

# **Biogeochemical Fe-S-cycling in a late Archean and Proterozoic Ocean Model Habitat – the high alpine Arvadi Spring**

## **Dissertation**

der Mathematisch-Naturwissenschaftlichen Fakultät  
der Eberhard Karls Universität Tübingen  
zur Erlangung des Grades eines  
Doktors der Naturwissenschaften  
(Dr. rer. nat.)

Vorgelegt von:

M. Sc. Elif Köksoy

aus Gäufelden-Nebringen

Tübingen, 2018

Gedruckt mit Genehmigung der Mathematisch-Naturwissenschaftlichen Fakultät der  
Eberhard Karls Universität Tübingen.

Tag der mündlichen Qualifikation: 25.04.2018

Dekan: Prof. Dr. Wolfgang Rosenstiel

1. Berichterstatter: Prof. Dr. Andreas Kappler

2: Berichterstatter: Dr. Itay Halevy





# TABLE OF CONTENTS

<b>Summary</b> .....	8
<b>Zusammenfassung</b> .....	12
<b>Chapter 1: Introduction</b> .....	17
Abstract .....	18
Precambrian seawater composition, biogeochemical processes and BIF deposition .....	19
Modern environments as ancient analogues .....	25
Lake stratification.....	27
Lake Matano .....	29
Lake Pavin .....	31
Lake La Cruz .....	32
Lake Nordbytjernet.....	33
Lake Vechten .....	34
Modern stratified lakes as models for Precambrian ocean conditions .....	35
Alternative field sites for studying Archean and Proterozoic ocean conditions.....	38
Outlook and future research needs .....	42
<b>Open question and objectives of this study</b> .....	51
<b>Chapter 2</b> .....	53
Abstract .....	54
Introduction.....	55
Materials and Methods .....	57
Results.....	64
Discussion.....	72

Implications for Fe-S-cycling in ferro-euxinic transition zones of shallow late Archean and Proterozoic ocean waters .....	80
<b>Chapter 3</b> .....	108
Abstract .....	109
Introduction.....	110
Material and Methods .....	111
Results and Discussion .....	112
Implications for Fe-S-mineralogy and nutrient cycling in ferro-euxinic intermixed waters of late Archean and Proterozoic Oceans .....	119
<b>Chapter 4</b> .....	136
Abstract .....	137
Introduction.....	138
Methods.....	140
Results.....	144
Discussion.....	155
Implications for Precambrian Fe-cycling .....	161
<b>General conclusions and outlook</b> .....	167
<b>Statement of personal contribution</b> .....	175
<b>Acknowledgements</b> .....	177
<b>Curriculum Vitae</b> .....	180



## SUMMARY

Earth is pictured to have been the scene for drastic environmental changes throughout the Precambrian while it developed into a life-hospitable setting. Among the most remarkable environmental developments of this time period is the redox evolution of the atmosphere and hydrosphere across the late Archean-Paleoproterozoic boundary that resulted by the emergence of oxygenic photosynthesis by about 2.7 Ga.

While anoxic and ferruginous (Fe(II)-enriched) conditions prevailed in the open deep ocean throughout much of the Precambrian, coastal seawater in mid-depths of the ocean is thought of having turned euxinic (sulfide-enriched) whereas ocean surface waters turned slightly oxic and presumably Fe(II)-poor due to abiotic Fe(II) oxidation by oxygen during the early Proterozoic. Great amounts of sulfate became mobilized by increased oxidative weathering of terrestrial pyrite and riverine runoff, resulting in enhanced sulfate reduction rates that were causal for the ferro-euxinic transition of seawater. The actual extend of ferruginous versus euxinic conditions has not been fully deciphered yet, and factors that controlled their formation and expansion as well as the identity of the major minerals that formed from such waters remain ambiguous. Deciphering the biogeochemistry of these highly complex ocean zones specifically is intriguing because of their postulated role in retarding biological diversification, particularly because euxinic waters are known to scavenge trace nutrients and metals as molybdenum and Fe(II) through their precipitation as Mo- and Fe(II)-sulfides.

Our grasp on this complex period remains vague as most of our knowledge comes from the interpretation of the geologic record that preserved biogeochemical signals, but however partly is incomplete and altered by diagenesis and metamorphism. The use of modern habitats that resemble ancient ocean conditions is a promising alternative way to gain information on ancient ocean composition and biogeochemical processes. Examples for ferruginous ocean analogues include Lake Matano (Indonesia), Lake Pavin (France), Lake La Cruz (Spain), Lake Cadagno (Switzerland), Lake Vechten (Netherlands) and Lake Nordbytjernet (Norway). Analogues of euxinic seawater are the Black Sea (Turkey, Georgia, Russia, Ukraine, Moldova, Romania and Bulgaria), the Cariaco Basin (Venezuela) and



Chesapeake Bay (USA). All of these habitats contain either Fe(II)- or sulfide-enriched waters, while h none of them comprises intermixed ferro-euxinic waters.

The Fe- and S-rich Arvadi Spring in the eastern Swiss Alps borrows strong potential as a model habitat for ferro-euxinic intermixed transition zones of oxygenated ancient oceans to study ancient biogeochemical Fe-S-cycling. Such conditions presumably prevailed mostly during the late Archean in oxygen oases and in surface waters of shallow Proterozoic oceans. The overall goal of this thesis was to decipher the controlling factors on the formation of ferruginous versus euxinic conditions by (1) evaluating the suitability of the Arvadi Spring as an analogue for ferro-euxinic transition zones of ancient oceans, (2) by identifying its geochemical, mineralogical and microbiological composition and finally, (3) by transferring our observations on present models of ancient Fe-S-cycling in ferro-euxinic transition zones of the ancient ocean.

Part I of this thesis followed the goal of evaluating the modern analogue value of the Arvadi Spring for ferro-euxinic transition zones of the ancient ocean by characterizing the geochemical composition of the Arvadi Spring water and sediment and comparing its geochemistry to modeled ancient seawater composition. We identified the Arvadi Spring water to have a circumneutral pH and cold temperature and to be fully saturated with oxygen. We found dissolved Fe(II) and sulfide to coexist at micromolar concentrations without reaching saturation with respect to Fe(II) sulfide (amorphous). Fe(III) primarily was observed in solid precipitates that covered the Arvadi Spring pond ground, while no dissolved Fe(III) was detectable in the Arvadi water. Overall, our results imply the Arvadi Spring to provide a suitable geochemical framework to study Fe-S-biogeochemistry in a natural laboratory, from which we can learn and transfer knowledge on ancient Fe-S-cycling.

In part II of this thesis, we examined the morphology and the mineralogical composition of red and white colored mineral precipitates (termed red and white flocs in the following) that abundantly formed in the Arvadi Spring. A suite of spectroscopic analyses including XRD, XAS, EXAFS and Mössbauer spectroscopy revealed red and white flocs to primarily consist of quartz, dolomite and calcite. We identified the Fe-mineralogy to be dominated by green

rust, lepidocrocite and ferrihydrite, while  $S^0$  constituted the dominating S-mineral in white flocs. Fe(II) sulfides were found only in small abundance at locally restricted hot spots in red flocs, which was consistent with a calculated undersaturation of the Arvadi Spring water with respect to amorphous Fe(II) sulfide. The observed Fe(II) sulfides at red flocs hot spots, including pyrite and mackinawite, presumably resulted from locally intense Fe(III) and sulfate reduction in anoxic sediment layers where Fe(II) and sulfide could accumulate to higher concentrations and precipitate as Fe(II) sulfides. The identified mineralogy in red and white flocs particularly suggests an important role for green rust and  $S^0$  as precursor minerals for geologic rock deposits.

The dense colonization of red and white flocs by microbial networks already implied respective minerals to be partly produced and/or consumed by microbes. Part III of this thesis addressed the identity, composition, abundance and metabolic activity of the observed microbial network in microbe-mineral assemblages and in the Arvadi Spring sediment. For this purpose, we carried out a suite of cultivation-based, molecular biological and controlled microcosm experiments. Generally, we found the microbial community in the Arvadi Spring sediment to be very diverse. We identified *Thiothrix* spec., a microaerophilic sulfide-oxidizer, to dominate the microbial community on the 16S rRNA gene level. We could show Fe- and S-metabolizers to coexist as part of the Arvadi Spring microbial community at different abundances, with microaerophiles being the dominant types of Fe- and S-metabolizers. Anaerobes were present at lower abundances, indicating the oxygen saturation of the spring to limit anaerobes in the availability of ecological niches that they could inhabit. We could show that Fe(II) was mainly oxidized abiotically by  $O_2$ , whereas no net Fe(II) oxidation was observed under anoxic conditions. Instead, Fe(III) reduction was the dominantly ongoing process in the Arvadi Spring sediment under anoxic incubation conditions, with the highest reduction intensity observed under the contemporaneous presence of sulfate reduction with elevated levels of organic carbon and ferrihydrite. Overall, our results imply a spatially separated cycling of Fe in the Arvadi Spring pond, with Fe(II) oxidation proceeding in oxic parts of the spring whereas Fe(III) reduction is ongoing in anoxic sediment layers. Generally, we suggest ferruginous conditions to have been promoted by sulfate reduction in ferro-

euxinic transition zones of the ancient ocean, if the availability of organic carbon was sufficient for sustaining both, dissimilatory sulfate reduction and Fe(III) reduction in parallel.

Collectively, our findings shed new light on the composition and ecosystem functioning in ferro-euxinic transition zones of ancient oceans and build the basis for future research with flow-through and column experiments to reconstruct stratified ancient oceans. Complementary data from such setups could ultimately reveal how the formation of ferruginous and euxinic conditions was controlled at different depths of stratified oceans, especially considering variations in microbial control due to a depth distribution pattern of different physiologies according to geochemical gradients in the water column.

# ZUSAMMENFASSUNG

Die präkambrische Erde wird als Schauplatz drastischer Umweltveränderungen während ihrer Entwicklung zu einem lebensfreundlichen Ort dargestellt. Zu den bemerkenswertesten Umweltentwicklungen dieser Zeit zählt die Redoxentwicklung der Atmosphäre und Hydrosphäre während des spätarchaisch-paläoproterozoischen Übergangs, die durch das erstmalige Auftreten oxygener Photosynthese vor etwa 2,7 Milliarden Jahren zustande kam.

Es wird angenommen, dass im gesamten Präkambrium anoxische und Fe(II)-reiche Bedingungen in der offenen Tiefsee vorherrschten, während sich im Paläoproterozoikum euxinische (Sulfid-angereicherte) Bedingungen in mittleren Tiefen der Küstengewässer entwickelten und Ozeanoberflächenwasser oxidierten und auf Grund abiotischer Fe(II)-Oxidation mit Sauerstoff an Fe(II) verarmten. Während dieser Zeit wurden große Mengen an Sulfat durch erhöhte oxidative Verwitterung terrestrischen Pyrits und Erosion in Küstengewässer eingetragen, was zu erhöhten Sulfatreduktionsraten führte welche für den ferro-euxinischen Wechsel der Meerwasserzusammensetzung verantwortlich waren.

Das tatsächliche Ausmaß von eisenhaltigen gegenüber euxinischen Wassermassen ist bislang nicht vollständig entschlüsselt, und insbesondere Faktoren, die ihre Bildung und Expansion sowie die Identität der Minerale, die sich aus solchen Gewässern ablagerten, kontrollierten, sind ungeklärt. Die Entschlüsselung der Biogeochemie dieser hochkomplexen Ozeanzonen ist aufgrund ihrer postulierten Rolle bei der Verzögerung der biologischen Diversifizierung von grossem Interesse, hauptsächlich auf der Ausfällung von Spurenelementen und Metallen wie Molybdän und Fe(II) durch euxinische Gewässer als Mo- und Fe(II)-Sulfide beruhend.

Unser Verständnis dieser komplexen Periode bleibt vage, da der Großteil unseres Wissens aus der Interpretation der geologischen Aufzeichnungen stammt, die zwar biogeochemische Signale konserviert haben, aber teilweise unvollständig und durch Diagenese und Metamorphose verändert sind. Die Nutzung moderner Habitate, welche in ihrer Zusammensetzung denen der Urozeane ähneln, ist ein vielversprechender alternativer Weg um Informationen über die Zusammensetzung der Urozeane und biogeochemische Prozesse

zu erhalten. Beispiele für eisenhaltige Ozeananaloga sind Lake Matano (Indonesien), Lake Pavin (Frankreich), Lake La Cruz (Spanien), Lake Cadagno (Schweiz), Lake Vechten (Niederlande) und Lake Nordbytjernet (Norwegen). Analoge Habitate für euxinische Gewässer sind das Schwarze Meer (Türkei, Georgien, Russland, Ukraine, Rep. Moldau, Rumänien und Bulgarien), das Cariaco Basin (Venezuela) und Chesapeake Bay (USA). All diese Habitate enthalten entweder Fe(II)- oder Sulfid-angereicherte Gewässer, wobei keines der genannten Habitate Fe(II)- und Sulfid-angereicherte Mischwässer enthält.

Die Fe- und S-reiche Arvadi-Quelle in den östlichen Schweizer Alpen birgt großes Potenzial als Modell-Habitat zur Untersuchung des biogeochemischen Fe-S-Umsatzes in ferro-euxinischen Übergangszonen oxygenierter Urozeane. Solche Bedingungen herrschten vermutlich hauptsächlich in spät archaischen Sauerstoffoasen und in seichten Ozeangewässern im Proterozoikum vor. Das übergeordnete Ziel dieser Arbeit war es, die Faktoren, welche die Bildung von eisenhaltigen gegenüber euxinischen Bedingungen kontrollierten, zu entschlüsseln, indem (1) die Tauglichkeit der Arvadi-Quelle als Analogon für ferro-euxinische Übergangszonen von Urozeanen bewertet wurde, (2) ihre geochemische, mineralogische und mikrobiologische Zusammensetzung analysiert wurde und schließlich (3) unserer Beobachtungen auf gegenwärtige Modelle des Fe-S-Umsatzes in ferro-euxinischen Übergangszonen des Urozeans übertragen wurden.

Teil I dieser Arbeit verfolgte das Ziel, den Nutzen der Arvadi-Quelle als Modell-Habitat für ferro-euxinische Übergangszonen des Urozeans zu bewerten, indem die geochemische Zusammensetzung des Arvadi-Quellwassers und -sediments analysiert und die ermittelte Geochemie mit der modellierten Meerwasserzusammensetzung des Urozeans verglichen wurde. Unsere Analysen ergaben, dass das Arvadi-Quellwasser einen neutralen pH-Wert, kalte Temperaturen und eine vollständige Sauerstoffsättigung vorweist. Wir fanden heraus, dass gelöstes Fe(II) und Sulfid in mikromolaren Konzentrationen im Quellwasser koexistieren, ohne Sättigung in Bezug auf Fe(II)-Sulfid (amorph) zu erreichen. Fe(III) wurde hauptsächlich in festen Niederschlägen beobachtet, die den Arvadi-Quellboden bedeckten, während im Arvadi-Wasser kein gelöstes Fe(III) nachweisbar war. Insgesamt deuten unsere Ergebnisse darauf hin, dass die Arvadi-Quelle einen geeigneten geochemischen Rahmen für

die Untersuchung der Fe-S-Biogeochemie im Rahmen eines natürlichen Labors bietet, von dem wir neue Erkenntnisse über den Fe-S-Zyklus im Urozean gewinnen und auf existierende Modelle transferieren können.

In Teil II dieser Arbeit untersuchten wir die Morphologie und die mineralogische Zusammensetzung von roten und weißen Mineralpräzipitaten (im Folgenden als rote und weiße Flocken bezeichnet), die in der Arvadi-Quelle in großen Mengen abgelagert wurden. Eine Reihe von spektroskopischen Analysen einschließlich XRD-, XAS-, EXAFS- und Mössbauer-Spektroskopie ergab, dass rote und weiße Flocken hauptsächlich aus Quarz, Dolomit und Calcit bestehen. Wir fanden heraus, dass die Fe-Mineralogie von Fougerit, Lepidokrokit und Ferrihydrit dominiert wird, während  $S^0$  das dominierende S-Mineral in weißen Flocken darstellt. Fe(II)-Sulfide wurden nur in kleinen Mengen an lokal begrenzten sogenannten 'hot-spots' in roten Flocken gefunden, was mit einer berechneten Untersättigung des Arvadi-Quellwassers in Bezug auf amorphes Fe(II)-Sulfid übereinstimmte. Die Fe(II)-Sulfide (einschließlich Pyrit und Mackinawit) in hot-spots der roten Flocken resultierten vermutlich aus lokal intensiver Fe(III)- und Sulfatreduktion in anoxischen Sedimentschichten, in denen sich Fe(II) und Sulfid zu höheren Konzentrationen anreichern und als Fe(II)-Sulfide ausfallen können. Die identifizierte Mineralogie in roten und weißen Flocken legt insbesondere eine wichtige Rolle für Fougerit und  $S^0$  als Vorläuferminerale für geologische Gesteinsablagerungen nahe.

Die dichte Kolonisierung von roten und weißen Flocken durch mikrobielle Netzwerke implizierte bereits, dass die vorhandenen Minerale teilweise von Mikroben produziert und/oder verbraucht wurden. Teil III dieser Arbeit befasste sich mit der Identität, Zusammensetzung, Abundanz und metabolischen Aktivität des mikrobiellen Netzwerks in roten und weißen Flocken und im Arvadi-Sediment. Zu diesem Zweck führten wir eine Reihe von Kultivierungs-basierten, molekularbiologischen und kontrollierten Mikrokosmen-Experimenten durch und fanden im Allgemeinen heraus, dass die mikrobielle Gemeinschaft im Arvadi-Sediment sehr divers ist. Wir identifizierten *Thiothrix spec.*, einen mikroaerophilen Sulfid-Oxidierer, die mikrobielle Gemeinschaft auf der 16S-rRNA-Gen-Ebene zu dominieren. Wir konnten zeigen, dass Fe- und S-Metabolisierer als Teil der

mikrobiellen Gemeinschaft der Arvadi-Quelle mit verschiedenen Abundanzen koexistieren, wobei Mikroaerophile deutlich dominierten. Anaerobe Fe-S-Metabolisierer waren gering abundant, was auf eine Limitierung der von Anaeroben bewohnbaren anoxischen ökologischen Nischen durch die Sauerstoffsättigung der Arvadi Quelle hinweist. Wir konnten zeigen, dass Fe(II) hauptsächlich abiotisch durch  $O_2$  oxidiert wird, während unter anoxischen Bedingungen keine Netto-Oxidation von Fe(II) nachgewiesen werden konnte. Stattdessen war Fe(III)-Reduktion der vorherrschende Prozess im Arvadi-Sediment unter anoxischen Inkubationsbedingungen, wobei die höchste Reduktionsintensität unter gleichzeitiger Anwesenheit von Sulfatreduktion und erhöhten Mengen an organischem Kohlenstoff und Ferrihydrit beobachtet wurde. Insgesamt deuten unsere Ergebnisse auf einen räumlich getrennten Fe-Umsatz im Arvadi-Quellteich hin, wobei Fe(II)-Oxidation in oxischen Teilen der Quelle abläuft, während Fe(III)-Reduktion in anoxischen Sedimentschichten fortschreitet. Im Allgemeinen schlagen wir vor, dass eisenhaltige Bedingungen durch Sulfatreduktion in ferro-euxinischen Übergangszonen des Urozeans gefördert wurden, vorausgesetzt organischer Kohlenstoff war in ausreichenden Mengen vorhanden, um sowohl dissimilatorische Sulfatreduktion als auch Fe(III)-Reduktion parallel aufrecht zu erhalten.

Zusammengefasst werfen unsere Ergebnisse ein neues Licht auf die Zusammensetzung und das Funktionieren von Ökosystemen in ferro-euxinischen Übergangszonen von Urozeanen und bilden die Grundlage für zukünftige Forschung mit Durchfluss- und Säulenexperimenten zur Rekonstruktion geochemisch stratifizierter Urozeane. Ergänzende Daten aus solchen Ansätzen könnten letztlich zeigen, wie die Bildung von eisenhaltigen und euxinischen Gewässern in verschiedenen Tiefen stratifizierter Urozeane kontrolliert wurde, insbesondere unter Berücksichtigung potentieller Differenzen in der mikrobiellen Kontrolle aufgrund eines Tiefenverteilungsmusters verschiedener physiologischer Gruppen gemäß geochemischer Gradienten in der Wassersäule.





# CHAPTER 1: INTRODUCTION

## **Using modern ferruginous habitats to interpret Precambrian banded iron formation deposition**

Elif Koeksoy<sup>1</sup>, Maximilian Halama<sup>1</sup>, Kurt O. Konhauser<sup>2</sup>, and Andreas Kappler<sup>1</sup>

<sup>1</sup>Geomicrobiology, Center for Applied Geosciences, University of Tuebingen, Germany

<sup>2</sup>Department of Earth and Atmospheric Sciences, University of Alberta, Edmonton, Canada

Published in: *International Journal of Astrobiology*, **15**, 215-217 (2016)

## **Abstract**

Early Earth processes are typically identified through the study of mineralogical, elemental and isotopic features in the rock record, including Precambrian banded iron formations (BIF). However, post-depositional processes often obscure the primary geochemical signals, making the use of BIF as proxies for paleo-seawater and the paleo-biosphere potentially imprecise. Thus, alternative approaches are required to complement the information gained from the rock record in order to fully understand the distinctive biogeochemical processes on ancient Earth. Simulating these conditions in the lab is one approach, but this approach can never fully replicate the complexity of a natural environment. Therefore, finding modern environments with a unique set of geochemical and microbiological characteristics to use as analogues for BIF depositional environments can provide invaluable information. In this review, we provide an overview of the chemical, physical and biological parameters of modern, ferruginous lakes that have been used as analogue BIF environments.

## **Precambrian seawater composition, biogeochemical processes and BIF deposition**

The composition of Archean seawater has largely been interpreted through the study of banded iron formations (BIF), Fe- and Si-rich chemical sedimentary rocks that precipitated directly out of seawater since at least 3.8 Ga years ago (Mloszewska et al., 2012). BIF are typically composed of quartz (in the form of chert), magnetite, hematite, Fe-rich silicate minerals (stilpnomelane, minnesotaite, greenalite, and riebeckite), carbonate minerals (siderite, ankerite, calcite, and dolomite), and minor amounts of sulfide minerals (pyrite and pyrrhotite). The presence of both, ferric and ferrous minerals give BIF an average oxidation state of  $\text{Fe}^{2.4+}$  (Klein and Beukes, 1992) which means that 60% of Fe in BIF is made up by Fe(II). The deposition of such a high quantity of iron as present in BIFs required transport of huge amounts of dissolved Fe(II), most probably introduced by hydrothermal venting to the seawater (Holland, 1973), to the deposition sites in Precambrian shelf regions where it was either microbially or abiotically oxidized (Posth et al., 2013b). A mostly anoxic water column was necessary to maintain Fe(II) remained in solution. Under such conditions, oxidized anions as sulfate ( $\text{SO}_4^{2-}$ ) were present in much lower concentrations (Table 1) than nowadays resulting in a different microbial community as well as a different elemental composition compared to modern oceans (Habicht et al. 2002).

The iron minerals in BIF are of particular interest in studies focusing on modelling the Precambrian seawater environment (Fig. 1), and have been used extensively as proxies for the abundance of trace metals in the ancient ocean (e.g., Bjerrum and Canfield, 2002; Konhauser et al., 2009; Mloszewska et al., 2012; Robbins et al., 2013; Partin et al., 2013). While BIF mineralogy reflects significant post-depositional alteration under diagenetic and metamorphic conditions, the layers of magnetite and hematite are interpreted to have formed from an initial Fe(III) (oxyhydr)oxide phase, e.g. ferrihydrite ( $\text{Fe}(\text{OH})_3$ ) (Klein, 2005; Posth et al., 2008). It is thought to have precipitated in the photic zone of the water column when dissolved ferrous iron ( $\text{Fe}^{2+}$ ) was oxidized and hydrolysed to poorly soluble ferric iron minerals. The Fe(III) (oxyhydr)oxide particles then sank through the water column and

deposited on the seafloor where they eventually transformed to: (1) magnetite or Fe(II)-containing carbonates by abiotic and microbial Fe(III) reduction, (2) the more stable Fe(III) oxide hematite in case the  $C_{org}$  content was low in sediments leading to dehydration of the Fe(III) (oxyhydr)oxides under elevated pressure and/or temperature, or (3) to iron silicates, possibly in the form of a precursor mineral such as greenalite, when silica-sorbed Fe(III) (oxyhydr)oxides reacted with other cationic species in the sediment pore waters (e.g., Johnson et al., 2008; Konhauser et al., 2005; Morris, 1993; Posth et al., 2013b; Posth et al., 2014; Rasmussen et al., 2015; Sun et al., 2015). Indeed, silica concentrations are assumed to have been high in the Precambrian oceans, reaching concentrations of at least 0.67 mM (supersaturation with respect to cristobalite), and possibly as high as 2.2 mM (Siever, 1992; Maliva et al., 2005; Konhauser et al., 2007) (Table 1).

Trace element sequestration by authigenic Fe(III) (oxyhydr)oxides, such as ferrihydrite, results from a continuum of adsorption and co-precipitation reactions. As a consequence, lumped-process distribution coefficient models can be used to relate the concentration of an element in the Fe(III) (oxyhydr)oxide to the dissolved concentration present at the time of precipitation. This predictive aspect of metal sorption reactions has been exploited to better understand the BIF record with respect to ancient seawater composition and nutrient limitations on Precambrian primary productivity. For instance, it has been proposed that low P concentrations in Archean and Paleoproterozoic BIF indicate limited marine phosphorous availability at that time (10-25% of present-day concentrations; Konhauser et al., 2007) (Table 1), which would have reduced levels of photosynthesis and carbon burial, thereby inhibiting long-term oxygen production on the early Earth (Bjerrum and Canfield, 2002). Similarly, it has been shown that the nickel content in BIF has changed dramatically over time, and that a drop in Ni availability in the oceans around 2.7 billion years ago would have had profound consequences for microorganisms that depended on it, that being methane-producing bacteria called methanogens (Konhauser et al., 2009). These bacteria have a unique Ni requirement for their methane-producing enzymes (< 100 nm; Schönheit et al., 1979), and importantly, these bacteria have been implicated in controlling oxygen levels on the ancient Earth as the methane they produced was reactive with oxygen and kept

atmospheric oxygen levels low. It is possible that a Ni famine eventually led to a cascade of events that began with reduced methane production, the expansion of cyanobacteria into shallow-water settings previously occupied by methanogens, and ultimately increased oxygenic photosynthesis that tipped the atmospheric balance in favor of oxygen, the so-called Great Oxidation Event (GOE) at 2.5 Gyr.

**Tab. 1:** Comparison of the chemical and physical composition of the Archean, Proterozoic and modern ocean including respective estimates on the atmospheric oxygen content given in % present atmospheric level (PAL).

	<b>Archean</b>	<b>Proterozoic</b>	<b>Modern</b>
<b>O<sub>2</sub> [% PAL]</b>	< 0.001 <sup>2</sup>	10–20 <sup>2</sup>	100
<b>Fe(II) [μM]</b>	40–120 <sup>1</sup>	0.1–0.5 <sup>2</sup>	< 0.001 <sup>2</sup>
<b>PO<sub>4</sub><sup>3-</sup> [μM]</b>	0.03–0.29 <sup>3</sup>	0.9 <sup>1</sup>	0.9 <sup>1</sup>
<b>SO<sub>4</sub><sup>2-</sup> [μM]</b>	0.06–0.08 <sup>4</sup>	500–3000 <sup>6</sup>	28000 <sup>5</sup>
<b>S<sup>2-</sup> [μM]</b>	n.a.	n.a.	< 0.001 <sup>2</sup>
<b>SiO<sub>2(aq)</sub> [μM]</b>	670–2200 <sup>7</sup>	670–2200 <sup>7</sup>	10–180 <sup>7</sup>
<b>pH</b>	>6.5 <sup>2</sup>	>6.5 <sup>2</sup>	8.1 <sup>2</sup>
<b>T [°C]</b>	~40–70 <sup>3</sup>	n.a.	-2–3 <sup>6</sup>

---

n.a. = not available

<sup>1</sup> Canfield (2005)

<sup>2</sup> Saito et al. (2003)

<sup>2</sup> Holland (2006)

<sup>3</sup> Grotzinger and Kasting (1993)

<sup>4</sup> Crowe et al. (2014)

<sup>5</sup> Jorgensen (1982)

<sup>6</sup> Canfield (1998)

<sup>7</sup> DeMaster et al. (1995)

---

It is widely accepted that photosynthetic bacteria played a crucial role in Fe(II) oxidation and the precipitation of BIF primary minerals throughout the Archean and Paleoproterozoic (see Posth et al., 2013b for review). Some of the earliest models of BIF deposition suggested that the abiotic oxidation of dissolved Fe(II) took place in the presence of free oxygen derived from oxygenic photosynthesis via the evolution of cyanobacteria (Cloud, 1973). However, on a dominantly anoxic Earth before 3.0 Ga (Crowe et al., 2013; Planavsky et al., 2014), the role of oxygen in terms of BIF deposition, if it existed, would have been limited. In this regard, anoxygenic photosynthetic bacteria (e.g., green and purple bacteria), which use Fe(II) as an electron donor for carbon assimilation rather than water and produce Fe(III) instead of dioxygen (e.g., Widdel et al., 1993), most probably colonized the anoxic waters of the Archean ocean. Laboratory experiments demonstrated that this form of metabolism could generate sufficient quantities of Fe(III) to account for all the oxidized iron in BIF even at rapid accumulation rates (Kappler et al., 2005; Konhauser et al., 2002). Fe(II) oxidation by anoxygenic phototrophs can be sustained in relatively deep waters (as much as one hundred meters of water depth) (Kappler et al., 2005), and their growth is not hindered by high concentrations of dissolved silica (Posth et al., 2008; Wu et al., 2014). Therefore, these organisms could easily have oxidized all of the upwelling Fe(II) before it made contact with the overlying oxygenated waters (if these existed) in the early Archean oceans (Czaja et al., 2013; Pecoits et al., 2015). As the redox state of the ocean most probably changed after the GOE in form of a slight oxygenation of the surface waters and anoxic bottom layers, the abundances of different types of bacteria must have changed crucially. For instance, microaerophilic Fe(II)-oxidizing bacteria likely thrived at the oxic-anoxic interface and contributed to the formation of Fe(III) (oxyhydr)oxides (Holm, 1989) in addition to anoxygenic photoferrotrophs that probably further colonized the anoxic photic zone. Because of the role microbes played in Fe(II) oxidation, the focus of a number of recent experimental studies on BIF deposition has been on how organic carbon may have (1) influenced trace metal sorption to the precursor ferrihydrite particles, and (2) affected the remobilization of trace metals during diagenesis and metamorphism when the heterotrophic respiration of the biomass would have been coupled to some form of terminal electron

accepting process, such as Fe(III) reduction. In the case of the former, Eickhoff et al. (2014) recently examined the partitioning of Ni to both abiogenic and biogenic ferrihydrite. They demonstrated that when normalized to specific surface area, biogenic ferrihydrite sorbed less Ni, apparently due to microbially derived organics or whole cells binding to the mineral surface and thereby competing with Ni for sorption sites. Given the potential for co-precipitating organic matter to depress partitioning of Ni, the Eickhoff study suggested that previous estimates for Ni concentrations in Archean seawater may be too low, and that the decline of Ni in Precambrian ocean may have occurred closer to the GOE, at 2.45 Ga. In the case of the latter, coupling the reduction of Fe(III) minerals to the oxidation of organic matter not only explains the low content of organic carbon in BIF (<0.5%; Gole and Klein, 1981), but it also explains the prevalence of light carbon isotope compositions in associated carbonate minerals (e.g., Walker, 1984), and light iron isotope compositions of magnetite and siderite (e.g., Johnson et al., 2008; Craddock and Dauphas, 2011). In this regard, Posth et al. (2013a) and Köhler et al. (2013) both demonstrated that by incubating ferrihydrite at 1.2 kbar and 170°C (conditions that mimic some BIF burial conditions) for only 14 days, the mineralogical transition from ferrihydrite to hematite is already accomplished. The addition of organic carbon to these diagenetic experiments led to the formation of reduced, i.e. Fe(II)-containing minerals in the post-diagenetic capsules, mainly a mixture of hematite, magnetite, and siderite, a composition broadly consistent with the modern day mineralogy of BIF. Robbins et al. (2015) took this one step further, demonstrating that during these diagenetic mineral transformations, Ni and Zn remained largely immobile.

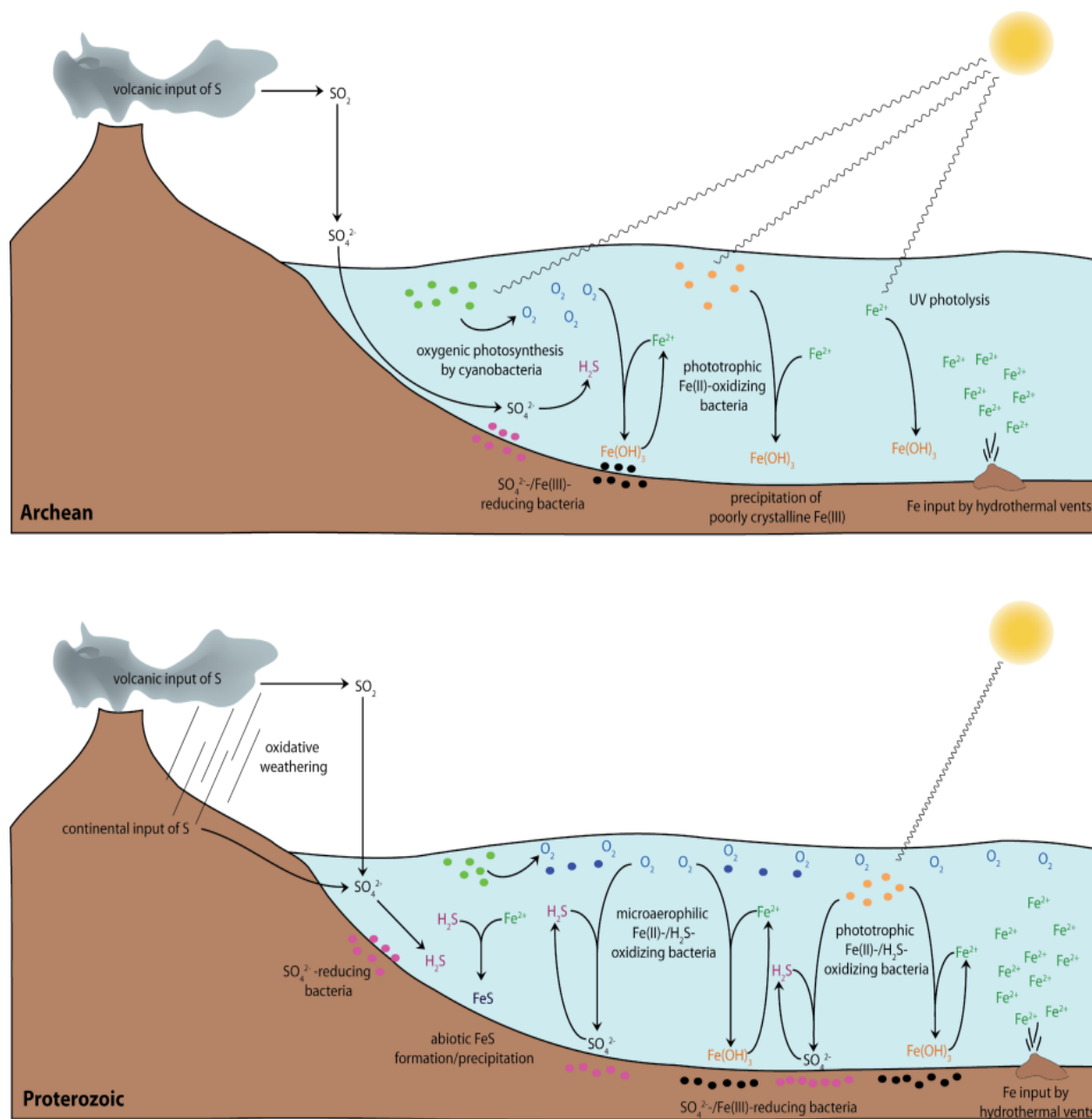


**Fig. 1:** Overview of the Fe-S biogeochemistry in the Archean and Proterozoic ocean. Archean: Fe(II) was introduced into the ocean hydrothermally and remained in its reduced state as oceans were dominantly anoxic. The occurrence of Fe(III) in the BIF record from that time can be explained by three different processes: (1) UV photolysis of Fe(II) (2) microbial oxidation of Fe(II) by photoautotrophic bacteria and (3) abiotic oxidation of Fe(II) by oxygen that started getting produced in minor amounts by cyanobacteria in the late Archean. Fe(III) was reduced to Fe(II) coupled to the oxidation of  $\text{H}_2$ /organic C by Fe(III)-reducing bacteria. Sulfate mainly was introduced into the ocean by volcanic input in form of  $\text{SO}_2$  that further got oxidized to  $\text{SO}_4^{2-}$  prior to its transfer to the ocean water. Sulfate-reducing bacteria



already produced small amounts of H<sub>2</sub>S by oxidizing H<sub>2</sub> and/or organic carbon. Proterozoic: The ocean surface was slightly oxic after the Great Oxidation Event (GOE) and O<sub>2</sub> starts accumulating also in the atmosphere. Increased oxidative weathering increased sulfate concentrations in the ocean by continental input in addition to volcanic input. Sulfate-reducing bacteria produced high amounts of sulfide which started accumulating under the reducing conditions of the deep ocean. Microaerophilic bacteria started flourishing under microoxic conditions and oxidized Fe(II) and H<sub>2</sub>S to Fe(III) and sulfate, respectively. Fe(II) and H<sub>2</sub>S reacted and precipitated in form of FeS minerals which is preserved in the rock record. Phototrophic sulfide-oxidizing bacteria started being highly active in the photic zone of the water column and oxidized accumulating H<sub>2</sub>S to sulfate.

### **Modern environments as ancient analogues**

A complete and accurate picture of all the important biogeochemical processes occurring in the Archean is impossible, if based solely on geological and geochemical observations, because the rock record is incomplete and has been altered by post-depositional processes (Sadler, 1981). Laboratory experiments that simulate BIF diagenesis or performing mineral precipitation experiments under Archean ocean compositions has also yielded valuable information (Kappler et al., 2005; Köhler et al., 2013; Konhauser et al., 2005; Posth et al., 2008; Posth et al., 2013a), but the conditions for these experiments are based on estimations for seawater conditions at that time, and the data derived are based on artificial systems which will never be able to represent the complexity of natural systems. There is thus a high probability of overlooking important parameters that are either impossible to integrate into the experimental setup or are basically ignored. Furthermore, proxies derived from geochemical modelling or from the rock record, on which the experimental designs are based on, might be inaccurate or imprecise (for example, estimates on the pH and temperature of the ancient ocean).

A way forward is through the study of modern environments that have geochemical conditions that might mimic Archean oceans. These analogues would include aqueous environments with the simultaneous presence of Si and Fe(II) at high concentrations, and a corresponding deficiency in sulfate in case of the Archean ocean. Correlation of observations

from such model habitats to results from simulative laboratory experiments can improve our current understanding of biogeochemical processes occurring in the Archean oceans (Fig. 2). In this review, we present five such model habitats which we evaluate for their suitability as modern analogues. All of them are redox-stratified lakes, either of meromictic or holomictic (Fig. 3; for definitions see the following section). In each case, ferruginous conditions can be found in a reducing bottom layer, which is assumed to have been the prevalent feature of the ancient ocean throughout much of the Precambrian and also the Phanerozoic (Zegeye et al., 2012). Two of the lakes – Lake Pavin and Lake Matano – are the best studied ferruginous basins with the purpose to transfer gained knowledge to models of the Precambrian ocean. The other three lakes – Lake La Cruz, Lake Vechten and Lake Nordbytjernet – were included to our study in order to present lakes with the potential to serve as ancient ocean analogues that have not been investigated as such, yet. By this, we aim to encourage scientists from different disciplines to investigate such environments in order to understand the ancient ocean in detail. Expanding on this unique feature of stratification, we first explain the basic definitions for different lake stratification scenarios in the following section and then compile information on Lake Pavin, Lake Matano, Lake La Cruz, Lake Vechten and Lake Nordbytjernet.

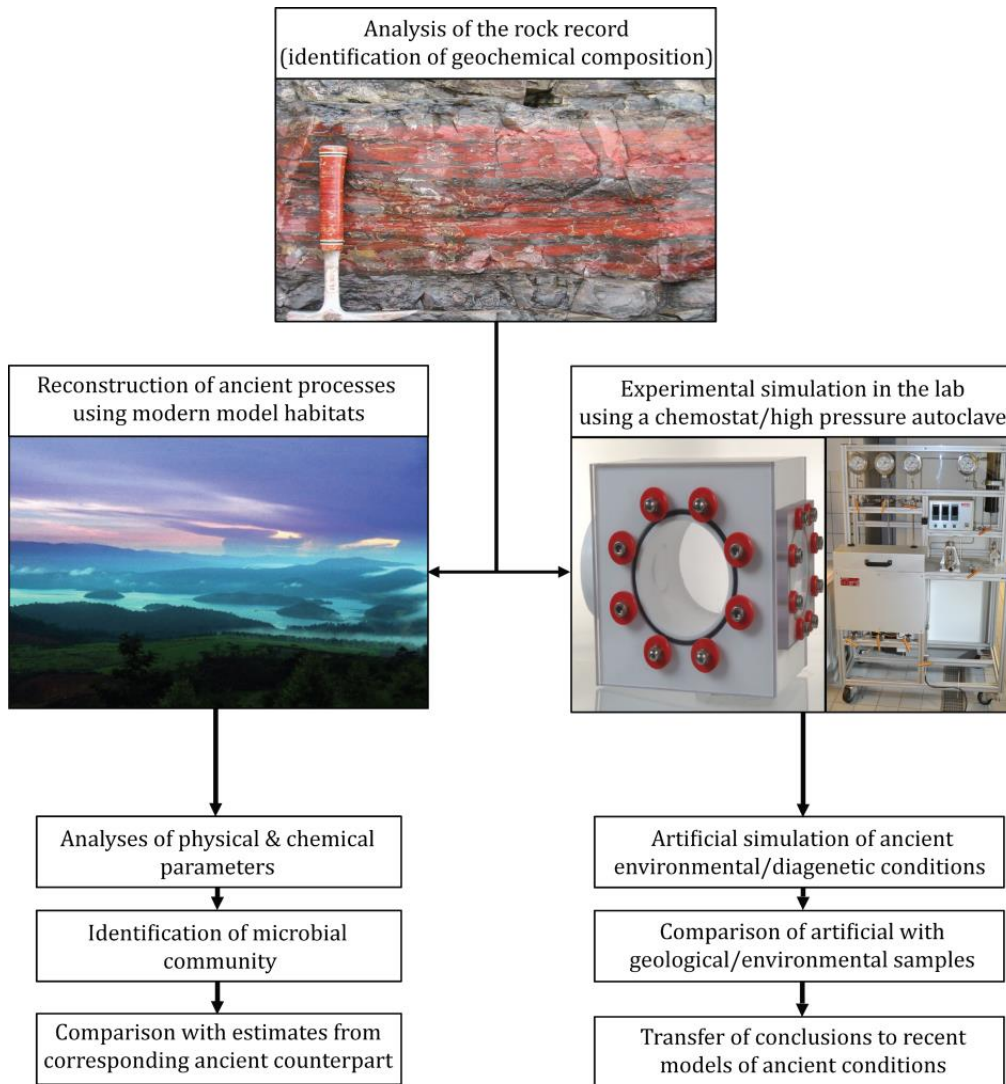


**Fig. 2:** Different approaches to evaluate the mineralogy, geochemistry and geomicrobiology of Archean and Proterozoic environments.

## Lake stratification

Water circulation in lakes is largely controlled by variations in water density at different depths, resulting from seasonal differences in surface temperature and dissolved ions (chemical gradients) (Boehrer and Schultze, 2008; Drever, 1997). The topmost layer in a

lake, the *epilimnion*, is exposed to solar radiation, heat-loss by long-wave radiation and thermal contact with the atmosphere. In contrast, the deeper water layer, the *hypolimnion*, is shielded from major heat sources, and is thus colder than epilimnetic waters. The epi- and hypolimnion are separated from each other by the *metalimnion*, a zone with a sharp temperature gradient (Andersson, 1997). Thus, lakes with sufficient depth tend to be stratified thermally during the warm season (separated into layers of different temperatures). When surface temperatures start exceeding those of the hypolimnion, warmer, more buoyant waters can only be mixed to a depth limited by colder, denser water. During stratification, the epilimnion and atmosphere exchange heat and volatile compounds (such as oxygen) resulting in the physical circulation of epilimnetic waters. Meanwhile, the hypolimnion is insulated from exchange with the atmosphere and thus the oxygen content steadily decreases in these deeper layers due to its consumption via aerobic respiration in the water column. The redox state of the lake differs in the hypo- and epilimnion, separated by a steep gradient of oxygen concentrations in the metalimnion, called *oxycline*. When epilimnetic temperatures start to decrease (e.g. during autumn) to values approaching hypolimnetic ones, density differences disappear, resulting in the complete vertical mixing of hypo- and epilimnetic waters (*fall turnover*). During this event, oxygen is mixed into the whole water column and is present at concentrations in equilibrium with air O<sub>2</sub> concentrations (Drever, 1997). When epilimnetic temperatures reach lower temperatures than hypolimnetic ones (e.g., during winter), density contrasts re-appear and stratification occurs, with a subsequent spring turnover. This phenomenon is observed in regions with seasonal temperature fluctuation, whereas changes in stratification pattern of lakes usually do not occur in areas with constant climate conditions.

Lakes with at least one annual turnover are collectively called *holomictic* (Fig. 3A). *Meromictic* lakes in contrast, contain an additional chemically distinct bottom layer, called the *monolimnion* that has not been recirculated for more than a year (Fig. 3B). This layer is usually anoxic, and overlain by the epi-, meta- and hypolimnion. Seasonal mixing of epi- and hypolimnion result in the mixolimnion.

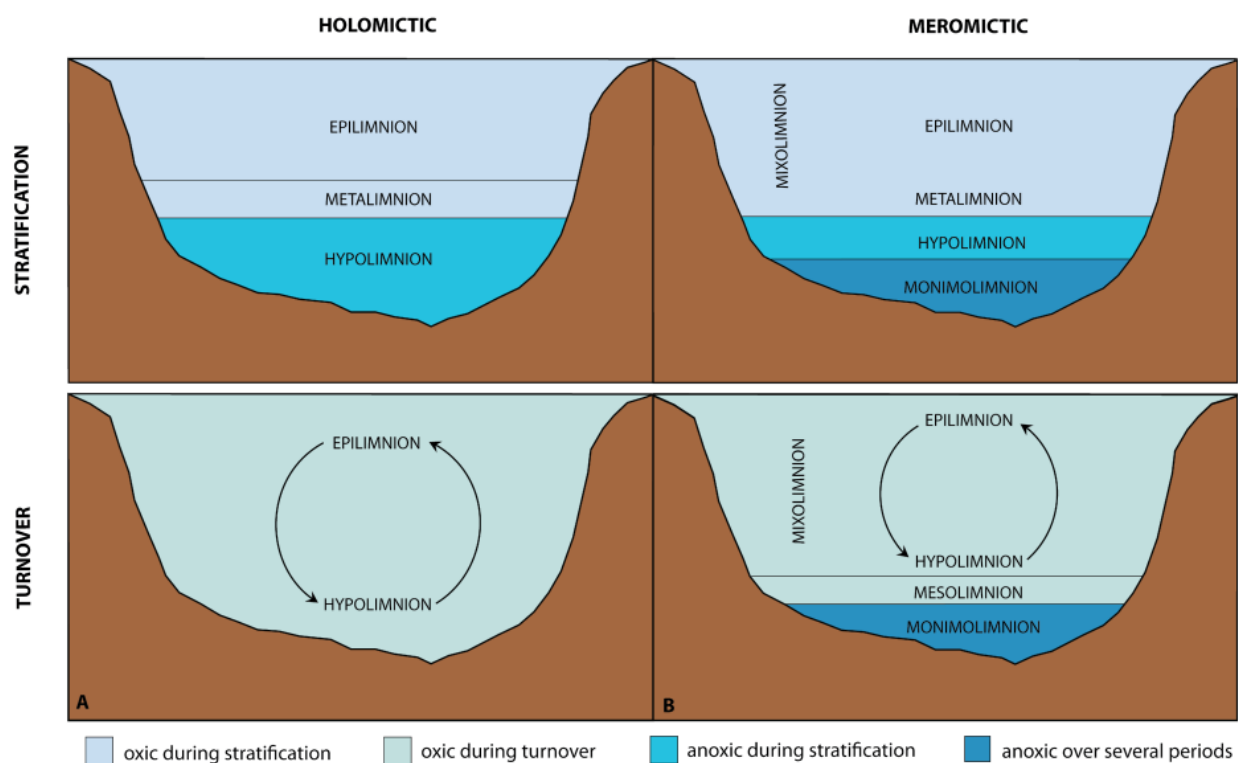


**Fig. 3:** Patterns of stratification and turnover in holomictic and meromictic lakes.

## Lake Matano

Lake Matano, the world's largest known ferruginous lake (Crowe et al., 2011), is located on Sulawesi Island, Indonesia (S2° 29' 9.215" E121° 22' 38.507"). The lake is categorized as meromictic (Crowe et al., 2008c), which results from the combination of its great depth (>590 m) with the absence of seasonal temperature fluctuations and a steep bathymetry (Crowe et al., 2008b; Crowe et al., 2008c). A persistent chemocline at ~100 m depth divides the lake into an oxic top and an anoxic bottom layer (Crowe et al., 2008c). Although it is not clear when the last mixing of the lake occurred, stable vertical profiles of redox-sensitive elements, such as Fe and Mn, suggest redox conditions to have prevailed on a millennial time scale (Crowe et al., 2008c). Dissolved Fe(II) is present at concentrations of up to 140  $\mu\text{M}$ , whereas dissolved Mn(II) reaches a maximum of 9.5  $\mu\text{M}$  in the hypolimnion. Chromium was

180 nM in the epilimnion, but it was not detectable in the hypolimnion. Similarly, sulfate was 20  $\mu\text{M}$  in the epilimnion, but was not detectable in the hypolimnion. Instead, trace concentrations of sulfide below 0.2  $\mu\text{M}$  were measured below the chemocline (Crowe et al., 2008c) as a result of slow sulfate reduction (Crowe et al., 2008b). Dissolved silica was measured below saturation at 300-420  $\mu\text{M}$  (Crowe et al., 2008b; Zegeye et al., 2012). An additional specific feature of Lake Matano results from the scavenging of phosphate by Fe(III) (oxyhydr)oxide phases, such as ferrihydrite, which limits primary productivity in the surface mixed layer. The lack of light-absorbing (in)organic particles in the water column enables light penetration down to a depth of 125 m, where oxygen is already absent. Combined with the supply of Fe(II), conditions favor the establishment of a large community of anoxygenic phototrophic bacteria, in this particular case green-sulfur bacteria (GSB), at a depth of 115-125 m (Crowe et al., 2008b). The shift from an oxygenic cyanobacteria population in the epilimnion to a community of anoxygenic phototrophs in the hypolimnion is accompanied with a transition in abundances of the photosynthetic pigments chlorophyll *a* that dominates the oxic waters to a similar quantity of bacteriochlorophyll *e*, which is used by *Chlorobiaceae*, a family of low light adapted green sulfur bacteria. The majority of this family are photolithoautotrophs that use sulfide as an electron donor with the exception of *C. ferrooxidans* that uses Fe(II) instead (Crowe et al., 2008b).

The mineralogy of the mineral particles formed during Fe(II) oxidation was determined, and showed the presence of carbonated green rust together with magnetite as abundant Fe minerals below the chemocline (Crowe et al., 2008c; Zegeye et al., 2012). Green rust is a mixed-valence intermediate Fe mineral formed by interaction of Fe(III) minerals with Fe(II) (Parmar et al., 2001). Lake Matano is so far the only stratified water body where green rust has been found (Zegeye et al., 2012). Whether the green rust is a microbial product by photoferrotrophy (Kappler and Newman, 2004) driven by the large GSB community or dissimilatory Fe(III) reduction (Zegeye et al., 2007) or whether an abiotic solid-phase transformation of ferrihydrite following Fe(II) adsorption is the pathway for its formation in Lake Matano remains unknown (Zegeye et al., 2012).

## Lake Pavin

Lake Pavin is a meromictic crater lake located 35 km southwest of Clermont-Ferrand (France) within the youngest volcano in the French Massif Central (N45° 29' 58.326" E2° 53' 12.743"). Surrounded by a ~50 m high ring of volcanic tuff, the lake is protected from physical mixing by wind. This, in combination with its almost circular geometry (750 m diameter, 0.44 km<sup>2</sup> surface and ~92 m maximum depth), results in a persistent redox stratification at a depth of ~60 m (Aeschbach-Hertig et al., 2002). The depth of the redoxcline can vary due to temporal variations resulting by annual meteorological differences and also was found at ~50 m depth in 2011 (Cosmidis et al., 2014). The mixolimnion (0- ca. 60 m depth) is oxygenated by seasonal fall and spring turnover, whereas the monimolimnion (ca. 60-92 m depth) remained anoxic for at least the last 100 years and thus reached a steady state (Busigny et al., 2014).

The mineralogy and oxidation state of Fe in the suspended particles was identified by Cosmidis et al. (2014) at different depths, revealing Fe to mainly be present in Fe(III) (oxyhydr)oxides and phyllosilicates at shallower depths, as Fe(II)-Fe(III)-phosphate mineral phases near the redoxcline, and Fe(II)-phosphates (vivianite-like) at the lake bottom. Under the reducing conditions in the monimolimnion, dissolved Fe(II) accumulates to a concentration of up to 1.2 mM (Bura-Nakic et al., 2009). Fe and Mn colloids (particle size <0.45 µm) as well as dissolved silica (H<sub>4</sub>SiO<sub>4</sub>) and phosphate are present at high concentrations (1.1 mM and 340 µM, respectively) in the bottom layer (Michard et al., 1994). Sulfate exists at low concentrations (15-20 µM) in the mixolimnion, and is absent in the monimolimnion (Assayag et al., 2008) as a result of microbial sulfate reduction. This metabolism leads to total dissolved sulfide concentrations between 0.6–16.7 µM just below the oxycline, with 80% of it being in colloidal FeS form as a consequence of Fe being the dominant metal involved into sulfur redox cycling (Bura-Nakic et al., 2009).

Lehours et al. (2005) identified the microbial community in Lake Pavin over different depths of the water column. They showed an elevated diversity of the archeal and bacterial communities in samples from anoxic water depths relative to samples from the oxic water

layers, with both changing in their structures over different lake depths (Lehours et al., 2005). The largest microbial community is represented by methanogens belonging to the genera *Methanosarcinales* and *Methanomicrobiales*, with 71% of the sequences related to *Methanosaeta concilii*. At the upper part of the chemocline (~60 m) sequences were related to methylotrophs as well as to the microaerophilic Fe(II)-oxidizer *Gallionella ferruginea* (with 97.5% sequence similarity), suggesting ongoing methane and microaerophilic Fe(II) oxidation at the oxic-anoxic redox transition zone of the lake. At a depth of 90 m, three sequences related to *Geothrix fermentans*, an Fe(III)-reducing  $\delta$ -Proteobacterium, were observed, suggesting the replenishment of Fe(II) at lower depths of the lake (Lehours et al., 2007).

### Lake La Cruz

Lake La Cruz is located at an altitude of 1000 m a.s.l. in the dolomitic karstic “Serrenia de Cuenca” mountains, near Cuenca, Spain (also called “Laguna de la Gitana”, N39° 59' 16.7" E1° 52' 25.0") (Rodrigo et al., 2001). Located inside a sink dissolution basin with steep vertical walls rising 20-30 m above water surface, the lake is protected from wind. In combination with its small surface to depth ratio it is also persistently stratified for the past four centuries now, however, unlike Lake Matano and Lake Pavin, stratification is not at a constant depth. Depending on the seasonal meteorology of the region within the respective year, its water depth and diameter vary annually. Measurements in 1987 and 1988 revealed variations in the redoxcline depth between 12.8-18.7 m. After intense rainfalls in spring 1988, maxima in depth and diameter with 24 m and 136 m were measured, respectively (Rodrigo et al., 2001). This resulted in a sharper and shallower thermocline, as well as a shallower oxic-anoxic boundary relative to periods with lower water levels (Romero-Viana et al., 2010). Nevertheless, values for iron and sulfide are constant in the anoxic bottom layer at ~900  $\mu$ M and <3  $\mu$ M, respectively. Sulfate is present at 0.05 mM (Rodrigo et al., 2000). One of the lake's main features is the annual summer 'whiting', a short-term precipitation event whereby



calcium carbonate is produced in the water column in sufficient quantities to be visible. The event is caused mainly by increased temperatures and increased CO<sub>2</sub> uptake by photosynthetic microorganisms, such that the carbonate crystals appear in light colored laminae alternating with dark laminae that result from the precipitation of organic matter throughout the year (Rodrigo et al., 1993).

Romero-Viana et al. (2010) identified photosynthetic pigments in the annual laminated sediment to reconstruct and interpret paleoproductivity in the lake. The study yielded the presence of marker pigments of phototrophic sulfur bacteria, including bacteriochlorophyll *a*, series of bacteriopheophytin *d*, and the bacterial carotenoids oktenone and chlorobactene (Romero-Viana et al., 2010). Correlating with solar radiation fluxes, the relative abundance of zeaxanthin suggests picocyanobacteria (e.g., *Synechococcus* sp.), to have dominated primary productivity in Lake La Cruz over the last four centuries (Romero-Viana et al., 2010). This is consistent with the general observation of promoted epicellular calcite precipitation in lakes with abundant picocyanobacteria communities (Romero-Viana et al., 2008). With midday solar fluxes  $>1 \mu\text{EM}^{-2}\text{s}^{-2}$ , light penetrates into the upper parts of the anoxic layer of the lake, enabling growth of a population of purple sulfur bacteria (*Amoebobacter purpureus*) immediately above green sulfur bacteria (*Pelodictyon chlatratiforme*). *A. purpureus* is capable of anaerobic photolithotrophy by metabolizing hydrogen sulfide, elemental sulfur and thiosulfate (Eichler and Pfennig, 1988) while *P. chlatratiforme* is capable of photosynthesis under low-sulfide and low-light conditions (Pfennig and Cohenbaz.G, 1967).

## Lake Nordbytjernet

Lake Nordbytjernet is located in the Upper Romerike area, 40 km northeast of Oslo, Norway (N60° 9' 23.299" E11° 9' 50.9"). The endogenic meromictic kettle lake has a maximum depth of 23 m, a persistent monimolimnion below 20 m and a surface area of 0.28 km<sup>2</sup> (Hongve, 2003). The major constituents of the anoxic zone are iron, manganese and phosphate with

concentrations reaching up to 710  $\mu\text{M}$ , 1180  $\mu\text{M}$  and 1130  $\mu\text{M}$ , respectively. Most of the Fe and Mn originate from a stream flowing through a forest area that has been artificially drained in modern times. The reducing conditions in the monimolimnion of Lake Nordbytjernet are maintained by the production of organic matter in the trophogenic zone. In contrast to other lakes, sulfate is present at high concentrations (up to 416  $\mu\text{M}$ ) in the oxic zone but is depleted in the anoxic bottom (Hongve, 2003). According to this author, conditions in Lake Nordbytjernet below 22 m favor the precipitation of both siderite ( $\text{FeCO}_3$ ) and vivianite ( $\text{Fe}_3(\text{PO}_4)_2 \cdot 8\text{H}_2\text{O}$ ), but played a role in Fe sedimentation from the monimolimnion. Instead, Fe(III) (oxyhydr)oxides, dominated by goethite, were the important Fe compounds in newly formed bottom sediments.

### Lake Vechten

Lake Vechten is a man-made gravel lake located in the municipality of Bunnik, the Netherlands (N52° 3' 40.23" E5° 9' 36.31") that was excavated in 1941 (Steenbergen and Korthals, 1982). It consists of two basins with maximum depths of 11.9 m and 10.5 m and a surface area of 4.7 ha, divided by a ridge at about 6 m depth (Steenbergen and Verdouw, 1982). The lake's water balance is regulated by meteorological conditions and horizontal groundwater flow. Of the five lakes presented here, Lake Vechten is the only holomictic lake with a summer stratification from May until October. A pronounced thermocline separates a cold hypolimnion (Crowe et al., 2014) from a warm epilimnion (0-5 m), resulting in hypolimnetic  $\text{O}_2$  depletion and thus a chemocline just below the thermocline. During summer, Fe(II) and Mn(II) can accumulate at concentrations up to 690  $\mu\text{M}$  and 180  $\mu\text{M}$  in the reducing bottom layer, respectively. In addition, sulfide concentrations nearly reach millimolar levels just below the oxic-anoxic boundary (Riera, 1988), above which sulfate reaches  $\sim 400$   $\mu\text{M}$  (Steenbergen and Verdouw, 1982). Sulfide decreases largely with increasing depth as Fe(II) becomes abundant enough to control sulfide levels (Riera, 1988; Verdouw and Dekkers, 1980). Availability of P and Si (52-104 and 3-17  $\mu\text{M}$ , respectively)

strongly depends on the autumnal turnover, with 2- to 5-fold concentrations in the whole mixed water column during winter compared to epilimnetic values during summer.

The deepest light penetration was found during summer stratification with Secchi disk depths of 3.5 to 4.5 m (extinction coefficients for green (0.38-0.85 m<sup>-1</sup>), yellow-orange (0.73-0.75 m<sup>-1</sup>), red (0.73-1.02 m<sup>-1</sup>) and blue light (0.69-1.42 m<sup>-1</sup>)). Thus, dense populations of phototrophic bacteria establish themselves in the metalimnion and upper hypolimnion where the chemocline starts. According to pigment analyses by Steenbergen and Korthals (1982) the total concentration of chlorophyll is up to 200 mg m<sup>-3</sup> during stratification, corresponding to several oxygenic photosynthesizers, including the genera *Synechococcus*, *Chloronema*, *Chromatium* and *Thiopedia*. At lake depths below 8 m, where light intensities are lower and sulfate concentrations decrease, abundances of sulfide-oxidizing bacteria, such as the families Chlorobiaceae and Chromatiaceae (Steenbergen and Korthals, 1982). A population of brown Chlorobiaceae, mainly *Chlorobium phaeobacteroides* was found where sulfide was measured at 870 μM, just beneath a population of green Chlorobiaceae where sulfide concentrations were <50 μM. As light extinction occurred mainly at the depths where *Synechococcus*-type cells and green Chlorobiaceae developed dense communities, brown Chlorobiaceae grew under very low light conditions with 0.001% incident surface light (Riera, 1988). As anaerobic bacteria respire low-molecular weight organic carbon compounds, such as acetate and lactate, in the lake sediment as well as the lower hypolimnion layers, fixation of produced CO<sub>2</sub> coupled to sulfide oxidation by purple sulfur bacteria at depths below 8 m is likely (Steenbergen and Korthals, 1982).

## **Modern stratified lakes as models for Precambrian ocean conditions**

From the presented five stratified lakes, four are meromictic and one, Lake Vechten, possesses a warm-holomixis stratification pattern. Their maximum depths vary greatly with Lake Matano showing the greatest depth (~590 m) followed by Lake Pavin (92 m), while the

other three are much shallower with similar depths (between 11.9-24.5 m, respectively, Table 2). All five lakes are stratified with regard to dissolved oxygen concentration, resulting in anoxic reduced bottom layers which enable the accumulation of redox-sensitive elements, such as Fe(II). Additionally, Si concentrations in respective bottom layers are relatively high (around 1 mM) combined with sulfate being almost deficient. Collectively their compositions suggest that all five lakes could serve as analogues for various times in the Archean and Paleoproterozoic.

In terms of the Fe(II) content, only Lake Matano approximates the estimated upper limit for Archean seawater Fe(II) (given as 120  $\mu\text{M}$  by Canfield, 2005) (Table 1) with a concentration of 140  $\mu\text{M}$  (Table 2). By contrast, the other lakes (with Fe concentrations between 690–1200  $\mu\text{M}$ ) significantly exceed Archean estimates (Table 2). In terms of Si, the 420  $\mu\text{M}$  in Lake Matano and the 500  $\mu\text{M}$  in Lake Nordbytjernet Si (Table 2) are below the suggested Archean Si lower limit of 670  $\mu\text{M}$  (Maliva et al., 2005) (Table 1), whereas Lake Pavin and Lake La Cruz contain Si concentrations within the estimated range of Precambrian Si (1100  $\mu\text{M}$  and 1178  $\mu\text{M}$ , respectively, Table 2). All five lakes exceed the upper estimate for Archean marine phosphate concentrations ( $5.3 \pm 2.6$   $\mu\text{M}$ , Konhauser et al., 2007) (Table 1), with Lake Matano exhibiting the lowest phosphate concentration of 9  $\mu\text{M}$ , followed by Lake Vechten (20  $\mu\text{M}$ ), Lake La Cruz (52.6  $\mu\text{M}$ ), Lake Pavin (340  $\mu\text{M}$ ) and Lake Nordbytjernet (1130  $\mu\text{M}$ , Table 2). Sulfate concentrations are very low in all lakes with values of  $<0.1$   $\mu\text{M}$  in case of Matano, Pavin and Nordbytjernet, while in Lake La Cruz and Lake Vechten sulfate is present at concentrations of around  $\sim 20$   $\mu\text{M}$  (Table 2), which is low but falls within the range of estimates for the Archean oceans of 200  $\mu\text{M}$  (Habicht et al., 2002) to only 80 nM (Crowe et al., 2014) (Table 1).

An important issue to take into account for the evaluation of Lake La Cruz as a model habitat is the annual summer whiting event, a massive calcium carbonate precipitation that likely changes lake geochemistry. This may limit the suitability of Lake La Cruz as a natural laboratory for ancient ocean conditions. In contrast, the geochemical composition of Lake Vechten is quite constant during stratification, which occurs during summer. However, for the evaluation of Lake Vechten as model habitat it is of greater importance to consider its

sulfide accumulation to high concentrations of up to 1000  $\mu\text{M}$  in the hypolimnion (Table 2). Such high sulfide values are comparable to suggested euxinic conditions in Proterozoic marginal marine settings. Thus, Lake Vechten represents a model habitat for the Proterozoic rather than for the Archean ocean due to the availability of ferruginous and euxinic conditions in its bottom. The simultaneous presence of both dissolved Fe(II) and sulfide is necessary for studying Fe-S biogeochemistry in model habitats for the Proterozoic ocean.

When comparing the microbial compositions of the different lakes, it is obvious that anoxygenic phototrophic green-sulfur bacteria (GSB) dominate the microbial communities in ferruginous basins, as is the case with the bottom waters of Lake Matano, Lake La Cruz and Lake Vechten. Anoxygenic photosynthesis is assumed to be an ancient metabolism indicated by the deep branching GSB and green non-sulfur bacteria (GNSB), as well as the utilization of one single photosystem to harvest light energy in contrast to the requirement of two photosystems for oxygenic photosynthesis (Woese, 1987; Blankenship, 1992). In samples from Lake Matano, the Fe(II)-oxidizing GSB *Chlorobium ferrooxidans* was identified as community member and to date is the only known GSB capable of photoferrotrophy (Heising et al., 1999). Since such GSB need a minimum concentration of 0.8  $\mu\text{M}$  free sulfide for sulfide oxidation (Vangemerden, 1984), it is likely that in an Fe(II)-rich environment, where sulfide availability was restricted to hydrothermal vents as in the Archean ocean, their preferred electron donor was Fe(II). In photic environments, where Fe(II) oxidation and Fe(III) mineral precipitation takes place, phosphorus was less available due to scavenging by Fe(III) (oxyhydr)oxides, and GSB further are suggested to have been the most active primary producing metabolism by photosynthetic C-fixation before cyanobacteria evolved confirmed by primary production rates of  $3.8 \times 10^{-3} \text{ mol C m}^{-2} \text{ d}^{-1}$  by photosynthetic C fixation in Lake Matano (Crowe et al., 2008b).

It is conceivable that the oxidation of hydrothermally derived Fe(II) and  $\text{H}_2\text{S}$  in the photic zone to sulfate and Fe(III) by GSB and GNSB, respectively, facilitated the activities of already evolved anaerobic sulfate- as well as Fe(III)-respiring bacteria in deeper layers of the water column. Chemoorganotrophic metabolisms were further facilitated by the formation of organic carbon by  $\text{CO}_2$  fixation driven by oxygenic photosynthesis as cyanobacteria likely

evolved around 3.0 Ga (Crowe et al., 2013; Planavsky et al., 2014). However, sulfate reduction rates were quantified to be low but still sufficient to remove all sulfate (<20  $\mu\text{M}$  in mixed layer, <0.1  $\mu\text{M}$  in bottom layer) in the water column of Lake Matano. Unlike Lake Matano, Lake La Cruz and Lake Vechten, the microbial community in Lake Pavin consists mainly of methylotrophs and microaerophilic Fe(II)-oxidizers in upper water layers whereas methanogens and Fe(III)-reducers dominate the monimolimnion (Lehours et al., 2005).

### **Alternative field sites for studying Archean and Proterozoic ocean conditions**

In addition to the five lakes described above, there are two examples of ferruginous lakes that have not been very well studied with respect to their biogeochemical properties so far but also provide conditions similar to those described for the other five lakes: Brownie Lake in Minnesota, USA (N44° 58' 4.483" W93° 19' 26.677") (Myrbo, 2011; Swain, 1984), and Canyon Lake in Michigan, USA (N46° 49' 58.069" W87° 55' 14.858") (Anderson-Carpenter, 2011; Davis, 2011; Smith, 1940). These lakes are redox-stratified and host ferruginous conditions with Fe(II) concentrations of 1500  $\mu\text{M}$  in Brownie Lake and 857  $\mu\text{M}$  in Canyon Lake, respectively. Both lakes are small with maximum depths of ~15 and ~25 m, respectively, compared to the well studied field sites Lake Matano and Lake Pavin.

**Tab. 2:** Comparison of five holo- or meromictic lakes regarding their physical and chemical properties.

	<b>L. Matano</b>		<b>L. Pavin</b>		<b>L. La Cruz</b>		<b>L. Nordbytjernet</b>		<b>L. Vechten</b>	
<b>Stratification</b>	meromixis <sup>1</sup>		meromixis <sup>5</sup>		meromixis <sup>8</sup>		meromixis <sup>9</sup>		monomixis <sup>10</sup>	
<b>Layer</b>	oxic	anoxic	oxic	anoxic	oxic	anoxic	oxic	anoxic	oxic	anoxic
<b>Depth [m]</b>	0-120 <sup>1</sup>	120-590 <sup>1</sup>	0-60 <sup>5</sup>	61-92 <sup>5</sup>	0-12/18 <sup>8</sup>	12/18-24.5 <sup>8</sup>	0-18/21 <sup>9</sup>	18/21-23 <sup>9</sup>	0-6 <sup>10</sup>	6/7-11.9 <sup>10</sup>
<b>Fe(II) [μM]</b>	0 <sup>1</sup>	140 <sup>1</sup>	0 <sup>5</sup>	>1200 <sup>5</sup>	0-10 <sup>8</sup>	10-1000 <sup>8</sup>	< 0.5 <sup>9</sup>	714 <sup>9</sup>	0 <sup>10</sup>	690 <sup>10</sup>
<b>Mn<sup>2+</sup> [μM]</b>	0.45 <sup>2</sup>	9.5 <sup>3</sup>	<27 <sup>5</sup>	<7 <sup>5</sup>	n.a.	n.a.	0.7 <sup>9</sup>	1180 <sup>9</sup>	0 <sup>10</sup>	180 <sup>10</sup>
<b>PO<sub>4</sub><sup>3-</sup> [μM]</b>	< 0.025 <sup>1</sup>	9 <sup>1</sup>	0 <sup>5</sup>	340 <sup>5</sup>	0.1 <sup>8</sup>	52.6 <sup>8</sup>	0 <sup>9</sup>	1130 <sup>9</sup>	52 - 104 <sup>10</sup>	20 <sup>10</sup>
<b>SO<sub>4</sub><sup>2-</sup> [μM]</b>	< 20 <sup>1</sup>	< 0.1 <sup>1</sup>	< 20 <sup>6</sup>	0 <sup>6</sup>	31.2 <sup>8</sup>	20.8 <sup>8</sup>	416 <sup>9</sup>	0 <sup>9</sup>	400 <sup>10</sup>	20 <sup>10</sup>
<b>S<sup>2-</sup> [μM]</b>	0 <sup>1</sup>	< 0.2 <sup>1</sup>	0 <sup>6</sup>	< 16.7 <sup>6</sup>	1-3 <sup>8</sup>	>15 <sup>8</sup>	n.a.	n.a.	n.a.	<1000 <sup>10</sup>
<b>Mo [μM]</b>	n.a.	n.a.	> 0.4 <sup>5</sup>	< 0.8 <sup>5</sup>	n. a.	n. a.	n.a.	n.a.	n.a.	n.a.
<b>Cr [μM]</b>	~0.18 <sup>3</sup>	<0.03 <sup>3</sup>	n.a.	n.a.	n. a.	n. a.	n.a.	n.a.	n.a.	n.a.
<b>SiO<sub>2(aq)</sub> [μM]</b>	300 <sup>1</sup>	420 <sup>1</sup>	0 <sup>5</sup>	1100 <sup>5</sup>	10.4 <sup>8</sup>	1178.6 <sup>8</sup>	<107.1 <sup>9</sup>	500 <sup>9</sup>	3.6 - 17.9 <sup>10</sup>	n.a.
<b>pH</b>	8.6 <sup>1</sup>	7.0 <sup>1</sup>	6.2 - 8.5 <sup>7</sup>	6.0-6.2 <sup>7</sup>	8.3-8.7 <sup>8</sup>	6.6-7.5 <sup>8</sup>	7.0-8.2 <sup>9</sup>	7.0-7.9 <sup>9</sup>	6.3-7.2 <sup>10</sup>	6.1-6.3 <sup>10</sup>
<b>T [°C]</b>	25-28 <sup>1</sup>	25-28 <sup>1</sup>	<17 <sup>7</sup>	<6 <sup>7</sup>	6-24 <sup>8</sup>	6-6.2 <sup>8</sup>	3.6-22 <sup>9</sup>	3.7-3.9 <sup>9</sup>	20-24 <sup>10</sup>	4-5 <sup>10</sup>

n.a. = not available

<sup>1</sup> Crowe et al. (2008b)

<sup>2</sup> Crowe et al. (2011)

<sup>3</sup> Crowe et al. (2008c)

<sup>4</sup> Crowe et al. (2008a)

<sup>5</sup> Busigny et al. (2014)

<sup>6</sup> Bura-Nakic et al. (2009)

<sup>7</sup> Cosmidis et al. (2014)

<sup>8</sup> Rodrigo et al. (2001)

<sup>9</sup> Hongve (1994)

<sup>10</sup> Riera (1988)

Furthermore, there are lakes with sulfidic bottom layers such as Green Lake in New York (United States, N43° 3' 5.965" W75° 57' 57.226") (Suits and Wilkin, 1998) and Lago Di Cadagno in the Swiss Alps (N46° 33' 2.246" E8° 42' 42.923") (Canfield et al., 2010), which both are not ferruginous since dissolved Fe(II) readily is scavenged by the sulfide and precipitates in form of iron sulfides in the water column. However, both lakes are subject of research projects already and contributed to the reconstruction of the ancient microbial sulfur cycle by analyses of the sulfur isotope compositions and contributions of microbial activities to the specific fractionation patterns (Canfield et al., 2010; Suits and Wilkin, 1998). Nevertheless, it remains unknown to which extent the iron cycle is coupled to the sulfur cycle in habitats that contain both Fe- and S-species, including questions on how bacterial abundances are spatially and temporally distributed and on which levels respective types of bacteria interact or compete for certain electron donors (Fe(II), sulfide, organic C) and electron acceptors (Fe(III), sulfate, nitrate). Since the holomictic Lake Vechten provides the presence of both, reduced Fe- and S-species at the same time, its investigation as modern model for Proterozoic oceans could improve our understanding of early biogeochemical Fe- and S-turnover and the coupling of these two cycles remarkably. One of the future challenges will be to find further habitats that are rich in Fe and S to evaluate and verify the observations from Lake Vechten. Such Fe- and S-rich habitats do not necessarily need to be stratified lakes but simply have to provide the simultaneous presence of dissolved Fe(II) and sulfide. One example for such a habitat is the Arvadi Spring, located in the higher Engadin window of the eastern Swiss Alps (N46° 40' 14.074" E9° 39' 52.956") within the Albula valley in the Canton of Grisons (Strauss et al., 2015). As one of several sulfur-containing springs of the area, the Arvadi spring stands out from the other springs by the presence of Fe- and S-species at tens of  $\mu\text{M}$  concentrations at the same time. Waters from two separate springs, namely the sulfide-containing Zuelper spring and a Fe(II)-containing spring, is mixed, resulting in the mixed Arvadi Spring water (Koeksoy, unpublished data). The spring is characterized by a distinct smell of sulfide and sediments of reddish colour, indicating the presence of Fe(III) (oxyhydr)oxides, covered with whitish flocks consisting probably of elemental sulfur (Fig. 4). Additionally, whitish biofilms cover parts of the spring sediment and most probably



contain sulfide-oxidizing bacteria such as *Thiothrix* spp. that store  $S^0$  in their cells (Kurt Hanselmann, personal communication). Identification of the  $S^0$  sulfur isotopic composition revealed a depletion in  $^{34}S$  with  $\delta^{34}S$  values between -26 to -23‰, suggesting dissolved sulfide to be generated by microbial reduction of sulfate that was quantified at high concentrations up to 10.4 mM (Strauss et al., 2015). The source of sulfate is assumed to be the dissolution of evaporitic gypsum that is overlain by the Silvretta nappe crystalline rocks on which the Albula valley is based on. Associated with a minor isotope effect, microbial oxidation of sulfide is suggested to occur at the oxic-anoxic redox boundary, also being the likely source of  $S^0$  flocks (Strauss et al., 2015). The spring is currently evaluated for its suitability as Proterozoic ocean model by the identification of its microbial community and geochemical composition and promises a high chance to achieve a better understanding of Proterozoic FeS biogeochemistry. First results of Most Probable Number (MPN) studies on sediment samples from the spring identified microaerophiles to be the most abundant Fe- and S-metabolizing bacteria (Koeksoy and Kappler, unpublished data) which is in accordance to what is assumed for the Proterozoic ocean due to the formation of a redox transition zone in surface water layers after the GOE. As the oxygen content of the spring water is high being close to saturation of 100%, anaerobic phototrophic and chemolithotrophic Fe- and S-metabolizing bacteria were quantified at lower cell numbers and thus are concluded to colonize only deeper and thus oxygen-depleted layers of the spring sediment. Further evaluation of microbial activities and interactions are ought to be identified with current experiments with the major goal of gaining a better understanding of spatial and temporal interactions of the Fe- and S-cycles on the microbial as well the geochemical levels.



**Fig. 4:** The Fe- and S-rich Arvadi Spring, located in the eastern Swiss Alps. Photograph was taken in February 2014. A Front view of the spring with the spring pond in the back and creek outflow. B View on the spring front from the top. The white S<sub>0</sub> flocks are distributed all over the spring pond, overlaying reddish Fe(III) minerals in the spring sediment. C White biofilms of *Thiobacillus* like bacteria sticking to stones at the creek outflow are a strong indication for the presence of sulfide-oxidizing bacteria in the spring. D Spring creek flows downwards into forest.

## Outlook and future research needs

The investigation of Precambrian environment-biosphere feedback systems to understand BIF deposition relies largely on circumstantial evidence to piece together an accurate picture of the functioning of ancient marine ecosystems. Our research approach must necessarily be multidisciplinary in this regard. While information obtained from the Precambrian rock record of banded iron formations sets the relevant geochemical parameters and laboratory experiments allow us to manipulate conditions in order to observe the effect of a set number of variables on processes relevant for BIF deposition, modern environments act as natural laboratories allowing us to observe the processes relevant for BIF deposition in situ. Therefore, there is need for well-suited natural habitats that provide conditions similar to

those on ancient Earth. Limited by the presence of specific features such as anoxic conditions as well as the presence of high Fe(II) concentrations, only a handful of lakes make suitable models for the ancient ocean. The two lakes that are currently used as modern analogues namely Lake Matano and Lake Pavin, are good but maybe not ideal, since they are diverging from estimated ancient seawater conditions in some aspects, such as high phosphate concentrations as well as probably too high Fe(II) concentrations relative to estimated ranges of respective compounds in Archean seawater. Alternatively, potential is hidden in Lake Vechten, Lake Nordbytjernet, Brownie Lake, and Canyon Lake, all ferruginous lakes that were not considered enough as model habitats so far. These lakes could be examined in more detail in the future, in order to compile insights comparable to those gained in the numerous studies of Lake Matano and Lake Pavin. The main challenge of our scientific community still is to find alternative habitats that also provide appropriate, and ideally, optimal conditions with parameters within the ranges delineated by the Precambrian rock record. However, more important than evaluating each habitat as a individual model for the ancient ocean is to connect the different aspects that we attain from each habitat and to transfer them to our current models of the Precambrian oceans and their biogeochemical processes. As there will never be the perfect model field site and as our view on ancient ocean conditions changes constantly, we will benefit most by answering different questions by using appropriate individual model habitats.

### **Acknowledgements**

The authors would like to thank H. Strauss (Muenster), K. Hanselmann (Zuerich) and R. Schoenberg/G. Albut (Tuebingen) for our collaboration studying the Arvadi spring. E.K. and M.H. are supported by the German Research Foundation (DFG) grants KA 1736/24-1 and KA1736/27-1. We also would like to thank A. Mloszewska for helpful comments and manuscript revisions.

## REFERENCES

- Aeschbach-Hertig W, Hofer M, Schmid M, Kipfer R, and Imboden DM. (2002) The physical structure and dynamics of a deep, meromictic crater lake (Lac Pavin, France). *Hydrobiologia*, 487: 111-136.
- Andersson C. (1997) Transfer function vs. modern analog technique for estimating Pliocene sea-surface temperatures based on planktic foraminiferal data, western equatorial Pacific Ocean. *Journal of Foraminiferal Research*, 27: 123-132.
- Assayag N, Jezequel D, Ader M, Viollier E, Michard G, Prevot F, and Agrinier P. (2008) Hydrological budget, carbon sources and biogeochemical processes in Lac Pavin (France): Constraints from delta O-18 of water and delta C-13 of dissolved inorganic carbon. *Applied Geochemistry*, 23: 2800-2816.
- Bachan, A. and L.R. Kump (2015) The rise of oxygen and siderite oxidation during the Lomagundi Event. *Proceedings of the National Academy of Sciences*, 112: p. 6562-6567.
- Bjerrum CJ, and Canfield DE. (2002) Ocean productivity before about 1.9 Gyr ago limited by phosphorus adsorption onto iron oxides. *Nature*, 417: 159-162.
- Blankenship RE. (1992) Origin and early evolution of photosynthesis. *Photosynthesis Research*, 33: 91-111.
- Boehrer B, and Schultze M. (2008) Stratification of lakes. *Reviews of Geophysics*, 46.
- Brocks JJ, Love GD, Summons RE, Knoll AH, Logan GA, and Bowden SA. (2005) Biomarker evidence for green and purple sulphur bacteria in a stratified Palaeoproterozoic sea. *Nature*, 437: 866-870.
- Bura-Nakic E, Viollier E, Jezequel D, Thiam A, and Ciglenecki I. (2009) Reduced sulfur and iron species in anoxic water column of meromictic crater Lake Pavin (Massif Central, France). *Chemical Geology*, 266: 311-317.
- Busigny V, Planavsky NJ, Jezequel D, Crowe S, Louvat P, Moureau J, Viollier E, and Lyons TW. (2014) Iron isotopes in an Archean ocean analogue. *Geochimica et Cosmochimica Acta*, 133: 443-462.
- Canfield DE. (1998) A new model for Proterozoic ocean chemistry. *Nature*, 396: 450-453.
- Canfield DE, and Raiswell R. (1999) The evolution of the sulfur cycle. *American Journal of Science*, 299: 697-723.
- Canfield DE. (2005) The early history of atmospheric oxygen: homage to Robert M. Garrels. *Annual Review of Earth and Planetary Sciences*, 33: 1-36.
- Canfield DE, Farquhar J, and Zerkle AL. (2010) High isotope fractionations during sulfate reduction in a low-sulfate euxinic ocean analog. *Geology*, 38: 415-418.

- Cloud P. (1973) Paleocological Significance of the Banded Iron-Formation. *Economic Geology*, 68: 1135-1143.
- Cosmidis J, Benzerara K, Morin G, Busigny V, Lebeau O, Jezequel D, Noel V, Dublet G, and Othmane G. (2014) Biomineralization of iron-phosphates in the water column of Lake Pavin (Massif Central, France). *Geochimica et Cosmochimica Acta*, 126: 78-96.
- Craddock PR, and Dauphas N. (2011). Iron and carbon isotope evidence for microbial iron respiration throughout the Archean. *Earth and Planetary Science Letters*, 303(1): 121-132.
- Crowe SA, Fowle DA, Katsev S, Sundby B, Mucci A, and Haffner GD. (2008a) Geochemistry of Mo in a modern Archean ocean analogue. *Geochimica et Cosmochimica Acta*, 72: A190-A190.
- Crowe SA, Jones C, Katsev S, Magen C, O'Neill AH, Sturm A, Canfield DE, Haffner GD, Mucci A, Sundby B and others. (2008b) Photoferrotrophs thrive in an Archean Ocean analogue. *Proceedings of the National Academy of Sciences of the United States of America*, 105: 15938-15943.
- Crowe SA, O'Neill AH, Katsev S, Hehanussa P, Haffner GD, Sundby B, Mucci A, and Fowle DA. (2008c) The biogeochemistry of tropical lakes: A case study from Lake Matano, Indonesia. *Limnology and Oceanography*, 53: 319-331.
- Crowe SA, Katsev S, Leslie K, Sturm A, Magen C, Nomosatryo S, Pack MA, Kessler JD, Reeburgh WS, Roberts JA and others. (2011) The methane cycle in ferruginous Lake Matano. *Geobiology*, 9: 61-78.
- Crowe SA, Dossing LN, Beukes NJ, Bau M, Kruger SJ, Frei R, and Canfield DE. (2013) Atmospheric oxygenation three billion years ago. *Nature*, 501: 535-538.
- Crowe SA, Paris G, Katsev S, Jones C, Kim S-T, Zerkle AL, Nomosatryo S, Fowle DA, Adkins JF, and Sessions AL. (2014a) Sulfate was a trace constituent of Archean seawater. *Science*, 346: 735-739.
- Czaja AD, Johnson CM, Beard BL, Roden EE, Li W, and Moorbath S. (2013) Biological Fe oxidation controlled deposition of banded iron formation in the ca. 3770 Ma Isua Supracrustal Belt (West Greenland). *Earth and Planetary Science Letters*, 363: 192-203.
- Davis MB. (1981) Outbreaks of forest pathogens in Quaternary history. *Proceedings of the IV International Palynological Conference, Lucknow*, 3: 216-226.
- DeMaster DJ, Leynaert A, and Queguiner B. (1995) The silica balance in the world ocean: a reestimate. *Science*, 268: 375-379.
- Drever JL. (1997) *The Geochemistry of Natural Waters*. Prentice-Hall International.
- Eickhoff M, Obst M, Schröder C, Hitchcock AP, Tyliczszak T, Martinez RE, Robbins LJ, Konhauser KO and Kappler A. (2014) Nickel partitioning in biogenic and abiogenic ferrihydrite: The influence of silica and implications for

- ancient environments. *Geochimica et Cosmochimica Acta*, 140: 65-79.
- Gole MJ, and Klein C. (1981) Banded iron-formations through much of the Precambrian time. *The Journal of Geology*, 169-183.
- Grotzinger JP, and Kasting JF. (1993) New constraints on Precambrian ocean composition. *The Journal of Geology*: 235-243.
- Habicht KS, Gade M, Thamdrup B, Berg P, and Canfield DE. (2002) Calibration of sulfate levels in the Archean ocean. *Science*, 298:2372-2374.
- Holland HD. (1973) The oceans; a possible source of iron in iron-formations. *Economic Geology*, 68: 1169-1172.
- Holland HD. (2006) The oxygenation of the atmosphere and oceans. *Philosophical Transactions of the Royal Society B-Biological Sciences*, 361: 903-915.
- Holm NG. (1989) The  $^{13}\text{C}/^{12}\text{C}$  ratios of siderite and organic matter of a modern metalliferous hydrothermal sediment and their implications for banded iron formations. *Chemical Geology*, 77: 41-45.
- Hongve D. (1994) Nutrient Metabolism (C, N, P, and Si) in the Trophogenic Zone of a Meromictic Lake. *Hydrobiologia*, 277: 17-39.
- Hongve D. (2003) Chemical stratigraphy of recent sediments from a depth gradient in a meromictic lake, Nordbytjernet, SE Norway, in relation to variable external loading and sedimentary fluxes. *Journal of Paleolimnology*, 30: 75-93.
- Johnson CM, Beard BL, and Roden EE. (2008) The Iron Isotope Fingerprints of Redox and Biogeochemical Cycling in Modern and Ancient Earth. *Annual Review of Earth and Planetary Sciences*, 36: 457-493.
- Jorgensen BB. (1982) Mineralization of Organic-Matter in the Sea Bed - the Role of Sulfate Reduction. *Nature*, 296: 643-645.
- Kappler A, Pasquero C, Konhauser KO, and Newman DK. (2005) Deposition of banded iron formations by anoxygenic phototrophic Fe(II)-oxidizing bacteria. *Geology*, 33: 865-868.
- Klein C, and Beukes NJ. (1992) Time distribution, stratigraphy, and sedimentologic setting, and geochemistry of Precambrian iron-formations. *The Proterozoic biosphere: A multidisciplinary study*. 139-146.
- Klein C. (2005) Some Precambrian banded iron-formations (BIFs) from around the world: Their age, geologic setting, mineralogy, metamorphism, geochemistry, and origin. *American Mineralogist*. 90: 1473-1499.
- Köhler I, Konhauser KO, Papineau D, Bekker A, and Kappler A. (2013) Biological carbon precursor to diagenetic siderite with spherical structures in iron formations. *Nature Communication*, 4: 1741.
- Konhauser KO, Hamade T, Raiswell R, Morris RC, Ferris FG, Southam G, and Canfield DE. (2002) Could bacteria have formed the Precambrian banded iron formations? *Geology*, 30: 1079-1082.

- Konhauser KO, Newman DK, and Kappler A. (2005) The potential significance of microbial Fe(III) reduction during deposition of Precambrian banded iron formations. *Geobiology*, 3: 167-177.
- Konhauser KO, Lalonde SV, Amskold L, and Holland HD. (2007) Was there really an Archean phosphate crisis? *Science*, 315: 1234-1234.
- Konhauser KO, Pecoits E, Lalonde SV, Papineau D, Nisbet EG, Barley ME, Arndt NT, Zahnle K, and Kamber BS. (2009) Oceanic nickel depletion and a methanogen famine before the Great Oxidation Event. *Nature*, 458: 750-753.
- Lehours AC, Bardot C, Thenot A, Debroas D, and Fonty G. (2005) Anaerobic microbial communities in Lake Pavin, a unique meromictic lake in France. *Applied and Environmental Microbiology*, 71: 7389-7400.
- Lehours AC, Evans P, Bardot C, Joblin K and Gérard F. (2007) Phylogenetic Diversity of Archea and Bacteria in the Anoxic Zone of a Meromictic Lake (Lake Pavin, France). *Applied and Environmental Microbiology*, 73: 2016-2019.
- Maliva RG, Knoll AH, and Simonson BM. (2005) Secular change in the Precambrian silica cycle: Insights from chert petrology. *Geological Society of America Bulletin*, 117: 835-845.
- Michard G, Viollier E, Jézéquel D, and Sarazin G. (1994) Geochemical study of a crater lake: Pavin Lake, France—identification, location and quantification of the chemical reactions in the lake. *Chemical Geology*, 115: 103-115.
- Mloszewska AM, Pecoits E, Cates NL, Mojzsis SJ, O'Neil J, Robbins LJ, and Konhauser KO. (2012) The composition of Earth's oldest iron formations: the Nuvvuagittuq Supracrustal Belt (Québec, Canada). *Earth and Planetary Science Letters*, 317: 331-342.
- Morris RC. (1993) Genetic modelling for banded iron-formation of the Hamersley Group, Pilbara Craton, Western Australia. *Precambrian Research*, 60: 243-286.
- Myrbo A, Murphy M and Stanley V. (2011) The Minneapolis Chain of Lakes by bicycle: Glacial history, human modifications, and paleolimnology of an urban natural environment. *Field Guides*, 24: 425-437.
- Parmar N, Gorby YA, Beveridge TJ, and Ferris FG. (2001) Formation of green rust and immobilization of nickel in response to bacterial reduction of hydrous ferric oxide. *Geomicrobiology Journal*, 18: 375-385.
- Partin CA, Lalonde SV, Planavsky NJ, Bekker A, Rouxel OJ, Lyons TW, and Konhauser KO. (2013) Uranium in iron formations and the rise of atmospheric oxygen. *Chemical Geology*. 362: 82-90.
- Pecoits E, Smith ML, Catling DC, Philippot P, Kappler A, and Konhauser KO. (2015) Atmospheric hydrogen peroxide and Eoarchean iron formations. *Geobiology*, 13: 1-14.

- Pfennig N, and Cohenbaz.G. (1967) Some Properties of Green Bacterium *Pelodictyon Clathratiforme*. *Archiv für Mikrobiologie*, 59: 226-236.
- Planavsky NJ, Reinhard CT, Wang X, Thomson D, McGoldrick P, Rainbird RH, Johnson T, Fischer WW, and Lyons TW. (2014) Low Mid-Proterozoic atmospheric oxygen levels and the delayed rise of animals. *Science*, 346: 635-638.
- Planavsky, N.J., Bekker, A., Hofmann, A., Owens J.D. and Lyons, T.W. (2012) Sulfur record of rising and falling marine oxygen and sulfate levels during the Lomagundi event. *Proceedings of the National Academy of Sciences*, 109: p. 18300-18305.
- Posth NR, Hegler F, Konhauser KO, and Kappler A. (2008) Alternating Si and Fe deposition caused by temperature fluctuations in Precambrian oceans. *Nature Geoscience*, 1: 703-708.
- Posth NR, Köhler I, D. Swanner ED, Schröder C, Wellmann E, Binder B, Konhauser KO, Neumann U, Berthold C, Nowak M and others. (2013a) Simulating Precambrian banded iron formation diagenesis. *Chemical Geology*, 362: 66-73.
- Posth NR, Konhauser KO, and Kappler A. (2013b) Microbiological processes in banded iron formation deposition. *Sedimentology*, 60: 1733-1754.
- Posth NR, Canfield DE, and Kappler A. (2014) Biogenic Fe(III) minerals: From formation to diagenesis and preservation in the rock record. *Earth-Science Reviews*, 135: 103-121.
- Rasmussen B, Krapež B, and Muhling JR. (2015) Seafloor silicification and hardground development during deposition of 2.5 Ga banded iron formations. *Geology*, 43: 235-238.
- Reinhard, C.T., Planavsky, N.J., Robbins, L.J., Partin, C.A., Gill, B.C., Lalonde S.V., Bekker, A., Konhauser, K.O. and Lyons, T.W. (2013) Proterozoic ocean redox and biogeochemical stasis. *Proceedings of the National Academy of Sciences*, 110: p. 5357-5362.
- Riera XG, Garcia-Gil, L. J., Abella, C. A. (1988) Lake Vechten, Schleinsee and Buchensee as examples of west central european holomictic lakes containing phototrophic bacteria. *SCIENTIA gerundensis*, 14: 57-69.
- Robbins LJ, Lalonde S, Saito MA, Planavsky N, Mloszewska A, Pecoits E, Scott C, Dupont C, Kappler A, and Konhauser K. (2013) Authigenic iron oxide proxies for marine zinc over geological time and implications for eukaryotic metallome evolution. *Geobiology*, 11: 295-306.
- Robbins LJ, Swanner ED, Lalonde SV, Eickhoff M, Paranich ML, Reinhard CT, Peacock CL, Kappler A, and Konhauser KO. (2015) Limited Zn and Ni mobility during simulated iron formation diagenesis. *Chemical Geology*, 402: 30-39.
- Rodrigo M, Vicente E, and Miracle M. (1993) Short-term calcite precipitation in the karstic meromictic Lake La Cruz (Cuenca, Spain). *Internationale Vereinigung für Theoretische und Angewandte Limnologie Verhandlungen*, 25: 711-719.



- Rodrigo MA, Vicente E, and Miracle MR. (2000) The role of light and concentration gradients in the vertical stratification and seasonal development of phototrophic bacteria in a meromictic lake. *Archiv für Hydrobiologie*, 148: 533-548.
- Rodrigo MA, Miracle MR, and Vicente E. (2001) The meromictic Lake La Cruz (Central Spain). Patterns of stratification. *Aquatic Sciences*, 63: 406-416.
- Romero-Viana L, Julia R, Camacho A, Vicente E, and Miracle MR. (2008) Climate signal in varve thickness: Lake La Cruz (Spain), a case study. *Journal of Paleolimnology*, 40: 703-714.
- Romero-Viana L, Keely BJ, Camacho A, Vicente E, and Miracle MR. (2010) Primary production in Lake La Cruz (Spain) over the last four centuries: reconstruction based on sedimentary signal of photosynthetic pigments. *Journal of Paleolimnology*, 43: 771-786.
- Sadler PM. (1981) Sediment Accumulation Rates and the Completeness of Stratigraphic Sections. *Journal of Geology*, 89: 569-584.
- Saito MA, Sigman DM, and Morel FMM. (2003) The bioinorganic chemistry of the ancient ocean: the co-evolution of cyanobacterial metal requirements and biogeochemical cycles at the Archean-Proterozoic boundary? *Inorganica Chimica Acta*, 356: 308-318.
- Siever R. (1992) The silica cycle in the Precambrian. *Geochimica et Cosmochimica Acta*, 56: 3265-3272.
- Steenbergen CLM, and Korthals HJ. (1982) Distribution of Phototropic Microorganisms in the Anaerobic and Microaerophilic Strata of Lake Vechten (the Netherlands) - Pigment Analysis and Role in Primary Production. *Limnology and Oceanography*, 27: 883-895.
- Steenbergen CLM, and Verdouw H. (1982) Lake Vechten - Aspects of Its Morphometry, Climate, Hydrology and Physicochemical Characteristics. *Hydrobiologia*, 95: 11-23.
- Smith LLJR. (1940) A limnological investigation of a permanently stratified lake in the Huron Mountain region of northern Michigan. *Papers of the Michigan Academy of Science Arts and Letters*. 26: 3-9.
- Strauss H, Chmiel H, Christ A, Fugmann A, Hanselmann K, Kappler A, Königer P, Lutter A, Siedenberg K, and Teichert BM. (2015) Multiple sulphur and oxygen isotopes reveal microbial sulphur cycling in spring waters in the Lower Engadin, Switzerland. *Isotopes in environmental and health studies*: 1-19.
- Suits NS, and Wilkin RT. (1998) Pyrite formation in the water column and sediments of a meromictic lake. *Geology*, 26: 1099-1102.
- Sun S, Konhauser KO, Kappler A, and Li Y-L. (2015) Primary hematite in Neoproterozoic to Paleoproterozoic oceans. *Geological Society of America Bulletin*, 127: 850-861.
- Swain EB. (1984) The paucity of blue-green algae in meromictic Brownie Lake: iron-limitation or heavy-metal

- toxicity [Ph.D. thesis]. *Minneapolis, University of Minnesota*, 362 p.
- Vangemerden H. (1984) The Sulfide Affinity of Phototrophic Bacteria in Relation to the Location of Elemental Sulfur. *Archives of Microbiology*, 139: 289-294.
- Verdouw H, and Dekkers EMJ. (1980) Iron and Manganese in Lake Vechten (the Netherlands) - Dynamics and Role in the Cycle of Reducing Power. *Archiv für Hydrobiologie*, 89: 509-532.
- Walker JCG. (1984) Suboxic diagenesis in banded iron formations. *Nature*, 309: 340-342.
- Widdel F, Schnell S, Heising S, Ehrenreich A, Assmus B, and Schink B. (1993) Ferrous iron oxidation by anoxygenic phototrophic bacteria. *Nature*, 362: 834-836.
- Woese CR. (1987) Bacterial evolution. *Microbiological Review*, 51: 221-271.
- Wu W, Swanner ED, Hao L, Zeitvogel F, Obst M, Pan Y, and Kappler A. (2014) Characterization of the physiology and cell-mineral interactions of the marine anoxygenic phototrophic Fe(II) oxidizer *Rhodovulum iodolum*-implications for Precambrian Fe(II) oxidation. *FEMS Microbiol Ecol*, 88: 503-515.
- Zegeye A, Ruby C, and Jorand F. (2007) Kinetic and thermodynamic analysis during dissimilatory gamma-FeOOH reduction: Formation of green rust 1 and magnetite. *Geomicrobiology Journal*, 24: 51-64.
- Zegeye A, Bonneville S, Benning LG, Sturm A, Fowle DA, Jones C, Canfield DE, Ruby C, MacLean LC, Nomosatryo S and others. (2012) Green rust formation controls nutrient availability in a ferruginous water column. *Geology*, 40: 59

## OPEN QUESTION AND OBJECTIVES OF THIS STUDY

Deciphering the geochemical and biological constraints in ferro-euxinic transition zones of oxygenated ancient oceans is inevitable to improve our understanding of the factors that on the one hand controlled biogeochemical stasis during the mid-Proterozoic and on the other hand triggered the diversification of the biosphere towards the Neoproterozoic-Cambrian boundary. Many questions regarding the composition of these complex and highly dynamic settings remain unsolved, including the actual areal extent of Fe(II)-rich versus sulfidic waters and factors that controlled their formation and extension. More specifically, the identity of Fe- and S-minerals that potentially co-precipitated from ferro-euxinic waters are of particular interest with respect to their role as precursor minerals in Banded Iron Formations and Black Shales. Furthermore, the response of the existing microbial community (that presumably consisted largely of Fe-metabolizers) to increasing sulfate levels and thereby triggered sulfate reduction rates and elevated sulfide concentrations requires elucidation. Especially their potential co-existence with emerging S-metabolizers and their competition for habitable niches and electron donors and acceptors needs to be deciphered.

These questions can partially be answered by analyzing the rock record, but based on its incomplete and partly diagenetically altered nature, additional verification from alternative approaches such as simulation-based laboratory and modeling experiments is required. The presented work in this thesis addressed the above described questions by the use of a modern model habitat for ferro-euxinic transition zones of ancient oceans, i.e. the Arvadi Spring. For the purpose of our goals, the objectives that we addressed as part of this thesis were:

- to evaluate the suitability of the Arvadi Spring as a modern model habitat for late Archean and Proterozoic ferro-euxinic ocean transition zones through a detailed geochemical characterization of the spring water. **Chapter 2** gives an overview about the geochemical composition of the Arvadi Spring water and compares its properties to ancient ocean conditions.

- to understand and evaluate the composition of ferro-euxinic ocean transition zones, specifically focussing on the equilibrium between dissolved Fe(II) and sulfide. While **Chapter 2** shows a detailed overview on the geochemical composition of the Arvadi Spring water, the mineral saturation index for Fe(II) sulfide and reasons for Fe(II) sulfide precipitation in the Arvadi Spring are elucidated in **Chapter 3**.
- to identify the composition, speciation and relative abundance of Arvadi Spring minerals, especially with regard to gaining insights on the identity of precursor minerals for Banded Iron Formation and Black Shale deposition. **Chapter 3** focusses on the Fe- and S-mineralogy in Arvadi Spring precipitates and discusses potential mineral formation mechanisms.
- to identify the microbial community composition, morphology, structure, relative abundance and activity, with the role of Fe- and S-metabolizing microorganisms being highlighted, which is discussed in **Chapter 2 and Chapter 4**.
- to assess the relative contribution of abiotic and biotic Fe- and S-redox transformations during different periods of ocean oxygenation based on the knowledge obtained from the Arvadi spring. All chapters included in this thesis comprise an implications part in which the specific results are integrated into currently existing models of biogeochemical Fe-S-cycling in ferro-euxinic transition zones of ancient oceans.

## CHAPTER 2

# **A case study for late Archean and Proterozoic biogeochemical iron- and sulphur-cycling in a modern habitat – the Arvadi Spring**

Elif Koeksoy<sup>1</sup>, Maximilian Halama<sup>1</sup>, Nikolas Hagemann<sup>1</sup>, Pascal R. Weigold<sup>1</sup>, Katja Laufer<sup>1,6</sup>,  
Sara Kleindienst<sup>1</sup>, James M. Byrne<sup>1</sup>, Anneli Sundman<sup>1</sup>, Kurt Hanselmann<sup>2</sup>, Itay Halevy<sup>3</sup>,  
Ronny Schoenberg<sup>4</sup>, Kurt O. Konhauser<sup>5</sup> and Andreas Kappler<sup>1,6\*</sup>

<sup>1</sup>Geomicrobiology, Center for Applied Geosciences, University of Tuebingen, Germany

<sup>2</sup>Geological Institute, ETH Zuerich, Switzerland

<sup>3</sup>Earth and Planetary Sciences, Weizmann Institute of Science, Israel

<sup>4</sup>Isotope Geochemistry, University of Tuebingen, Germany

<sup>5</sup> Earth and Atmospheric Sciences, University of Alberta, Canada

<sup>6</sup>Bioscience, Center for Geomicrobiology, Aarhus University, Denmark

Accepted for publication in: *Geobiology*

## Abstract

As a consequence of Earth's surface oxygenation, ocean geochemistry changed from ferruginous (iron(II)-rich) into more complex ferro-euxinic (iron(II)-sulphide-rich) conditions during the Paleoproterozoic. This transition must have had profound implications for the Proterozoic microbial community that existed within the ocean water and bottom sediment; in particular iron-oxidizing bacteria likely had to compete with emerging sulphur-metabolizers. However, the nature of their co-existence and interaction remains speculative. Here we present geochemical and microbiological data from the Arvadi Spring in the eastern Swiss Alps, a modern model habitat for ferro-euxinic transition zones in late Archean and Proterozoic oceans during high-oxygen intervals, which enables us to reconstruct the microbial community structure in respective settings for this geological era. The spring water is oxygen-saturated but still contains relatively elevated concentrations of dissolved iron(II) ( $17.2 \pm 2.8 \mu\text{M}$ ) and sulphide ( $2.5 \pm 0.2 \mu\text{M}$ ) with simultaneously high concentrations of sulphate ( $8.3 \pm 0.04 \text{ mM}$ ). Solids consisting of quartz, calcite, dolomite and iron(III) oxyhydroxide minerals as well as sulphur-containing particles, presumably elemental  $\text{S}^0$ , cover the spring sediment. Cultivation-based most probable number counts revealed microaerophilic iron(II)-oxidizers and sulphide-oxidizers to represent the largest fraction of iron- and sulphur-metabolizers in the spring, co-existing with less abundant iron(III)-reducers, sulphate-reducers and phototrophic and nitrate-reducing iron(II)-oxidizers. 16S rRNA gene 454 pyrosequencing showed sulphide-oxidizing *Thiothrix* species to be the dominating genus, supporting the results from our cultivation-based assessment. Collectively, our results suggest that anaerobic and microaerophilic iron- and sulphur-metabolizers could have co-existed in oxygenated ferro-sulphidic transition zones of the late Archean and Proterozoic ocean, where they would have sustained continuous cycling of iron and sulphur compounds.

## Introduction

Knowing the identity and composition of ancient microbial communities is vital in order to shed light onto the most compelling questions about the history of life, including the impact of rising oxygen levels in Earth's atmosphere and oceans on life's diversification. However, our understanding is incomplete as the remains of ancient metabolisms in the form of microfossils are rarely found in the rock record, and also because the interpretation of chemical fingerprints in ancient rocks is challenging due to diagenetic alteration and/or metamorphic overprinting (Klein, 2005; Koeksoy et al., 2016).

The majority of Precambrian oceans were dominantly anoxic and ferruginous (rich in iron(II) (Poulton & Canfield, 2011)) and the bulk ocean presumably remained like this until the later Neoproterozoic (1.0-0.5 Ga) (Canfield et al., 2008; Planavsky et al., 2011). Hence, iron-metabolizing microorganisms probably played a key role in shaping the Precambrian biogeochemical environment before more complex eukaryotic life forms emerged and diversified. Striking evidence for the existence of such microorganisms early in Earth's history comes from Banded Iron Formations (BIF), sedimentary rocks with a characteristic alternation of iron-rich and silica-rich layers that were deposited throughout the Archean (4.0-2.5 Ga) and Paleoproterozoic (2.5-1.6 Ga) (Bekker et al., 2014; Bekker et al., 2010). For instance, iron-isotope data in early Archean BIFs suggest the prevalence of phototrophic iron(II)-oxidizers by ca. 3.7 Ga (Czaja et al., 2013), while iron and neodymium isotopes together with rare Earth element analyses in late Archean BIFs suggest dissimilatory iron(III)-reducers to have recycled parts of continental iron in coastal sediments by ca. 2.5 Ga (Li et al., 2015; Johnson et al., 2008). Furthermore, microfossil data found in the Nuvvuagittuq supracrustal belt in Quebec, Canada, imply the very early existence of microaerophilic iron(II)-oxidizers already by 3.7 Ga, possibly even by 4.5 Ga (Dodd et al., 2017). Additional microfossil data from the Paleoproterozoic Jhamarkotra Formation, India (Crosby et al., 2014), and iron-isotope data in stromatolites from the Animkie basin of the Gunflint and Biwabik Formations, Canada and USA (Planavsky et al., 2009), indicate respective microorganisms to have flourished in slightly oxic surface zones of the ocean

during high-oxygen intervals. Respective conditions are thought of having been widespread during the late Archean in form of oxygen oases (Olson et al., 2013), during the Paleoproterozoic Great Oxidation Event (GOE) (Holland, 2006), and throughout the Proterozoic (Planavsky et al., 2014; see Lyons et al., 2014 for an overview).

Although these patches of information hint at the establishment of an ancient network of iron-metabolizers on Precambrian Earth, outstanding questions about their spatial distribution, community composition and interplay with metabolically different communities remain unsolved. Especially their response to the expanding sulphate-reducing microbial community in coastal parts of the water column and in underlying sediments as a consequence of the enhanced delivery of dissolved sulphate to neritic ocean regions through increased oxidative weathering of terrestrial pyrite during high-oxygen intervals (Canfield, 1998) is uncertain. As a consequence, the accumulation of euxinic (sulphide-rich) waters by enhanced sulphate reduction rates and their expansion to intermediate-depth ocean regions of high biological productivity (Poulton et al., 2004; Poulton et al. 2010; Canfield, 1998; Reinhard et al., 2009) likely triggered the proliferation of sulphur-oxidizers.

Deciphering the nature of the coexistence of iron- and sulphur-metabolizers in oxygenated ferro-euxinic transition zones of Precambrian oceans is essential to understand the biological and geochemical factors that controlled the extent of euxinic versus ferruginous conditions and that shaped the biogeochemical cycling of redox-active elements, including carbon, oxygen, iron and sulphur. As the available rock record data is insufficient to assemble a complete picture of ancient microbial community structure and activity, an alternative promising approach is the analysis of existing modern habitats that resemble conditions of relevant ancient settings (Koeksoy et al., 2016), such as Lake Matano (Crowe et al., 2008), Lake Pavin (Busigny et al., 2014), Lake La Cruz (Walter et al., 2014) and Kabuno Bay of Lake Kivu (Llirós et al., 2015). Accordingly, we present data from the iron- and sulphur-rich Arvadi Spring in the eastern Swiss Alps, which we posit to simulate the geochemical and microbial composition in shallow ferro-euxinic transition zones of late Archean and Proterozoic oceans during high-oxygen intervals. The main goals of this study were to (1) analyse the geochemical composition of the Arvadi Spring, (2) to identify and quantify the



key players of the iron- and sulphur-metabolizing bacterial communities, and (3) to predict late Archean and Proterozoic ocean geochemical and microbial community composition.

## Materials and Methods

**Field site description.** The highly mineralized Arvadi Spring is located in the Albula valley close to Bad Alvaneu (canton of Grisons, Switzerland) at an altitude of 928 m above sea level (46°40'17.4" N 9°39'18.8"E). It is situated in an alpine orogeny area comprising erosion of the Austroalpine overthrusts and the underlying Penninic rocks. Exposure of Jurassic oceanic crustal rocks and overlying sedimentary rocks resulted in the discharge of deeply circulating waters from lithologically variable rock units. The Arvadi Spring discharges from the crystalline rocks of the Silvretta nappe, which overlays carbonates and evaporitic gypsum, of which the latter is the source of sulphur species in the Arvadi Spring water (Strauss et al., 2016). The contemporaneous presence of both, iron and sulphur species, in the spring water results from a mixture of sulphur-rich water from a sulphide spring with iron-rich water from a second unknown subsurface water source. A scheme of the water flow system is provided in the supplementary information file (Fig. S1). Unfortunately, we had no access to the subsurface sources of the parental waters and hence cannot provide information on their geochemistry. The iron(II) and sulphide content of sulphide- and iron(II)-rich water could be identified, however, at a connection point between the two different sourced waters in a mixing tunnel (CP2, Fig. S1) and were found to be  $13.81 \pm 1.33$   $\mu\text{M}$  and  $8.00 \pm 0.79$   $\mu\text{M}$ , respectively, at full oxygen saturation. From connection point 2 the intermixed water flows ca. 35 m downhill before it crops out into a manmade pond (the Arvadi spring) with a diameter of 3.3 m and a water depth of  $\sim 20$  cm (Fig. 1). From the pond, the water flows into a creek of ca. 13 m length and converges with a second creek at 16.5 m distance from the spring discharge (Fig. 1), which dilutes the Arvadi Spring water. The sediment of the spring pond is completely covered by soft reddish particles, which are overlain partly by fluffy whitish flocs that apparently have a lower density (Fig. 2A, 2B). Rock

surfaces in the spring pond are partly covered by white biofilms with filamentous elongations and partly by orange-brownish biofilm-like crusts. The soft red and white flocs are not present along the spring creek. Instead, the creek floor is covered by a thin orange-whitish crust.

**Field measurements of physical and chemical parameters and sampling.** Major physical and chemical parameters (pH, temperature, oxygen content, electrical conductivity and salinity) were determined by in-situ measurements at 7 locations in the spring water (Fig. 1). Measurements were performed with a field multimeter (WTW, Multi 3430), containing an oxygen sensor (FDO®925, 0-200 ± 1.5% dissolved oxygen at 20°C), a conductivity electrode (TetraCon®925, conductivity range 1 µS cm<sup>-1</sup> - 1 S cm<sup>-1</sup> ± 0.5% of measured value) and a pH sensor (SenTix®, pH range 0.000-14.000 ± 0.004) with an additional temperature sensor. The pH and conductivity sensors were calibrated at room temperature according to manual instructions of the WTW Multi 3430 field multimeter. The pH sensor was calibrated with a three-point calibration using technical buffers at pH values 4.01, 7.00 and 10.00. The conductivity electrode was calibrated using a 0.01 mol L<sup>-1</sup> KCl conductivity standard with a conductivity of 1413 µS cm<sup>-1</sup> at 25°C. The oxygen sensor is factory calibrated for the whole sensor lifetime with values stored in an internal memory chip within the sensor cap. The mean residence time of the pond water was identified by using NaCl as a tracer and conductivity measurements with the WTW TetraCon®925. The conductivity of the Arvadi Spring water at location 1 (L1, Fig. 1) was doubled by dissolving the NaCl tracer in the spring water. The tracer was distributed homogeneously in the spring pond by stirring the pond water over the length of the experiment. The conductivity was logged until it returned to initial values.

Spring water for geochemical analyses was collected from two locations within the spring pond (L1 and L2, Fig. 1). Samples were filtered to 0.45 µm in order to quantify major anions and cations by ion chromatography, dissolved organic (DOC) and inorganic carbon (DIC) by a carbon analyzer (highTOC, Elementar, Germany) and silica by Microwave Plasma – Atomic Emission Spectroscopy (MP-AES) (4200, Agilent Technologies, USA). Samples for Si

quantification additionally were acidified with 2% HNO<sub>3</sub> prior to analyses. Water for bicarbonate analyses was sampled without headspace and titrated in the laboratory against 1 M HCl. To prevent oxidation of iron(II) by air-O<sub>2</sub> during sampling, water and red floc samples from L1 and L2 for iron quantification were directly added to 0.5 M HCl on site (Porsch & Kappler, 2011). Iron(II) and total iron were quantified in respective samples by the spectrophotometric ferrozine assay (Stookey, 1970) with a microplate reader (FlashScan 550, Analytic Jena, Germany). For the quantification of total iron, samples were added to 10% hydroxylamine hydrochloride (HAHCl) solution in order to reduce all iron(III) to iron(II). The iron(II) content in HAHCl reduced samples therefore represents total iron. Iron(III) concentrations were calculated by subtraction of iron(II) concentrations from total iron concentrations. Hydrogen sulphide was quantified in water samples from L1 and L2 by the methylene blue method after Cline (1969) with a photometer (FlashScan 550, Analytic Jena, Germany). Sulphide was prevented from oxidation by air-O<sub>2</sub> during sampling by fixation of samples in 2% (w/v) zinc-acetate solution (Cline, 1969).

**Mineralogical analyses.** The mineralogy of the red flocs was identified by Mössbauer spectroscopy (Larese-Casanova et al., 2012). Precipitates were collected at L2 (Fig. 1) and stored without headspace at 4°C in the dark prior to further treatment in the laboratory. Samples were dried by applying low pressure inside an anoxic glovebox (100% N<sub>2</sub>) to avoid oxidation of potentially present redox-sensitive iron(II) minerals. The dried samples were ground in a mortar, filled in a flat cylinder-shaped plexiglas holder (with open top and an inner diameter of 1.5 cm) and fixed by a second smaller sample holder. For measurements, samples were inserted into a closed-cycle exchange gas cryostat (Janis cryogenics, USA). Spectra were recorded at 77 K and 4.2 K in transmission geometry using a constant acceleration drive system (WissEL GmbH, Germany). A <sup>57</sup>Co source embedded in a Rhodium matrix was used as gamma radiation source. The sample spectra were calibrated against a 7-µm-thick α-<sup>57</sup>Fe foil at room temperature. The RECOIL software suite (University of Ottawa, Canada) was used for calibration and modelling of the spectra. The spectra were modelled using Voigt-based line shapes (Rancourt & Ping, 1991). The Lorentz half-width-

half-maximum value (HWHM) was kept constant at 0.126 mm/s (determined from the minimum line width of the 3 and 4 peaks of the calibration foil) in the models. The Gauss' sigma ( $\sigma$ ) parameter was used to account for line broadening until the fitting was reasonable. Sample spectra were analysed with respect to the centre shift (CS), shift/quadrupole splitting/ ( $\epsilon/QS$ ) and hyperfine field (H).

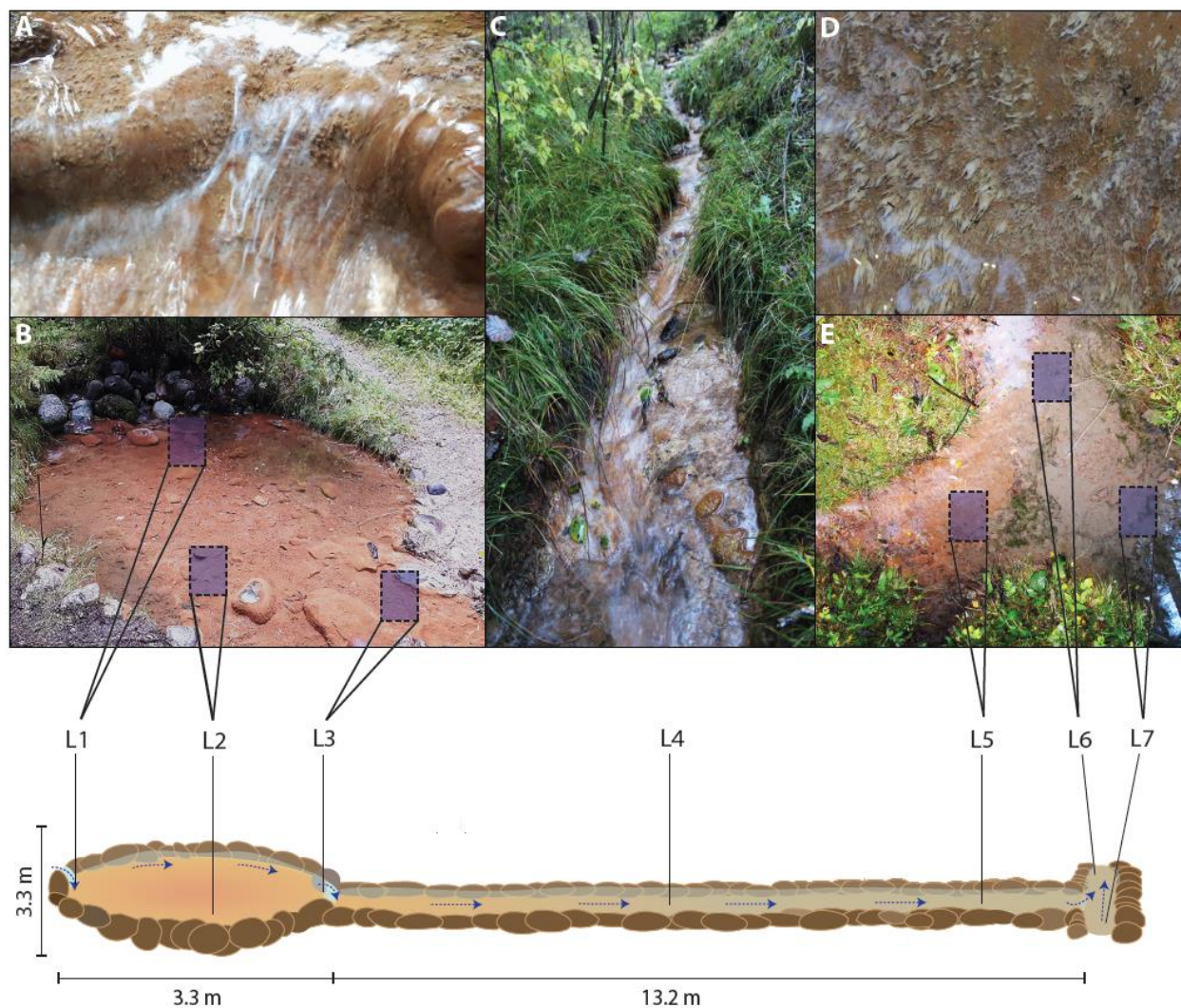


**Figure 1:** Schematic overview of the Arvadi Spring. Locations L1 and L2 are situated within the spring pond (B). L1 is located at the spring discharge and L3 at the transition of the water from the spring pond into the spring creek. Image (A) shows the transition of the spring pond to the creek at L3. Image (C) shows how the spring water flows via location L4 from the

spring pond to location L5. Image (D) shows whitish biofilms grown at several locations within the spring creek. Image (E) shows how water from another creek (L7) gets mixed into Arvadi Spring water. The mixed water flows out into forestal area (L6).

**Microscopy.** White and red flocs were sampled and stored at 4°C in the dark until analysis with a BMS 133 Trino binocular microscope (BMS Microscopes, NL). Samples for light microscopy were fixed in 2% paraformaldehyde. For fluorescence microscopy, samples were stained with SYTO9 stain (BacLight, Invitrogen, Carlsbad, CA) before analysis with a Leica DM 5500 B microscope (Leica Microsystems, Germany). Biofilm samples were fixed in 2.5% glutaraldehyde in the field to preserve biotic structures for Scanning Electron Microscopy (SEM) (Schädler et al., 2008). The samples were then transported on ice and in the dark back to the laboratory where they were stored in a cold-room over-night. The next day, samples were prepared on TEM grids or on glass slides, both pre-treated with poly-lysine. The TEM grids were dipped into the preserved samples and then taken through a dehydration series consisting of 30, 70, 95 and 100% ethanol (with the samples being immersed for ca. 5 seconds in each solution) and 2 final steps with hexamethyldisilazane before samples were left to air dry. Samples were prepared on glass slides by first adding a droplet of sample onto the slide, after which excess liquid was pipetted away and each of the solutions in the dehydration series above were added to the glass slide and left for 10-15 minutes before being exchanged. Finally, all samples were placed on aluminium stubs with carbon tape and sputter-coated with platinum (6-8 nm, SCD005, BAL-TEC, Liechtenstein, 35 mm working distance, 30 mA, 60 s). SEM micrographs were recorded with a secondary electron detector of a Leo Model 1450VP SEM (Carl Zeiss SMT AG, Germany) operated at 7 kV and 6 mm working distance.

**Quantification of cell abundance by Most Probable Number (MPN) counts.** Red and white flocs were collected separately from each location (L1 and L2; Fig. 1) and stored without headspace at 4°C in the dark prior to the experiment. The red flocs were used for

MPN enumerations of iron-metabolizers, while white flocs were used for MPN counts of sulphur-metabolizers after Oblinger and Koburger (Oblinger & Koburger, 1975; Straub et al., 2005). First, red and white flocs were homogenized separately. A  $10^{-1}$  dilution was prepared by the addition of approximately 1 g wet weight of red flocs to 9 mL of freshwater (FW) medium and 1 g wet weight of white flocs to 9 mL of basal mineral (BM) medium, respectively (for detailed description of media composition, see SI). Starting with the  $10^{-1}$  dilution, a ten-fold dilution series was prepared by sample transfer in a 1:10 ratio up to a dilution of  $10^{-12}$ . The dilutions were used as inoculum for MPN experiments. Anaerobic iron- and sulphur-metabolizers were cultivated in anoxic growth media with selective additives, as listed below (Hegler et al., 2008; Straub et al., 2005). Microaerophilic iron(II)- and sulphide-oxidizers were cultivated in gradient tubes after Emerson et al. (2005). Both types of MPN experiments were conducted as described by Laufer et al. (2016).

Iron-metabolizers were cultivated in FW medium amended with 30 mM  $\text{NaHCO}_3$ . Phototrophic iron(II)-oxidizers were cultivated with 10 mM  $\text{FeCl}_2$  as iron(II) source and 5 mM  $\text{Na}_2\text{MoO}_4$  to inhibit growth of sulphate-reducers. Nitrate-reducing iron(II)-oxidizers were cultivated in FW medium amended with 10 mM  $\text{FeCl}_2$ , 5 mM  $\text{Na}_2\text{MoO}_4$ , 4 mM  $\text{NaNO}_3$  and 0.5 mM Na-acetate. Iron(III)-reducers were cultivated in FW medium amended with 5 mmol  $\text{L}^{-1}$  ferrihydrite as iron(III) source, 5 mM Na-acetate and 5 mM Na-lactate.

Phototrophic sulphide-oxidizers (purple and green sulphur bacteria as well as non-sulphur bacteria) were cultivated in BM medium amended with 30 mM  $\text{NaHCO}_3$ . BM medium for non-sulphur bacteria contained 0.1 mM  $\text{Na}_2\text{S}$ , 5 mM Na-acetate, 5 mM succinic acid and 5 mM maleic acid and had a final pH of 6.8. BM medium for purple sulphur bacteria was amended with 1.2 mM  $\text{Na}_2\text{S}$  and was adjusted to a final pH of 7.6. BM medium for green sulphur bacteria contained 2.5 mM  $\text{Na}_2\text{S}$  and was adjusted to a pH of 6.8. Nitrate-reducing sulphide-oxidizers were cultivated in BM medium amended with 1 mM  $\text{NaNO}_3$ , 1 mM  $\text{Na}_2\text{S}$ , 0.5 mM Na-acetate and 30 mM  $\text{NaHCO}_3$ .

Sulphate-reducers were cultivated in BM medium amended with 30 mM  $\text{Na}_2\text{SO}_4$ , 1 mM  $\text{Na}_2\text{S}$  and 10 mM Na-acetate. Microaerophiles were cultivated in gradient tubes prepared with

Modified Wolfe's Mineral Medium (MWMM) (see SI) containing an iron(II) bottom plug in case of iron(II)-oxidizers, while gradient tubes for sulphide-oxidizers contained a Na<sub>2</sub>S bottom layer.

Generally, anoxic MPN deep-well plates and MPN gradient tubes were evaluated visually for positive growth due to a colour change in test wells and tubes, either from (1) light greenish or colourless to orange-brownish indicating the presence of iron(III) (oxyhydr)oxide precipitates and thus iron(II) oxidation or (2) from reddish to black indicating the precipitation of ferrous sulphides or mixed-valent iron(II)/iron(III) minerals and thus iron(III) reduction or (3) from colourless to blackish indicating precipitation of ferrous sulphides and thus sulphate reduction or (4) from colourless to purple indicating growth of purple (non-)sulphur bacteria or (5) from colourless to greenish indicating growth of green (non-)sulphur bacteria. In case of no visible colour change as it was the case for nitrate-reducing sulphide-oxidizers, growth was evaluated by sampling of the test wells and subsequent quantification of sulphide.

**DNA extraction, 454 pyrosequencing of 16S rRNA gene amplicons & sequence analyses.** Sediment samples for DNA extraction and subsequent 454 pyrosequencing were collected from L2 (pond) and L5 (creek) (Fig. 1). DNA was extracted from each sample with the Powersoil® DNA Isolation Kit (MoBio Laboratories, Carlsbad, CA, USA). DNA quality and quantity was determined spectrophotometrically using NanoDrop™ (ND 2000, PEQLAB biotechnology GmbH, Germany). Bacterial 16S rRNA genes were amplified using primers 27F (5'-AGAGTTTGATCMTGGCTCAG-3', (Lane, 1991)) and 534R (5'-ATTACCGGGCTGCTGGC-3', (Liu et al., 2007)) targeting the variable regions V1-V3 (507 bp). Both primers contained Roche 454 pyrosequencing barcodes. Primer 27F and 534R contained Roche 454-pyrosequencing adaptor sequences A and B, respectively. PCR was performed on each DNA extract in duplicate using the FastStart High Fidelity PCR system (Roche Diagnostics, Rotkreuz, Switzerland). PCR products were pooled in equal amounts. The amplified DNA was quantified using the Quant-iT™ PicoGreen® dsDNA assay kit (Life Technologies, Carlsbad, CA, USA) and a QuantiFluor®-ST fluorometer (Promega, Madison,

WI, USA). 454 pyrosequencing was performed on a Roche GS Junior Sequencer (454 Life Sciences, Branford, CT, USA) according to the manufacturer's instructions for amplicon sequencing. Amplicon reads have been deposited in the NCBI Sequence Read Archive (accession number: SRP124992, bioproject: PRJNA417005).

Curation of the obtained sequencing data including quality control, sequence alignment and sequence classification was performed using the software package MOTHUR, version 1.35.1 (Schloss et al., 2009). Pyrosequencing noise including primer dimers, single base errors and PCR chimeras were removed with the MOTHUR-implemented algorithms PyroNoise (Quince et al., 2009) and UCHIME (Edgar et al., 2011). Sequences shorter than 200 bp and homopolymers longer than 8 bp were removed from the dataset. All remaining high-quality sequences were aligned against the SILVA SSU Ref rRNA database (v119) (Pruesse et al., 2007) and pre-clustered with the single linkage algorithm at a threshold of 2% (Huse et al., 2010). Sequences were assigned to operational taxonomic units (OTUs) based on 3% genetic distance using the average neighbour algorithm (Schloss & Westcott, 2011). Sequence classification was performed using the Naïve Bayesian Classifier (Wang et al., 2007) and the SILVA SSU rRNA reference database with a minimum bootstrap confidence cut-off value of 60%. Random subsampling was performed prior to alpha diversity analyses to normalize the dataset to the sample with the lowest number of reads. Rarefaction curves, richness estimators (Chao1, ACE) and diversity indices (Shannon diversity, Simpson diversity) were calculated based on 3% genetic distance using MOTHUR's implementation DOTUR (Schloss & Handelsman, 2005).

## Results

**Geochemical composition of the Arvadi Spring water.** Geochemical parameters were constant in the spring pond (locations L1, L2, L3; Fig. 1; Tab. S1), as well as over the creek length with increasing distance from the spring discharge (locations L4, L5, L6; Fig. 1; Tab. S1). Differences were observed at location L7, which is in the second creek and not the Arvadi



Spring (Fig. 1). The spring water in the pond had a circumneutral pH and a temperature of 7.0 to 7.3°C (Tab. 1). The water was saturated with oxygen ( $337.5 \pm 1.3 \mu\text{M}$ , average  $\pm$  standard deviation,  $n=3$ , Table 1) but still contained dissolved iron(II) and sulphide at concentrations of  $17.2 \pm 2.8 \mu\text{M}$  and  $2.5 \pm 0.2 \mu\text{M}$  ( $n=5$ , Table 1), respectively. Dissolved iron(III) was not detected in the spring water. The average concentrations of the main anions and cations in the spring pond (L1-L3, Table S2; Table S3,  $n=3$ ) were sulphate ( $8.3 \pm 0.1 \text{ mM}$ ), magnesium ( $3.2 \pm 0.0 \text{ mM}$ ) and calcium ( $7.0 \pm 0.0 \text{ mM}$ ). Total carbon was quantified at  $50.9 \pm 0.3 \text{ mg L}^{-1}$ , of which  $1.3 \pm 0.7 \text{ mg L}^{-1}$  was DOC ( $n=3$ , Table S4). The bicarbonate content of the spring water was  $4.5 \pm 0.0 \text{ mM}$  ( $n=3$ , Table 1). Silica was quantified at  $134.3 \pm 4.4 \mu\text{M}$  in the spring pond water ( $n=6$ , Table 1). On the basis of the conductivity measurements, which reflected the loss of the NaCl spike from the pond water, the mean residence time of the spring water in the pond was 16 minutes.

**Structure and composition of precipitates.** The spring pond ground was completely covered by red floc precipitates partly overlain by whitish flocs (Fig. 2A, 2B). Light microscopy showed the red floc material to be bulky and densely packed (Fig. 2C), while white flocs consisted of filaments interspersed with smaller nodule structures (Fig. 2D). Staining of the red and white flocs with SYTO9, a nucleic acid dye, indicated that both types of flocs consisted mainly of biotic structures (Fig. 2E, 2F). SEM analyses of red and white biofilm samples recovered from rock surfaces at L3 (Fig. 1D) revealed similar results as the microscopic analyses of red and white floc samples. The red biofilm contained mainly bulky and heterogeneous structures (Fig. 2G) that were similar to the red floc morphology, whereas the white biofilm rather consisted of a web of filamentous structures (Fig. 2H), as found in white flocs.

Quantification of the iron(II):iron(III) ratios in red flocs by the spectrophotometric ferrozine assay after acidic dissolution revealed iron(III) to be the dominant redox state, although the relative amounts varied between samples from L1 and L2. Red flocs from L1 had  $77.0 \pm 2.2\%$  (average  $\pm$  standard deviation,  $n=5$ ) iron(III) and a lower amount of iron(II) of  $23.1 \pm 2.2\%$ .

By contrast, red flocs from L2 contained  $55.0 \pm 3.7\%$  and  $45.0 \pm 3.7\%$  of iron(III) and iron(II), respectively.

Analysis by  $\mu$ XRD revealed the crystalline part of the red flocs to be dominated by quartz, calcite and dolomite (Figure 3). The Mössbauer spectrum collected at 77 K is best fitted by three doublets corresponding to paramagnetic iron phases with an additional phase having broad quadrupole splitting indicating the partial onset of magnetic ordering. The narrow paramagnetic doublet at 77K (Fig. 3; CS = 0.5 mm/s; QS = 0.6 mm/s (Table S5)) can potentially correspond to a number of mineral phases, such as lepidocrocite, or iron(II) sulphides, including mono- and disulphides such as pyrrhotite and pyrite (Jeandey et al., 1991; Montano and Seehra, 1976). The 4.2K spectrum is dominated by several magnetically ordered sextets in addition to two doublets (Fig. 3). The sextets are characteristic for poorly crystalline iron(III) (oxyhydr)oxide phases, with large inner-line broadening that are suggestive of an association with organic matter (Eusterhues et al., 2008; Shimizu et al., 2013). The wide paramagnetic doublet at 4.2K (Fig. 3; CS = 1.3 mm/s; QS=2.7 mm/s (Table S5)) corresponds to an iron(II) phase, that could be either vivianite, green rust, siderite or even sorbed iron(II) (Domes et al., 1986). Based on the fitting of the spectrum collected at 4.2K, the calculated iron(II):iron(tot) ratio in the sample is 0.169.

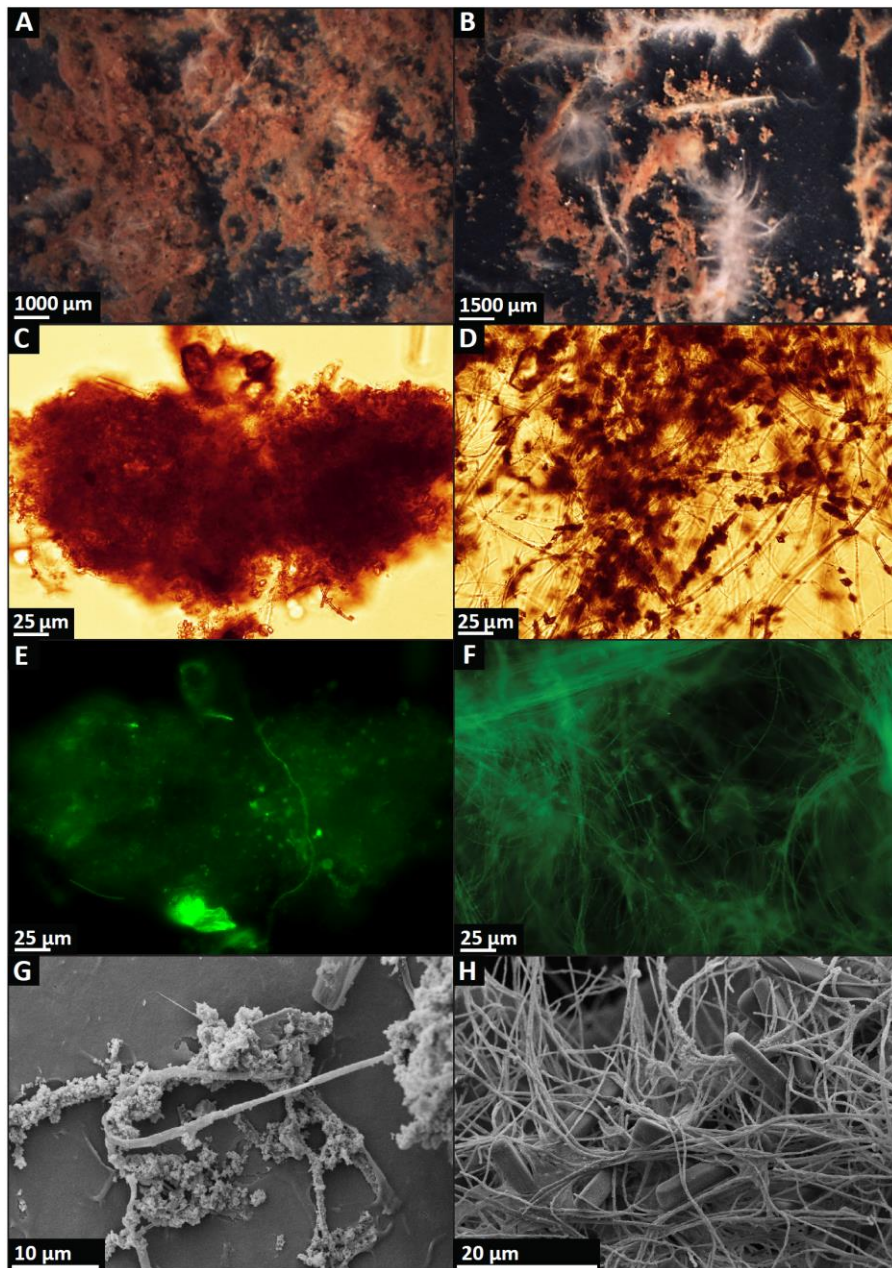


**Figure 2:** Binocular and microscopy images of red and white flocs and biofilm. Binocular images of a mixture of red and white flocs that cover the Arvadi Spring ground at L2 (A & B). Microscopy images of a red floc (C & E; taken from L2); red biofilm (G, taken from L3), white flocs (D & F, taken from L2) and white biofilm (H, taken from location 3). Binocular images (A & B) were taken at 10x magnification (A) and 15x magnification (B). Brightfield (C & D) and fluorescence mode images (E & F) were taken at 400x magnification. SEM images (G & H) were taken at 5000x (G) and 2000x (H) magnification.

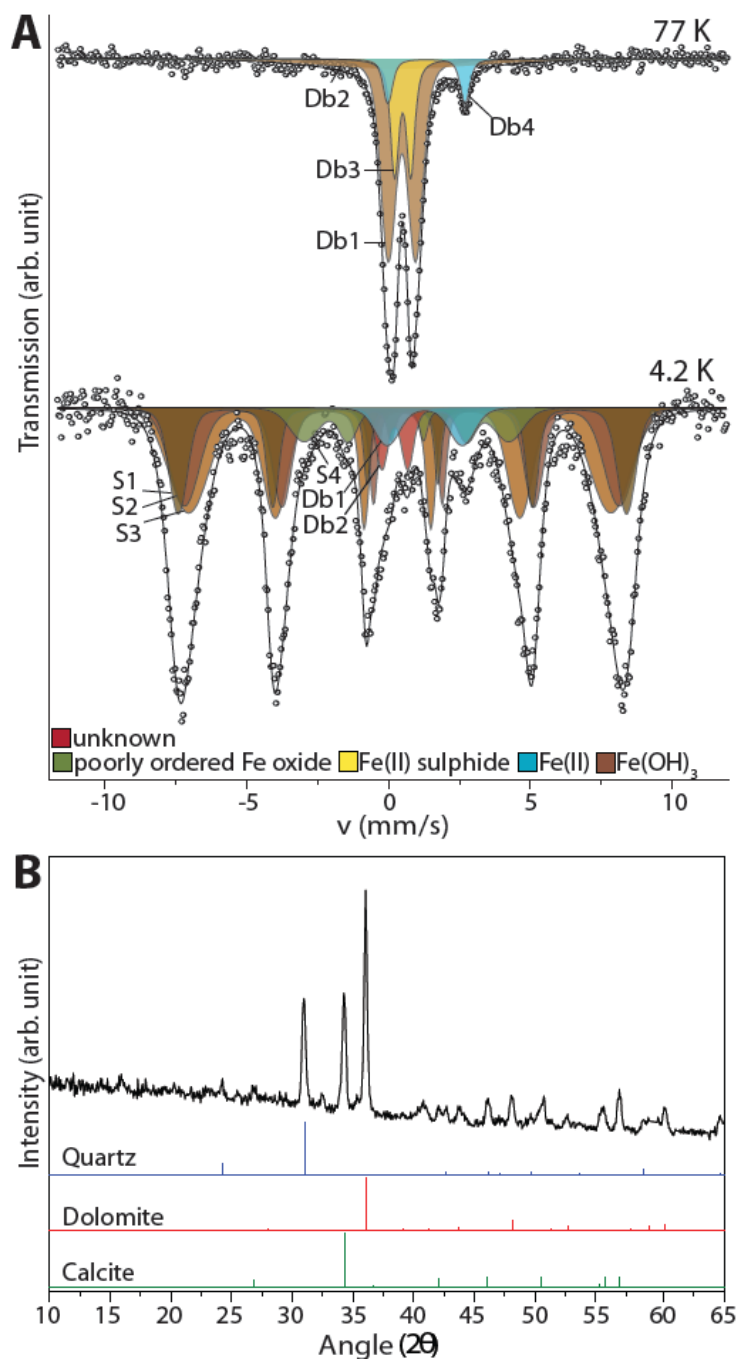


**Figure 3:** Mössbauer spectra obtained at 77 K and 4.2 K (A) and X-ray diffractograms (B) of red flocs.

**Microbial community composition and abundance of iron- and sulphur-metabolizers.**

The abundance of iron- and sulphur-metabolizing bacteria in red and white flocs was quantified by MPN counts (Fig. 4). Microaerophilic sulphide-oxidizers were most abundant at L1 and L2, with  $2.47 \times 10^5$  and  $2.40 \times 10^5$  cells  $g^{-1}$  in the white flocs, respectively, followed by microaerophilic iron(II)-oxidizers with  $2.47 \times 10^4$  and  $2.40 \times 10^4$  cells  $g^{-1}$  in the red flocs. Anaerobic iron- and sulphur-metabolizers were quantified at lower abundances, with the lowest abundance among phototrophic iron(II)-oxidizers ( $6.03 \times 10^1$  and  $5.26 \times 10^2$  cells  $g^{-1}$  red flocs), nitrate-reducing iron(II)-oxidizers ( $3.14 \times 10^3$  and  $2.98 \times 10^2$  cells  $g^{-1}$  red flocs) and sulphate-reducers ( $3.05 \times 10^2$  and  $2.40 \times 10^2$  cells  $g^{-1}$  white flocs). Iron(III)-reducers were the most abundant anaerobes among the iron- and sulphur-metabolizers with  $2.47 \times 10^3$  and  $2.97 \times 10^4$  cells  $g^{-1}$  red flocs). MPN numbers could not be determined for phototrophic and nitrate-reducing sulphide-oxidizers as only very few tubes inoculated for purple (non-) sulphur bacteria were positive and did not show a clear trend or growth for green (non-) sulphur bacteria and nitrate-reducing sulphide-oxidizers.

454 pyrosequencing of bacterial 16S rRNA genes revealed that the Arvadi Spring pond and creek sediments contained diverse bacterial communities with 213 genera identified in total (Table S6). The most abundant phyla in both samples were Proteobacteria (57.8% and 59.0% rel. sequence abundance, respectively), Bacteroidetes (17.8% and 14.8% rel. sequence abundance, respectively) and Cyanobacteria (9.5% and 9.9% rel. sequence abundance; Fig. 5A). On the genus level, the samples were dominated by *Thiothrix* (14.0% and 17.2% rel. sequence abundance, respectively), *Thiobacillus* (4.1% and 5.9%, respectively), and *Gemmobacter* (3.3% and 2.5%, respectively) (Fig. 5B). Genera with relative sequence abundances below 1% were summarized as 'Other' and made up 17.5% and 19.2% of the total community, respectively. This group included various genera known to comprise iron- and sulphur-metabolizers such as *Acidiferrobacter*, *Acidithiobacillus*, *Acidovorax*, *Albidiferax*, *Desulfathirabdium*, *Desulfocapsa*, *Ferrithrix*, *Nitrospira*, *Sideroxydans*, *Sulfuricella*, *Sulfuricurvum*, *Sulfuritalea*, and *Sulfurospirillum* (Table S6). Rarefaction analyses indicated that sampling did not fully recover the total estimated diversity (Fig. S1). Richness estimators (Tab. S7) further suggested that the observed richness covered on average 57 to

72% of the estimated total bacterial richness in the pond and creek samples. In general, the observed and estimated richness (based on Chao1 and ACE richness estimators) were higher in the pond compared to the creek sample. Diversity indices (Shannon and Simpson) suggested the pond and creek samples to be diverse to a similar extent.

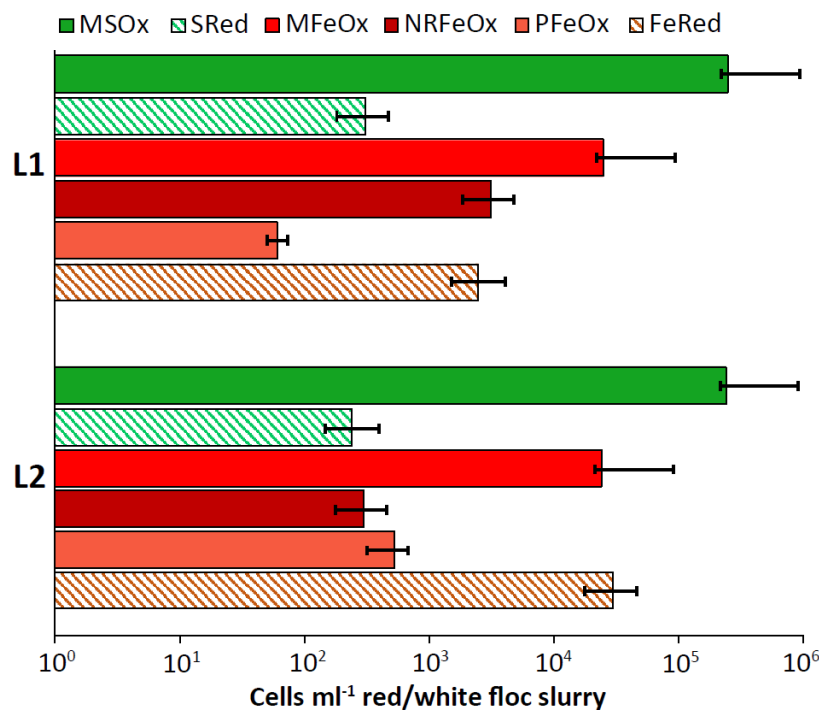


**Figure 4:** MPNs of iron- and sulphur-metabolizers in red and white flocs at locations L1 and L2: Microaerophilic sulphide-oxidizers (MSOx), sulphate-reducers (SRed), microaerophilic (MFeOx), nitrate-reducing (NRFeOx) and phototrophic iron(II)-oxidizers (PFeOx) as well as iron(III)-reducers (FeRed). The error bars indicate upper and lower limits of the 95% confidence intervals for the estimates.

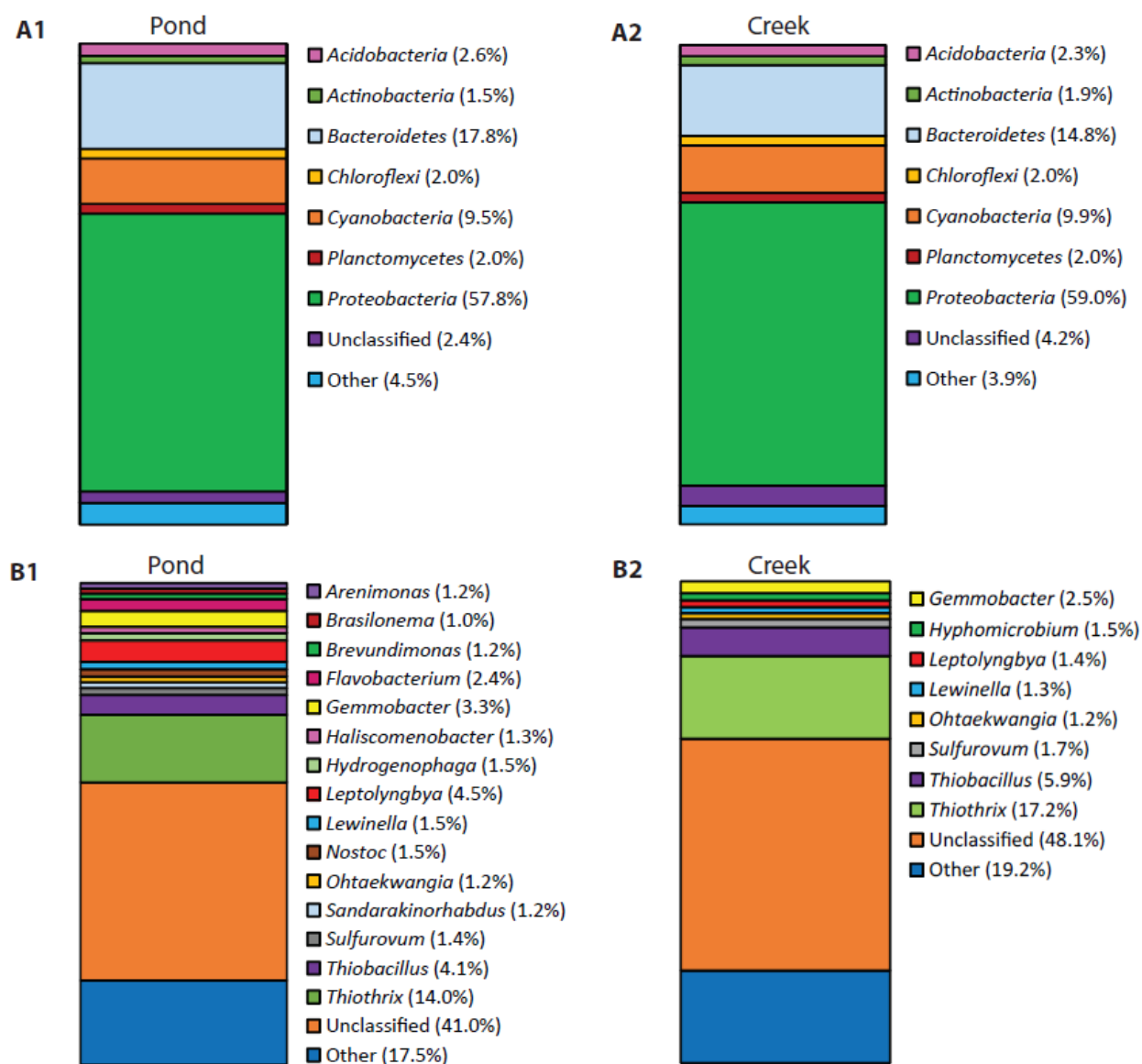


**Figure 5:** Taxonomic identity and relative sequence abundance of bacterial 16S rRNA genes on the class (A) and genus level (B) in Arvadi Spring pond and creek. For detailed information, see Table S6.

## Discussion

The Arvadi Spring is characterized by O<sub>2</sub> saturation, low concentrations of iron(II) and sulphide, considerable amounts of sulphate, and high light availability. Figure 6 shows a model for biogeochemical iron and sulphur cycling in the Arvadi Spring that we hypothesize to apply to ferro-euxinic intermixed transition zones along redox interfaces of Proterozoic surface ocean waters and possibly also of late Archean oxygen oases during high-oxygen intervals (Fig. 6B, Table 1). We evaluated iron(II)- and sulphide-consuming and -producing processes and identified the present geochemical iron and sulphur species in the Arvadi Spring to determine the factors that limit iron(II) and sulphide bioavailability, aiming to better understand Precambrian biogeochemical iron- and sulphur-cycling under high-oxygen conditions.

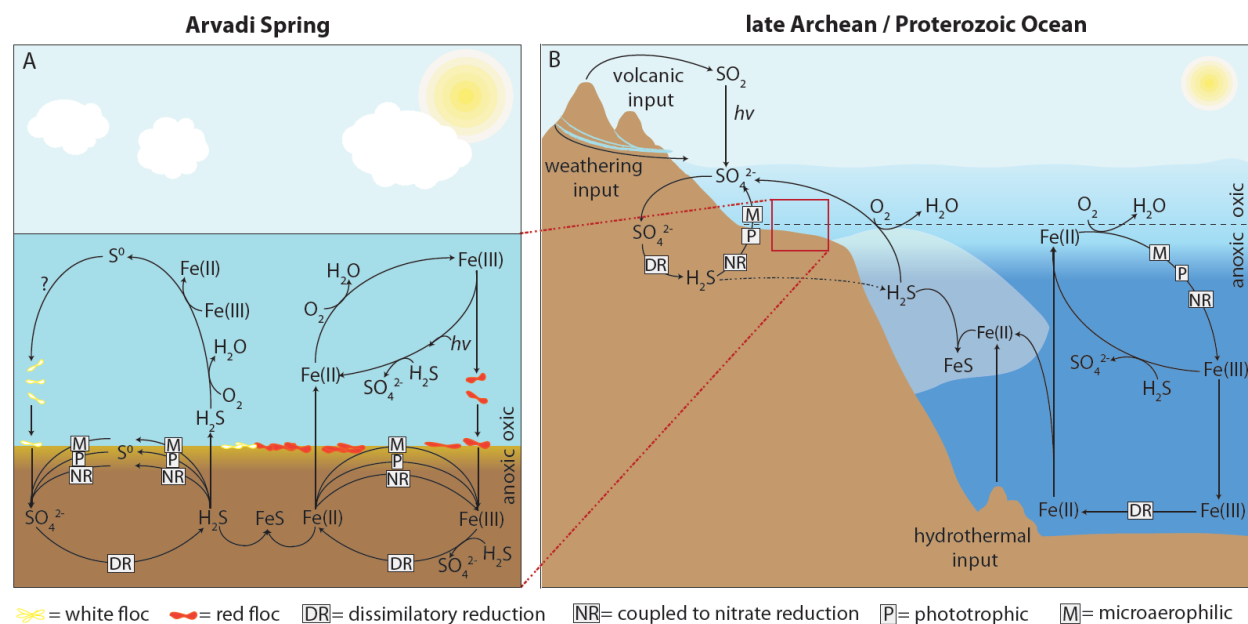


**Figure 6:** Simplified model of biogeochemical iron and sulphur cycling in the Arvadi Spring and its relevance for late Archean and Proterozoic ocean iron and sulphur cycling. **A:** Abiotic oxidation reactions in the Arvadi Spring pond occur mainly in the oxic water, producing S<sup>0</sup> and iron(III) that are further metabolized in the spring sediment. Red and white flocs are potential products of abiotic and biotic iron(II) and sulphide oxidation. White flocs are expected to contain S<sup>0</sup>, while red flocs consist of iron(III) minerals. These compounds get metabolized by microbial processes (indicated by squares, see legend) at the oxic-anoxic



sediment surface and in anoxic deeper sediment layers. The same biotic and abiotic redox processes are also expected to occur in red and white flocc precipitates (not shown). B: The Arvadi Spring model possibly represents conditions near the redox-cline in late Archean and Proterozoic oceans (see red dashed lines and box), where enough light and/or oxygen were available to support phototrophic and aerobic microbial processes and where sulphide-rich and iron(II)-rich waters were mixed with oxygenated surface waters. The iron cycle on the right hand side of the image probably also contemporaneously took place in neritic sediments (not shown). The grey shaded area indicates euxinic water masses formed by dissimilatory sulphate reduction.

**Iron(II)- and sulphide-producing and -consuming biogeochemical processes in the Arvadi Spring.** Under full oxygenation and at the circumneutral pH of the Arvadi Spring water, dissolved iron(II) is expected to become oxidized abiotically by O<sub>2</sub> within minutes (Millero et al., 1987a; Pham & Waite, 2008). As we found microaerophilic, phototrophic, and nitrate-reducing iron(II)-oxidizing microorganisms to colonize Arvadi Spring red flocs, we conclude that a significant fraction of the total iron(II) budget is consumed by their metabolic processes (Fig. 6A). The low but constant steady-state concentration of total dissolved iron(II) that we quantified (17.2 μM) is likely the result of a balance between its different sources and sinks. A certain fraction of dissolved iron(II) likely stems from dissimilatory iron(III) reduction, while iron(II) may also be formed by abiotic iron(III) reduction processes including photoreduction of ligand-bound iron(III) (Barbeau et al., 2001), the abiotic reaction of O<sub>2</sub> with ligand-bound or dissociated iron(III) (Rush & Bielski, 1985), or iron(III) reduction coupled to abiotic sulphide oxidation (Yao & Millero, 1996; Lohmayer et al., 2014). The initial concentration of iron(II) introduced to the Arvadi Spring pond together with the iron(II) from reductive processes may be sufficient to avoid being completely consumed by abiotic and biotic oxidation processes during the mean water residence time of 16 minutes in the pond, leaving residual iron(II) in solution. Other reasons for the low but stable iron(II) concentrations may be the presence of humic ligands that can stabilize iron(II) (Hopwood et al., 2015; Statham et al., 2012) and the large amounts of sulphate in the Arvadi water that can retard the abiotic oxidation of iron(II) to a certain extent (Millero, 1985).

Microbial reduction of gypsum-derived sulphate that is present in large amounts in the Alpine orogeny is the major source of sulphide in the Arvadi Spring (Strauss et al., 2016). Compared to iron(II), sulphide is oxidized abiotically by  $O_2$  much more slowly, i.e., on the order of hours to days (Luther et al., 2011; Millero et al., 1987b). Hence, we expect the majority of aqueous sulphide to be oxidized microbially and not abiotically, since the water residence time in the pond is only 16 minutes. Our MPN and 16S rRNA gene sequence analyses suggest microaerophilic sulphide-oxidizers to play a major role in sulphide consumption within the Arvadi Spring, as *Thiothrix*, a genus representative of aerobic sulphide-oxidizers (Nielsen et al., 2000), was identified to dominate the Arvadi Spring microbial community. The observed growth of *Thiothrix*-like filamentous biofilms (Bland & Staley, 1978) at several locations (Fig. 1A, 1D) gives hints on respective microorganisms to flourish in the Arvadi Spring. Minor sulphide portions may be metabolized by phototrophic and nitrate-reducing sulphide-oxidizers (Fig. 6A) that were indicated to be part of the Arvadi Spring community based on 16S rRNA gene sequencing data (phototrophic sulphide-oxidizers in the families *Chlorobiaceae*, *Chromatiaceae*, *Chloroflexi* and nitrate-reducing sulphide-oxidizers in the genera *Arcobacter* and *Thiobacillus*, respectively; see Table S6). However, we could neither determine taxonomic identity on the strain level nor whether respective microorganisms actually perform phototrophic and nitrate-reducing sulphide oxidation in situ. Furthermore, as we could not quantify the (probably low) abundance of respective microorganisms by MPN counts and do not have evidence for their metabolic activity in the Arvadi Spring, the overall role that phototrophic and nitrate-reducing sulphide-oxidizers play in the Arvadi Spring requires further investigations in the future.

We expect elemental sulphur ( $S^0$ ) - a key intermediate during sulphur metabolism that is stored intra- or extracellularly by sulphide-oxidizing microorganisms such as *Thiothrix* spp. (Nielsen et al., 2000) - to be present in Arvadi Spring solids, in particular in white floc precipitates (Fig. 6A) and whitish biofilms (Fig. 1D). However, additional mineralogical and speciation experiments are required to decipher the identity of sulphur intermediates and related processes such as  $S^0$  disproportionation or  $S^0$  oxidation in Arvadi Spring precipitates in order to uncover their relative importance on the overall sulphur budget in the Arvadi

Spring and, by inference, in parts of ferro-euxinic transition zones along redox-interfaces and chemoclines of shallow Proterozoic and late Archean ocean waters during high-oxygen intervals.

**Table 1:** Geochemical parameters in the Arvadi Spring pond water and approximations for respective parameters in late Archean and Proterozoic oceans from the literature.

	Arvadi Spring Pond	Late Archean & Proterozoic ocean (surface)
T [°C]	7.2±0.1	20-70 <sup>1,2</sup>
pH	8.0±0.0	6.5-8.5 <sup>3,4</sup>
O <sub>2</sub> [μM]	337.5±1.3	1-10 in late Archean oxygen oases <sup>5</sup> 0.2 in mid-Proterozoic <sup>6</sup> >1 in Paleoproterozoic <sup>7</sup>
Salinity [‰]	0.7	35-70 <sup>8</sup>
HCO <sub>3</sub> <sup>-</sup> [mM]	4.5±0.0	~70 <sup>3</sup>
Sulphate [mM]	8.3±0.0	~0.08 for the late Archean <sup>9</sup> 1.0-4.5 for the Paleo- & Mesoproterozoic <sup>10,11</sup>
Sulphide [μM]	2.5±0.3	n.a.
Fe(II) [μM]	17.2±2.8	40-120 in Archean oceans <sup>11</sup> <100 in Proterozoic oceans <sup>13</sup>
SiO <sub>2(aq)</sub> [μM]	134.3±4.4	670-2200 <sup>14</sup>

Values for the Arvadi Pond are average±standard deviation for  $n=3$  (L1-L3, see also Tab. S1, S2)

<sup>1</sup> Pinti, 2005

<sup>2</sup> Robert & Chaussidon, 2006

<sup>3</sup> Grotzinger & Kasting, 1993

<sup>4</sup> Halevy & Bachan, 2017

<sup>5</sup> Olson et al., 2013

<sup>6</sup> Tang et al., 2016

<sup>7</sup> Hardisty et al., 2014

<sup>8</sup> Knauth, 2005

<sup>9</sup> Jamieson et al., 2013

<sup>10</sup> Canfield et al., 2010

<sup>11</sup> Kah et al., 2004

<sup>12</sup> Canfield, 2005

<sup>13</sup> Planavsky et al., 2011

<sup>14</sup> Konhauser et al., 2007

The coexistence of iron(II) and sulphide at the  $\mu\text{M}$  concentration range in the Arvadi Spring water likely applies to respective ancient habitats (Fig. 6B). However, respective values should not be taken as representative for the bulk of ancient seawater, as anoxia was the prevailing feature of Precambrian oceans. The (reductive) sources of iron(II) and sulphide probably exceeded their sinks (microaerophilic/abiotic oxidation and precipitation) during anoxic intervals, with iron(II) and sulphide concentrations presumably having peaked at higher concentrations (e.g. iron(II) reaching 40-120  $\mu\text{M}$  as suggested for Archean oceans (Canfield, 2005)).

**Iron redox speciation in the Arvadi Spring and iron(II) bioavailability for iron(II)-oxidizing microorganisms.** Fe(III) is poorly soluble at neutral pH and dissolved iron(III) only occurs as colloidal or ligand-bound (complexed) iron(III) (Cornell & Schwertmann, 2003). As we could not detect dissolved iron(III) in the spring water, iron(III) complexes must play a relatively minor role in the Arvadi Spring water, with most iron(III) precipitating directly after formation as iron(III) minerals. Wet-chemical extraction followed by ferrozine analyses and Mössbauer spectroscopy clearly showed red flocs to consist of poorly crystalline iron(III) (oxyhydr)oxides similar to ferrihydrite (Table S5, Fig. 3). This is in accordance with the common observation of ferrihydrite formation through abiotic iron(II) oxidation by  $\text{O}_2$  or by microaerophilic iron(II)-oxidizers in other cold-water springs with circumneutral pH (Jambor & Dutrizac, 1998; James & Ferris, 2004; Konhauser et al., 2011; Hegler et al., 2012). Thus, red flocs probably form through a combination of biotic and abiotic iron(II) oxidation (Fig. 6A).

The Mössbauer spectra (Table S5) and ferrozine analyses showed iron(II) to be present in red flocs, which likely stems from dissimilatory iron(III) reduction proceeding in red flocs in addition to iron(II) oxidation based on our MPN results. Interestingly, the iron(II) content of 45% as determined in red flocs from location L2 using acidic extraction and the spectrophotometric ferrozine assay contradicts our Mössbauer results which suggest an iron(II):iron(tot) ratio of 16.9% in the sample. This discrepancy may be due to abiotic

reduction of iron(III) by sulphide that is released during acidic extraction and thus made available for iron(III) reduction. Also, sulphide produced by potentially more intensely ongoing sulphate reduction in closely associated white flocs from L2 (see MPN results) may be responsible for the observed discrepancy.

Generally, we suggest the iron(II) in red flocs to be consumed by iron(II)-oxidizers that colonize red flocs. However, the bioavailability of iron(II) in red flocs depends on its speciation as for instance the bioavailability of mineral-bound iron(II) depends on mineral solubility (Zhao et al., 2016; Kappler & Newman, 2004). Iron(II) in more stable minerals is less bioavailable, as for instance, pyrite (solubility product (KSP) =  $10^{-16.4 \pm 1.2}$  (Davison, 1991)) was shown not to be metabolized by phototrophic iron(II)-oxidizers at neutral pH, whereas other iron(II) minerals (such as poorly crystalline FeS (KSP =  $10^{-2.95 \pm 0.1}$ ; (Davison, 1991)) or iron(II) carbonate (KSP =  $10^{-2.94 \pm 0.4}$ ; (Bénezeth et al., 2009)) with higher solubility were oxidized (Kappler & Newman, 2004). Intuitively, based on the presence of iron(II), sulphide and high carbonate content in the Arvadi Spring water, we considered the possibility that a fraction of the iron(II) in the red flocs occurs as iron(II) sulphide and as siderite minerals. Being highly reactive towards each other, iron(II) and sulphide precipitate as poorly crystalline ferrous sulphide if their concentrations reach supersaturation (Rickard & Luther, 2007) and transform further into more stable iron(II) sulphides (i.e. pyrite or pyrrhotite) (Rickard, 2006; Rickard & Luther, 2007). However, under the given Arvadi Spring water geochemistry and a calculated saturation index of -7.42 for amorphous FeS, such FeS-mineral phases are unlikely to precipitate in the Arvadi Spring, although the formation of dissolved and/or colloidal FeS complexes and nanoparticulate higher crystalline FeS species such as mackinawite at hotspots where higher sulphide and iron(II) are present (for example in deeper sediments) cannot be excluded (Luther & Rickard, 2005). Our Mössbauer results indicate the narrow paramagnetic doublet at 77K to potentially account for an FeS phase, suggesting locally formed iron(II) and sulphide from iron(III) and sulphate reduction that proceed in close association in red and white flocs to reach supersaturation and hence to result in the formation of different FeS-minerals at spatially restricted sites (Fig. 6A). Our Mössbauer results further indicate siderite to be formed in the

Arvadi Spring, which is in line with a calculated saturation index of 2.67 for siderite formation based on the Arvadi water geochemistry. As these conclusions are mostly based on theoretical considerations using the geochemical conditions in the Arvadi water, further investigation of the iron- (and sulphur-) speciation in red and white flocs is required to understand the actual mineral identity and the mechanisms behind their formation.

Our observations suggest that dissolved iron(III) was probably absent in Precambrian ocean margins with intermixed ferro-euxinic-oxic waters, except in low abundances of ligand-bound or colloidal forms. Moreover, the iron(III) minerals formed by microaerophilic and abiotic iron(II) oxidation were likely poorly crystalline and ferrihydrite-like. The formed iron(III) particles may have been similar in their structure and composition to Arvadi Spring red flocs and probably were colonized by microorganisms, in particular by iron-metabolizers, during and after sinking to the ocean floor. These particles likely also contained ferrous minerals, which resulted from dissimilatory iron(III) reduction. Respective iron(II) phases could have included green rust (Halevy et al., 2017), as well as iron(II) sulphides that precipitated directly from the ferro-euxinic surface ocean waters (Canfield, 1998; Lyons, 2008). These iron sulphides likely settled together with red floc-like particles and transformed over time to more stable iron(II) sulphides (e.g., pyrite).

**Adaptation of iron and sulphur metabolizers to Arvadi Spring's high O<sub>2</sub> content.** Our results show the co-occurrence of phototrophic, nitrate-reducing and microaerophilic iron(II)-oxidizers and microaerophilic sulphide-oxidizers with dissimilatory iron(III)- and sulphate-reducers in an iron- and sulphur-rich environment. Based on bioturbation in the spring ground by movement of the prevalent macrobiota together with the apparently low density of red and white flocs and hence their subjection to water movement from the top, we assume intermixing of different sediment layers with red and white flocs to proceed over the whole year and hence the different metabolic types of microorganisms to co-occur in different ecological niches throughout the seasons (especially as our results were reproducible with samples from different seasons, data not shown). Partial introduction of

certain metabolic types of microorganisms from the ambient water is inevitable and hence may have a minor impact on the observed composition.

The dense microbial networks associated with Arvadi Spring red and white flocs (Fig. 2E, 2F) contain heterotrophic aerobic respiring bacteria (Gemmobacter, Hydrogenophaga and Pseudomonas, see Tab. S6). Oxygen consumption by these microbes, alongside abiotic O<sub>2</sub>-consuming reactions, e.g., abiotic O<sub>2</sub>-dependent sulphide and iron(II) oxidation can create microoxic or anoxic microniches in otherwise oxic environments (Brune et al., 2000). Based on the significant numbers of anaerobic and microaerophilic Fe- and S-metabolizing microorganisms that we found in MPN experiments, we suggest anoxic and microoxic microniches to be present in the Arvadi Spring and that such microsites should be analyzed in future experiments for example using O<sub>2</sub>-, Fe- or Eh-microelectrodes. Based on the lower abundance of anaerobes compared to microaerophiles, the high O<sub>2</sub> content in the Arvadi Spring is probably limiting obligate anaerobes in their growth and activity. Additionally, it has to be considered that potentially some anaerobes could have been washed from other locations to the spots that were sampled and based on our data it is not possible to fully distinguish between scenarios where the different types of organisms really co-occur in association with each other or whether they just co-occur in the collected sample.

Aerobic microorganisms are unlikely to have dominated the bulk of the late Archean and Proterozoic ocean microbiome as anoxia was the prevailing feature by that time with the exception of settings that were similar to the Arvadi Spring. Our finding of a predominance of microaerophiles over anaerobes therefore should only be understood as a likely scenario for redox-stratified ocean waters in paleo-shorelines during high-oxygen intervals. In respective settings, O<sub>2</sub>-tolerant and even O<sub>2</sub>-dependent lifestyles may have evolved and became widespread. We suggest that in settings similar to the Arvadi Spring, phototrophic and nitrate-reducing iron(II)-oxidizers would not have been abundant, if not generally metabolically inactive. Nitrate may have been scarce in Precambrian oceans (Fennel et al., 2005; Godfrey & Falkowski, 2009) as it is the case in the Arvadi Spring, whereby a recent study by Michiels et al. (2017) on N-cycling in ferruginous Kabuno Bay implies the contrast, suggesting significant contribution of nitrate-reducing iron(II)-oxidizers to global

Proterozoic N-retention. Further, the redox stratification of the Precambrian ocean with the first appearance of oxic conditions and the accompanying formation of oxy- and chemoclines may have re-arranged the spatial distribution of microbial communities, with microaerophiles presumably having colonized topmost oxic (and photic) layers. They likely co-existed with phototrophs, but competing for iron(II), phototrophs may have decreased in their abundance in oxic intervals at respective sites.

## **Implications for Fe-S-cycling in ferro-euxinic transition zones of shallow late Archean and Proterozoic ocean waters**

The present study provides new insights from a modern iron(II)-, sulphide- and O<sub>2</sub>-rich model habitat regarding the potential network of iron- and sulphur-metabolizing microorganisms in shallow ferro-euxinic transition zones of Precambrian oceans that were influenced by the presence of O<sub>2</sub> in the water and atmosphere. The Arvadi Spring data implies the iron- and sulphur-metabolizing microbial community that presumably co-existed in respective ancient sites to have been dominated by microaerophiles. However, considering a higher prevalence of anoxia for the bulk of Precambrian oceans, anaerobic iron- and sulphur-metabolizers presumably would have still been dominating over microaerophiles on the global level. Comparing the observed morphology in red and white flocs (Fig. 2) to microfossil structures found in the rock record that are interpreted as remains of early microorganisms (Schopf et al., 2015) we suggest similar microbial networks to have colonized mineral particles that settled from ferro-euxinic intermixed surface waters of the late Archean and Proterozoic ocean.

Collectively, the Arvadi Spring helps us to understand how O<sub>2</sub> consumption by aerobic microorganisms, and production of reduced compounds by anaerobic respiring microorganisms (e.g., iron(II), sulphide), could have affected the abundance, activity, and survival of anaerobic members of the upper, oxygenated ancient ocean metabolic network by forming anoxic niches. Especially for the interpretation of signatures found in the rock record the Arvadi Spring can help to understand which biotic and abiotic processes resulted



in the isotope composition that was preserved in the rock record (Strauss et al., 2016), to decipher the identity of the primary minerals prior to diagenesis, and to know the morphology of the microbial community that exists under envisaged conditions prior to preservation in form of microfossils. To further improve our model and our understanding of the metabolic network of iron- and sulphur-metabolizing microorganisms, we need to know the factors controlling the interrelation and competition of iron- and sulphur-metabolizers with abiotic reactions in the Arvadi Spring. This includes understanding the relative importance of different metabolic types of iron- and sulphur-metabolizers by determining rates of the individual processes. To evaluate the impact of changing redox conditions on the microbial community activities, controlled laboratory microcosm experiments are required, which include variations in O<sub>2</sub> availability and in iron(II) and sulphide concentrations. The quantification of microbial versus abiotic rates of iron(II) and sulphide oxidation, as well as rates of iron(III) and sulphate reduction in the Arvadi Spring by iron- and sulphur-metabolizers, is a prerequisite to decipher biogeochemical iron and sulphur cycling in detail. Only by unravelling the response of a living microbial community to postulated geochemical frameworks, we can reconstruct the ancient biosphere and geosphere as a whole.

### **Acknowledgements**

We thank E. Struve for DOC, anion/cation and bicarbonate measurements and W. Ruschmeier for gradient tube preparation. Furthermore, we thank Karin Stoegerer for 454 pyrosequencing. We would like to thank A. Mloszewska, as well as the editor and two anonymous reviewers for helpful comments that significantly improved the manuscript. This study was funded by a German Research Foundation (DFG) grant (No. KA 1736/27-1).

## REFERENCES

- Barbeau K, Rue E, Bruland K, Butler A (2001) Photochemical cycling of iron in the surface ocean mediated by microbial iron (III)-binding ligands. *Nature*, **413**, 409-413.
- Bekker A, Planavsky NJ, Krapež B, Rasmussen B, Hofmann A, Slack JF, Rouxel OJ, Konhauser KO (2014) Iron formations: their origins and implications for ancient seawater chemistry. In: *Treatise on Geochemistry* (eds Holland H, Turekian K). Elsevier Ltd, Waltham, MA, USA, pp. 561-628.
- Bekker A, Slack JF, Planavsky N, Krapež B, Hofmann A, Konhauser KO, Rouxel OJ (2010) Iron formation: the sedimentary product of a complex interplay among mantle, tectonic, oceanic, and biospheric processes. *Economic Geology*, **105**, 467-508.
- Bénézech P, Dandurand JL, Harrichoury JC (2009) Solubility product of siderite (FeCO<sub>3</sub>) as a function of temperature (25–250 °C). *Chemical Geology*, **265**, 3-12.
- Bland JA, Staley JT (1978) Observations on the biology of Thiobacillus. *Archives of Microbiology*, **117**, 79-87.
- Brune A, Frenzel P, Cypionka H (2000) Life at the oxic-anoxic interface: microbial activities and adaptations. *Federation of European Microbiological Societies Microbiology Reviews*, **24**, 691-710.
- Busigny V, Planavsky NJ, Jézéquel D, Crowe S, Louvat P, Moureau J, Viollier E, Lyons TW (2014) Iron isotopes in an Archean ocean analogue. *Geochimica et Cosmochimica Acta*, **133**, 443-462.
- Canfield DE (1998) A new model for Proterozoic ocean chemistry. *Nature*, **396**, 450-453.
- Canfield DE (2005) The early history of atmospheric oxygen: Homage to Robert M. Garrels. *Annual Review of Earth and Planetary Sciences*, **33**, 1-36.
- Canfield DE, Poulton SW, Knoll AH, Narbonne GM, Ross G, Goldberg T, Strauss H (2008) Ferruginous conditions dominated later Neoproterozoic deep-water chemistry. *Science*, **321**, 949-952.
- Canfield DE, Farquhar J, Zerkle AL (2010) High isotope fractionations during sulfate reduction in a low-sulfate euxinic ocean analog. *Geology*, **38**, 415-418.
- Cline JD (1969) Spectrophotometric determination of hydrogen sulfide in natural waters. *Limnology and Oceanography*, **14**, 454-458.
- Cornell RM, Schwertmann U (2003) The iron oxides: structure, properties, reactions, occurrences and uses. Wiley-VCH, Weinheim.
- Crosby CH, Bailey JV, Sharma M (2014) Fossil evidence of iron-oxidizing chemolithotrophy linked to phosphogenesis in the wake of the Great Oxidation Event. *Geology*, **42**, 1015-1018.

- Crowe SA, Jones C, Katsev S, Magen C, O'Neill AH, Sturm A, Canfield DE, Haffner GD, Mucci A, Sundby B (2008) Photoferrotrophs thrive in an Archean Ocean analogue. *Proceedings of the National Academy of Sciences*, **105**, 15938-15943.
- Czaja AD, Johnson CM, Beard BL, Roden EE, Li WQ, Moorbath S (2013) Biological Fe oxidation controlled deposition of banded iron formation in the ca. 3770 Ma Isua Supracrustal Belt (West Greenland). *Earth and Planetary Science Letters*, **363**, 192-203.
- Davison W (1991) The solubility of iron sulphides in synthetic and natural waters at ambient temperature. *Aquatic Sciences*, **53**, 309-329.
- Dodd MS, Papineau D, Grenne T, Slack JF, Rittner M, Pirajno F, O'Neil J, Little CTS (2017) Evidence for early life in Earth's oldest hydrothermal vent precipitates. *Nature*, **543**, 60-64.
- Domes H, Leupold O, Nagy DL, Ritter G, Spiering H, Molnár B, Szücs IS (1986) Mössbauer study of short range order in frozen aqueous solutions of Fe(ClO<sub>4</sub>)<sub>2</sub>. *The Journal of Chemical Physics*, **85**, 7294-7300.
- Edgar RC, Haas BJ, Clemente JC, Quince C, Knight R (2011) UCHIME improves sensitivity and speed of chimera detection. *Bioinformatics*, **27**, 2194-2200.
- Emerson D, Floyd MM (2005) Enrichment and isolation of iron-oxidizing bacteria at neutral pH. *Methods in Enzymology*, **397**, 112-123.
- Eusterhues K, Wagner FE, Häusler W, Hanzlik M, Knicker H, Totsche KU, Kögel-Knabner I, Schwertmann U (2008) Characterization of ferrihydrite-soil organic matter coprecipitates by x-ray diffraction and Mössbauer spectroscopy. *Environmental Science & Technology*, **42**, 7891-7897.
- Fennel K, Follows M, Falkowski PG (2005) The co-evolution of the nitrogen, carbon and oxygen cycles in the Proterozoic ocean. *American Journal of Science*, **305**, 526-545.
- Godfrey LV, Falkowski PG (2009) The cycling and redox state of nitrogen in the Archean ocean. *Nature Geoscience*, **2**, 725-729.
- Grotzinger JP, Kasting JF (1993) New constraints on Precambrian ocean composition. *The Journal of Geology*, **101**, 235-243.
- Halevy I, Bachan I (2017) The geologic history of seawater pH. *Science*, **355**, 1069-1071.
- Halevy I, Alesker M, Schuster EM, Popovitz-Biro R, Feldman Y (2017) A key role for green rust in the Precambrian oceans and the genesis of iron formations. *Nature Geoscience*, **10**, 135-139
- Hardisty DS, Lu Z, Planasky NJ, Bekker A, Philippot P, Zhou X, Lyons TW (2014) An iodine record of Paleoproterozoic surface ocean oxygenation. *Geology*, **42**, 619-622.
- Hegler F, Posth NR, Jiang J, Kappler A (2008) Physiology of phototrophic iron(II)-oxidizing bacteria: implications for modern and ancient environments. *Federation of European Microbiological Societies Microbiology Ecology*, **66**, 250-260.

- Hegler F, Lösekann-Behrens T, Hanselmann K, Behrens S, Kappler A (2012) Influence of seasonal and geochemical changes on the geomicrobiology of an iron carbonate mineral water spring. *Applied and Environmental Microbiology*, **78**, 7185-7196.
- Holland HD (2006) The oxygenation of the atmosphere and oceans. *Philosophical Transactions of the Royal Society B: Biological Sciences*, **361**, 903-915.
- Hopwood MJ, Statham PJ, Skrabal SA, Willey JD (2015) Dissolved iron(II) ligands in river and estuarine water. *Marine Chemistry*, **173**, 173-182.
- Huse SM, Welch DM, Morrison HG, Sogin ML (2010) Ironing out the wrinkles in the rare biosphere through improved OTU clustering. *Environmental Microbiology*, **12**, 1889-1898.
- Jambor JL, Dutrizac JE (1998) Occurrence and constitution of natural and synthetic ferrihydrite, a widespread iron oxyhydroxide. *Chemical Reviews*, **98**, 2549-2585.
- James RE, Ferris FG (2004) Evidence for microbial-mediated iron oxidation at a neutrophilic groundwater spring. *Chemical Geology*, **212**, 301-311.
- Jamieson JW, Wing BA, Farquhar J, Hannington MD (2013) Neoproterozoic seawater sulphate concentrations from sulphur isotopes in massive sulphide ore. *Nature Geoscience*, **6**, 61-64.
- Jeandey C, Oddou JL, Mattei JL, Fillion G (1991) Mössbauer investigation of the pyrrhotite at low temperature. *Solid State Communications*, **78**, 195-198.
- Johnson CM, Beard BL, Klein C, Beukes NJ, Roden EE (2008) Iron isotopes constrain biologic and abiologic processes in banded iron formation genesis. *Geochimica et Cosmochimica Acta*, **72**, 151-169.
- Kappler A, Newman DK (2004) Formation of Fe(III)-minerals by Fe(II)-oxidizing photoautotrophic bacteria. *Geochimica et Cosmochimica Acta*, **68**, 1217-1226.
- Kah LC, Lyons TW, Frank TD (2004) Low marine sulphate and protracted oxygenation of the Proterozoic biosphere. *Nature*, **431**, 834-838.
- Koeksoy E, Halama M, Konhauser KO, Kappler A (2016) Using modern ferruginous habitats to interpret Precambrian banded iron formation deposition. *International Journal of Astrobiology*, **15**, 205-217.
- Klein C (2005) Some Precambrian banded iron-formations (BIFs) from around the world: Their age, geologic setting, mineralogy, metamorphism, geochemistry, and origin. *American Mineralogist*, **90**, 1473-1499.
- Knauth LP (2005) Temperature and salinity history of the Precambrian ocean: implications for the course of microbial evolution. *Paleogeography, Paleoclimatology, Paleoecology*, **219**, 53-69.
- Konhauser KO, Lalonde SV, Amskold L, Holland HD (2007) Was there really an Archean phosphate crisis? *Science*, **315**, 1234.
- Konhauser KO, Kappler A, Roden EE (2011) Iron in microbial metabolisms. *Elements*, **7**, 89-93.

- Lane DJ (1991) 16S/23S rRNA sequencing. In: *Nucleic Acid Techniques in Bacterial Systematics* (eds Stackebrandt E, Godfellow, M. ). Wiley, New York, pp. 115-175.
- Larese-Casanova P, Kappler A, Haderlein SB (2012) Heterogeneous oxidation of Fe(II) on iron oxides in aqueous systems: identification and controls of Fe(III) product formation. *Geochimica et Cosmochimica Acta*, **91**, 171-186.
- Laufer K, Byrne JM, Glombitze C, Schmidt C, Jorgensen BB, Kappler A (2016) Anaerobic microbial Fe(II) oxidation and Fe(III) reduction in coastal marine sediments controlled by organic carbon content. *Environmental Microbiology*, **18**, 3159–3174.
- Li W, Beard BL, Johnson CM (2015) Biologically recycled continental iron is a major component in banded iron formations. *Proceedings of the National Academy of Science*, **112**, 8193-8198.
- Liu ZZ, Lozupone C, Hamady M, Bushman FD, Knight R (2007) Short pyrosequencing reads suffice for accurate microbial community analysis. *Nucleic Acids Research*, **35**.
- Llirós M, García-Armisen T, Darchambeau F, Morana C, Triadó-Margarit X, Inceoğlu Ö, Borrego CM, Bouillon S, Servais P, Borges AV, Descy JP, Canfield DE, Crowe SA (2015) Pelagic photoferrotrophy and iron cycling in a modern ferruginous basin. *Scientific Reports*, **5**, 13803.
- Lohmayer R, Kappler A, Lösekann-Behrens T, Planer-Friedrich B (2014) Sulfur species as redox partners and electron shuttles for ferrihydrite reduction by *Sulfurospirillum deleyianum*. *Applied and Environmental Microbiology*, **80**, 3141-3149.
- Luther GW, Rickard DT (2005) Metal sulfide cluster complexes and their biogeochemical importance in the environment. *Journal of Nanoparticle Research*, **7**, 389-407.
- Luther GW, Findlay AJ, Macdonald DJ, Owings SM, Hanson TE, Beinart RA, Girguis PR (2011) Thermodynamics and kinetics of sulfide oxidation by oxygen: a look at inorganically controlled reactions and biologically mediated processes in the environment. *Frontiers in Microbiology*, **2**.
- Lyons TW (2008) Ironing out ocean chemistry at the dawn of animal life. *Science*, **321**, 923-924.
- Lyons TW, Reinhard CT, Planavsky NJ (2014) The rise of oxygen in Earth's early ocean and atmosphere. *Nature*, **506**, 307-315.
- Michiels CC, Darchambeau F, Roland FA, Morana C, Lliros M, García-Armisen T, Thamdrup B, Borges AV, Canfield DE, Servais P (2017) Iron-dependent nitrogen cycling in a ferruginous lake and the nutrient status of Proterozoic oceans. *Nature Geoscience*, **10**, 217-221.
- Millero FJ (1985) The effect of ionic interactions on the oxidation of metals in natural waters. *Geochimica et Cosmochimica Acta*, **49**, 547-553.
- Millero FJ, Sotolongo S, Izaguirre M (1987a) The oxidation kinetics of Fe(II) in seawater. *Geochimica et Cosmochimica Acta*, **51**, 793-801.

- Millero FJ, Hubinger S, Fernandez M, Garnett S (1987b) Oxidation of H<sub>2</sub>S in seawater as a function of temperature, pH, and ionic strength. *Environmental Science and Technology*, **21**, 439-443.
- Montano PA, Seehra MS (1976) Magnetism of iron pyrite (FeS<sub>2</sub>) — a Mössbauer study in an external magnetic field. *Solid State Communications*, **20**, 897-898.
- Nielsen PH, De Muro MA, Nielsen JL (2000) Studies on the in situ physiology of *Thiothrix* spp. present in activated sludge. *Environmental Microbiology*, **2**, 389-398.
- Oblinger JL, Koburger JA (1975) Understanding and teaching most probable number technique. *Journal of Milk and Food Technolgy*, **38**, 540-545.
- Olson SL, Kump LR, Kasting JF (2013) Quantifying the areal extent and dissolved oxygen concentrations of Archean oxygen oases. *Chemical Geology*, **362**, 35-43.
- Pham AN, Waite TD (2008) Oxygenation of Fe(II) in natural waters revisited: Kinetic modeling approaches, rate constant estimation and the importance of various reaction pathways. *Geochimica et Cosmochimica Acta*, **72**, 3616-3630.
- Pinti LD (2005) The origin and evolution of the oceans. In: *Lectures in Astrobiology* (eds Gargaud M, Barbier B, Martin H, Reisse J). Springer, Heidelberg, pp 83-112.
- Planavsky N, Rouxel O, Bekker A, Shapiro R, Fralick P, Knudsen A (2009) Iron-oxidizing microbial ecosystems thrived in late Paleoproterozoic redox-stratified oceans. *Earth and Planetary Science Letters*, **286**, 230-242.
- Planavsky NJ, Mcgoldrick P, Scott CT, Li C, Reinhard CT, Kelly AE, Chu X, Bekker A, Love GD, Lyons TW (2011) Widespread iron-rich conditions in the mid-Proterozoic ocean. *Nature*, **477**, 448-451.
- Planavsky NJ, Reinhard CT, Wang X, Thomson D, Mcgoldrick P, Rainbird RH, Johnson T, Fischer WW, Lyons TW (2014) Low Mid-Proterozoic atmospheric oxygen levels and the delayed rise of animals. *Science*, **346**, 635-638.
- Porsch K, Kappler A (2011) Fe<sup>II</sup> oxidation by molecular O<sub>2</sub> during HCl extraction. *Environmental Chemistry*, **8**, 190-197.
- Poulton SW, Fralick PW, Canfield DE (2004) The transition to a sulphidic ocean ~1.84 billion years ago. *Nature*, **431**, 173-177.
- Poulton SW, Fralick PW, Canfield DE (2010) Spatial variability in oceanic redox structure 1.8 billion years ago. *Nature Geoscience*, **3**, 486-490.
- Poulton SW, Canfield DE (2011) Ferruginous conditions: A dominant feature of the ocean through Earth's history. *Elements*, **7**, 107-112.
- Pruesse E, Quast C, Knittel K, Fuchs BM, Ludwig WG, Peplies J, Glockner FO (2007) SILVA: a comprehensive online resource for quality checked and aligned ribosomal RNA sequence data compatible with ARB. *Nucleic Acids Research*, **35**, 7188-7196.
- Quince C, Lanzen A, Curtis TP, Davenport RJ, Hall N, Head IM, Read LF, Sloan WT (2009) Accurate determination of

- microbial diversity from 454 pyrosequencing data. *Nature Methods*, **6**, 639-641.
- Rancourt D, Ping J (1991) Voigt-based methods for arbitrary-shape static hyperfine parameter distributions in Mössbauer spectroscopy. *Nuclear Instruments and Methods in Physics Research Section B: Beam Interactions with Materials and Atoms*, **58**, 85-97.
- Reinhard CT, Raiswell R, Scott C, Anbar AD, Lyons TW (2009) A late Archean sulfidic sea stimulated by early oxidative weathering of the continents. *Science*, **326**, 713-716.
- Rickard D (2006) The solubility of FeS. *Geochimica et Cosmochimica Acta*, **70**, 5779-5789.
- Rickard D, Luther GW (2007) Chemistry of iron sulfides. *Chemical Reviews*, **107**, 514-562.
- Robert F, Chaussidon M (2006) A paleotemperature curve for the Precambrian oceans based on silicon isotopes in cherts. *Nature*, **443**, 969-972.
- Rush JD, Bielski BH (1985) Pulse radiolytic studies of the reaction of HO<sub>2</sub>/O<sub>2</sub><sup>-</sup> with Fe(II)/Fe(III) ions. The reactivity of HO<sub>2</sub>/O<sub>2</sub><sup>-</sup> with ferric ions and its implication on the occurrence of the Haber-Weiss reaction. *The Journal of Physical Chemistry*, **89**, 5062-5066.
- Schädler S, Burkhardt C, Kappler A (2008) Evaluation of electron microscopic sample preparation methods and imaging techniques for characterization of cell-mineral aggregates. *Geomicrobiology Journal*, **25**, 228-239.
- Schloss PD, Handelsman J (2005) Introducing DOTUR, a computer program for defining operational taxonomic units and estimating species richness. *Applied and Environmental Microbiology*, **71**, 1501-1506.
- Schloss PD, Westcott SL, Ryabin T, Hall JR, Hartmann M, Hollister EB, Lesniewski RA, Oakley BB, Parks DH, Robinson CJ, Sahl JW, Stres B, Thallinger GG, Van Horn DJ, Weber CF (2009) Introducing mothur: open-source, platform-independent, community-supported software for describing and comparing microbial communities. *Applied and Environmental Microbiology*, **75**, 7537-7541.
- Schloss PD, Westcott SL (2011) Assessing and improving methods used in operational taxonomic unit-based approaches for 16S rRNA gene sequence analysis. *Applied and Environmental Microbiology*, **77**, 3219-3226.
- Schopf JW, Kudryavtsev AB, Walter MR, Van Kranendonk MJ, Williford KH, Kozdon R, Valley JW, Gallardo VA, Espinoza C, Flannery DT (2015) Sulfur-cycling fossil bacteria from the 1.8-Ga Duck Creek Formation provide promising evidence of evolution's null hypothesis. *Proceedings of the National Academy of Sciences*, **112**, 2087-2092.
- Shimizu M, Zhou JH, Schroder C, Obst M, Kappler A, Borch T (2013) Dissimilatory reduction and transformation of ferrihydrite-humic acid coprecipitates. *Environmental Science and Technology*, **47**, 13375-13384.

- Statham PJ, Jacobson Y, Van Den Berg CMG (2012) The measurement of organically complexed Fe<sup>II</sup> in natural waters using competitive ligand reverse titration. *Analytica Chimica Acta*, **743**, 111-116.
- Stookey LL (1970) Ferrozine - a new spectrophotometric reagent for iron. *Analytical Chemistry*, **42**, 779-781.
- Straub KL, Kappler A, Schink B (2005) Enrichment and isolation of ferric-iron- and humic-acid-reducing bacteria. *Methods in Enzymology*, **397**, 58-77.
- Strauss H, Chmiel H, Christ A, Fugmann A, Hanselmann K, Kappler A, Koniger P, Lutter A, Siedenberg K, Teichert BMA (2016) Multiple sulphur and oxygen isotopes reveal microbial sulphur cycling in spring waters in the Lower Engadin, Switzerland. *Isotopes in Environmental and Health Studies*, **52**, 75-93.
- Tang D, Shi X, Wang X, Jiang G (2016) Extremely low oxygen concentration in mid-Proterozoic shallow seawater. *Precambrian Research*, **276**, 145-157.
- Walter XA, Picazo A, Miracle MR, Vicente E, Camacho A, Aragno M, Zopfi J (2014) Phototrophic Fe(II)-oxidation in the chemocline of a ferruginous meromictic lake. *Frontiers in Microbiology*, **5**, 713.
- Wang Q, Garrity GM, Tiedje JM, Cole JR (2007) Naive Bayesian classifier for rapid assignment of rRNA sequences into the new bacterial taxonomy. *Applied and Environmental Microbiology*, **73**, 5261-5267.
- Yao WS, Millero FJ (1996) Oxidation of hydrogen sulfide by hydrous Fe(III) oxides in seawater. *Marine Chemistry*, **52**, 1-16.
- Zhao CM, Campbell PGC, Wilkinson KJ (2016) When are metal complexes bioavailable? *Environmental Chemistry*, **13**, 425-433.



**SUPPLEMENTAL INFORMATION FOR**

**A case study for late Archean and Proterozoic  
biogeochemical iron- and sulphur-cycling in a modern  
habitat – the Arvadi Spring**

Elif Koeksoy<sup>1</sup>, Maximilian Halama<sup>1</sup>, Nikolas Hagemann<sup>1</sup>, Pascal R. Weigold<sup>1</sup>, Katja Laufer<sup>1,6</sup>,  
Sara Kleindienst<sup>1</sup>, James M. Byrne<sup>1</sup>, Anneli Sundman<sup>1</sup>, Kurt Hanselmann<sup>2</sup>, Itay Halevy<sup>3</sup>,  
Ronny Schoenberg<sup>4</sup>, Kurt O. Konhauser<sup>5</sup> and Andreas Kappler<sup>1,6\*</sup>

<sup>1</sup>Geomicrobiology, Center for Applied Geosciences, University of Tuebingen, Germany

<sup>2</sup>Geological Institute, ETH Zuerich, Switzerland

<sup>3</sup>Earth and Planetary Sciences, Weizmann Institute of Science, Israel

<sup>4</sup>Isotope Geochemistry, University of Tuebingen, Germany

<sup>5</sup> Earth and Atmospheric Sciences, University of Alberta, Canada

<sup>6</sup>Bioscience, Center for Geomicrobiology, Aarhus University, Denmark

Accepted for publication in: *Geobiology*

**SI. 1: Metabolism-selective growth media.** All media were prepared anoxically with a N<sub>2</sub>:CO<sub>2</sub> (90:10) headspace and were buffered with 30 mM NaHCO<sub>3</sub>. FW medium contained following salts per litre: 0.6 g of KH<sub>2</sub>PO<sub>4</sub>, 0.3 g of NH<sub>4</sub>Cl, 0.025 g of MgSO<sub>4</sub>\*7H<sub>2</sub>O, 0.4 g of MgCl<sub>2</sub>\*6H<sub>2</sub>O and 0.1 g of CaCl<sub>2</sub>\*2H<sub>2</sub>O. BM medium contained following salts per litre: 1.0 g of NaCl, 0.4 g of MgCl<sub>2</sub>\*6H<sub>2</sub>O, 0.15 g of CaCl<sub>2</sub>\*2H<sub>2</sub>O, 0.2 g of KH<sub>2</sub>PO<sub>4</sub>, 0.5 g of KCl, 0.25 g of NH<sub>4</sub>Cl. MWMM contained following salt per litre: 0.1 g of NH<sub>4</sub>Cl, 0.2 g of MgSO<sub>4</sub>\*7H<sub>2</sub>O, 0.1 g of CaCl<sub>2</sub>\*2H<sub>2</sub>O and 0.05 g of K<sub>2</sub>HPO<sub>4</sub>. The pH was adjusted to 7.2 with either 1 M HCl or 0.5 M Na<sub>2</sub>CO<sub>3</sub>. Trace metals (selenite-tungstate solution & SL10 solution after Widdel et al., 1983) and vitamins (7-vitamine solution after Widdel & Pfennig, 1981) were added to all media in same amounts (1 ml L<sup>-1</sup>), metabolism selectivity was established by the addition of different electron donors and acceptors to respective media.

**SI. 2: MPN experiments with anaerobic Fe- and S- metabolizers.** MPN counts for anaerobic Fe- and S-metabolizers were performed in 96-deep-well microtiter plates (Laufer et al., 2016). One MPN plate was prepared per sampling location and per type of bacterial metabolism. First, 900 µL of growth medium with respective metabolism-selective additives were dispersed to the test wells and inoculated with 100 µL of previously prepared sample dilutions in seven replicates. One row of negative control wells contained 1000 µL of medium without inoculum. After pipetting, plates were sealed with transparent plastic foils and inserted into incubation bags. In order to provide anoxic growth conditions, oxygen consuming catalyst bags (Anaerocult® A mini, Merck GmbH, Germany) and redox indicator stripes (Anaerotest®, Merck GmbH, Germany) were inserted to each incubation bag. The incubation bags were sealed oxygen-tight with Anaeroclip® (Merck GmbH, Germany) plastic clips. Plates were prepared under anoxic conditions in a glove box (100% N<sub>2</sub>) and were incubated afterwards for 8 to 10 weeks at 20°C under metabolism-selective conditions. MPN plates for the cultivation of phototrophic iron(II)-oxidizers were incubated under infra-red (IR) light (>730 nm) in order to prevent growth of cyanobacteria. IR light conditions were provided in a dark incubation box with an IR light filter on top, through which only the IR

spectrum of a 40 W bulb could pass. MPN plates for the cultivation of nitrate-reducing iron(II)-oxidizers, iron(III)-reducers and sulphate-reducers were incubated in the dark.

**SI. 3: MPN experiments with microaerophilic Fe- and S-metabolizers.** MPN counts for microaerophilic iron(II)- and sulphide-oxidizers were performed in gradient tubes. Gradient tubes were prepared two days prior to inoculation in order to enable establishment of electron donor and acceptor gradients. For this, an electron donor (iron(II) or sulphide) and agarose-containing bottom layer was prepared either with FeS or Na<sub>2</sub>S. After solidification in the test tube, the bottom layer was overlain by a MWMM top layer. The whole procedure was performed anoxically in order to prevent oxidation of the electron donors. Tubes were inoculated in duplicates with the same sample dilutions as used for anaerobic MPNs. Thereby, tubes were opened for 1 minute under sterile conditions to let air enter the tube headspace in order to create an oxygen gradient from the top to the bottom of each tube. Afterwards, 100 µL of sample were injected homogeneously with a syringe starting at about 0.5 cm above the bottom layer over the whole length of the top layer. Tubes were closed air-tight and incubated for 2-3 days at 20°C in the dark.

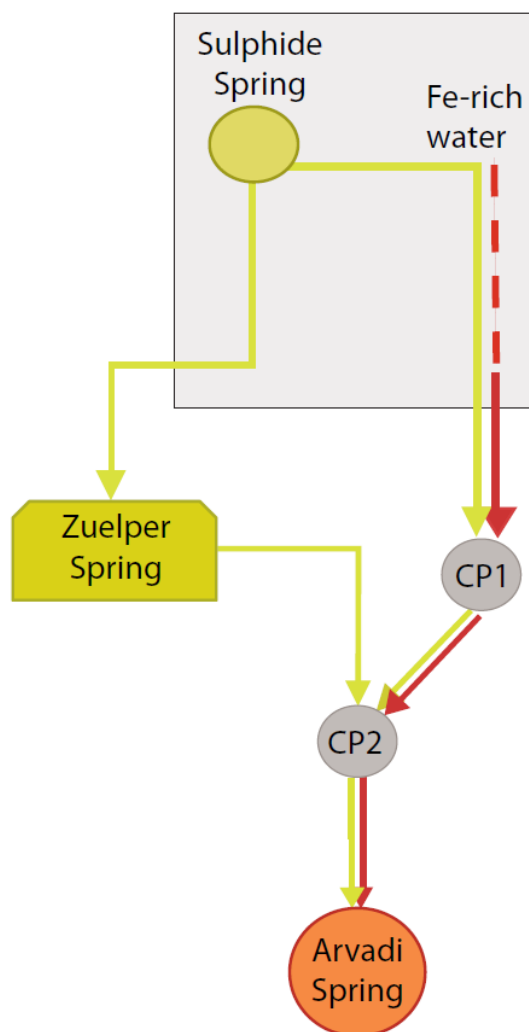


**Figure S1:** Water flow scheme between the Sulphide Spring, Zuelper Spring, Fe-rich waters and the Arvadi Spring. The grey shaded rectangle indicates the inaccessible concrete tunnel, in which the Sulphide Spring is located that is the parental water source to Arvadi Spring sulphide. Also, Fe-rich waters with unknown source emanate in the tunnel and get mixed with sulphide-rich water. In an intermixed form, the Fe- and S-rich water is transported through a pipe system to connection points 1 and 2 (CP1, CP2). From the latter, water samples were taken for Fe(II), Fe(tot) and sulphide quantification. Fe-S-rich water further gets transported to the Arvadi Spring pond where it crops out. The Sulphide Spring water additionally flows into the Zuelper Spring, where no Fe-rich water is introduced. Zuelper Spring water flows additionally into CP2 and further to the Arvadi Spring pond.

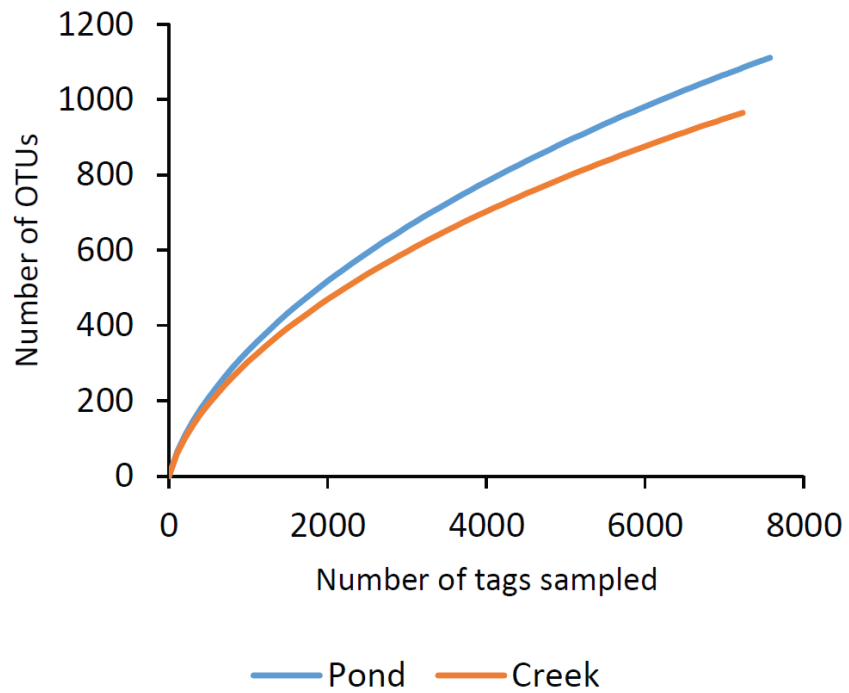


**Figure S2:** Rarefaction curves representing the number of observed OTUs in the Arvadi Spring pond and creek bacterial community based on OTU clustering at a genetic distance of 3%.

**Table S1:** Major geochemical parameters in Arvadi Spring water at different locations.

<b>location</b>	<b>pH</b>	<b>T [°C]</b>	<b>O<sub>2</sub> [mg L<sup>-1</sup>]</b>	<b>O<sub>2</sub> [%]</b>	<b>σ [μS cm<sup>-1</sup>]</b>
<b>1</b>	7.9	7.2	10.8	101.1	1442.0
<b>2</b>	8.0	7.3	10.9	100.7	1450.0
<b>3</b>	8.0	7.0	11.0	100.8	1450.0
<b>4</b>	8.0	7.0	10.9	100.4	1449.0
<b>5</b>	8.1	6.8	11.0	101.0	1450.0
<b>6</b>	8.2	5.8	11.2	99.7	1436.0
<b>7</b>	8.1	6.7	11.0	111.1	1450.0

---

Numbers of different locations refer to numbers in Fig. 1

---

**Table S2:** Concentrations of major anions [ $\mu\text{M}$ ] in Arvadi Spring water at different locations.

location	F <sup>-</sup>	Cl <sup>-</sup>	NO <sub>2</sub> <sup>-</sup>	Br <sup>-</sup>	NO <sub>3</sub> <sup>-</sup>	PO <sub>4</sub> <sup>3-</sup>	SO <sub>4</sub> <sup>2-</sup>
1	96.7	14.0	b.d.l.	b.d.l.	b.d.l.	b.d.l.	8268.5
2	98.4	14.6	b.d.l.	b.d.l.	b.d.l.	b.d.l.	8357.2
3	97.7	15.6	b.d.l.	b.d.l.	b.d.l.	b.d.l.	8337.3
4	100.6	15.2	b.d.l.	b.d.l.	b.d.l.	b.d.l.	8307.7
5	100.7	15.5	b.d.l.	b.d.l.	b.d.l.	b.d.l.	8344.1
6	96.8	15.4	b.d.l.	b.d.l.	b.d.l.	b.d.l.	8165.7
7	100.0	15.5	b.d.l.	b.d.l.	b.d.l.	b.d.l.	8317.5

---

b.d.l.= below detection limit

Numbers of different locations refer to numbers in Fig. 1

---

**Table S3:** Overview of major cations [ $\mu\text{M}$ ] in Arvadi Spring water at different locations.

<b>location</b>	<b>Na<sup>+</sup></b>	<b>NH<sub>4</sub><sup>+</sup></b>	<b>K<sup>+</sup></b>	<b>Mg<sup>2+</sup></b>	<b>Ca<sup>2+</sup></b>
<b>1</b>	38.9	b.d.l.	26.1	3251.6	6981.0
<b>2</b>	39.1	b.d.l.	26.4	3275.8	7038.6
<b>3</b>	39.5	b.d.l.	26.4	3272.7	7062.3
<b>4</b>	39.4	b.d.l.	27.0	3245.9	7044.3
<b>5</b>	39.8	b.d.l.	26.9	3269.6	7061.3
<b>6</b>	39.1	b.d.l.	26.8	3208.4	6909.5
<b>7</b>	39.5	b.d.l.	27.3	3280.4	7095.1

---

b.d.l.= below detection limit

Numbers of different locations refer to numbers in Fig. 1

---



**Table S4:** Overview of total carbon (TC), total inorganic carbon (TIC) and dissolved organic carbon (DOC) content [mg/L] in Arvadi Spring water at different locations.

<b>location</b>	<b>TIC</b>	<b>DOC</b>	<b>TC</b>
<b>1</b>	49.9	3.5	53.4
<b>2</b>	49.8	3.7	53.5
<b>3</b>	49.8	2.4	52.2
<b>4</b>	49.5	3.6	53.1
<b>5</b>	49.2	3.6	52.7
<b>6</b>	48.6	3.0	51.6
<b>7</b>	50.3	1.8	52.1

---

Numbers of different locations refer to numbers in Fig. 1

---

**Table S5:** Mössbauer data collected for red flocs at 77K and 4.2K.

<b>T</b> <b>[K]</b>			<b>CS</b> <b>[mm/s]</b>	<b><math>\epsilon/QS</math></b> <b>[mm/s]</b>	<b>H</b> <b>[T]</b>	<b><math>\sigma</math></b> <b>[mm/s]</b>	<b>pop</b> <b>[%]</b>	<b><math>\chi^2</math></b>
<b>77</b>	Db1	Fe(III) (oxyhydr)oxide	0.5	1.0		0.4	58.0	0.6
	Db2	Fe(III) (oxyhydr)oxide	0.4	4.3		5.0	12.7	
	Db3	Fe(II) sulphide	0.5	0.6		0.2	21.0	
	Db4	Fe(II)	1.3	2.7		0.2	9.1	
<b>4.2</b>	Db1	Fe(II)	1.3	2.7		0.8	4.4	0.7
	Db2	Unknown	0.2	0.9		0.3	3.7	
	S1	Fe(III) (oxyhydr)oxide	0.5	0.0	49.1	1.7	18.9	
	S2	Fe(III) (oxyhydr)oxide	0.4	0.0	46.2	4.1	37.4	
	S3	Fe(III) (oxyhydr)oxide	0.6	-0.1	47.6	2.9	26.7	
	S4	Poorly ordered Fe oxide	0.7	-0.01	22.4	2.8	8.8	

Db = doublet

S = sextet

CS = centre shift

 $\epsilon/QS$  = shift/quadrupole splitting

H = hyperfine field

 $\sigma$  = Gauss' sigma parameter

pop = population

 $\chi^2$  = goodness of fitting

**Table S6:** Bacterial genera (including the number of sequences and relative sequence abundance per genus, respectively) in the Arvadi Spring pond and creek sediment samples.

Genus	No. of sequences		Rel. sequence abundance[%]	
	Pond	Creek	Pond	Creek
<i>Acetivibrio</i>	0	1	0.00	0.01
<i>Acidaminobacter</i>	2	1	0.03	0.01
<i>Acidiferrobacter</i>	26	38	0.34	0.53
<i>Acidisoma</i>	1	0	0.01	0.00
<i>Aciditerrimonas</i>	2	1	0.03	0.01
<i>Acidithiobacillus</i>	2	1	0.03	0.01
<i>Acidovorax</i>	1	0	0.01	0.00
<i>Actinomycetospora</i>	0	1	0.00	0.01
<i>Adhaeribacter</i>	0	1	0.00	0.01
<i>Afipia</i>	14	9	0.18	0.12
AKYG587	7	4	0.09	0.06
<i>Albidiferax</i>	55	23	0.73	0.32
<i>Amaricoccus</i>	9	0	0.12	0.00
<i>Anaerolinea</i>	1	0	0.01	0.00
<i>Anaeromyxobacter</i>	4	1	0.05	0.01
<i>Aquicella</i>	2	0	0.03	0.00
<i>Aquimonas</i>	7	13	0.09	0.18
<i>Arcobacter</i>	1	0	0.01	0.00
<i>Arcticibacter</i>	0	2	0.00	0.03
<i>Arenimonas</i>	89	49	1.17	0.68
<i>Armatimonas</i>	3	1	0.04	0.01
<i>Asticcacaulis</i>	11	2	0.15	0.03
<i>Aureimonas</i>	0	1	0.00	0.01
<i>Aureispira</i>	1	1	0.01	0.01

<i>Azotobacter</i>	0	1	0.00	0.01
<i>Bacteriovorax</i>	3	0	0.04	0.00
<i>Bacteroides</i>	0	1	0.00	0.01
<i>Bauldia</i>	5	2	0.07	0.03
<i>Bdellovibrio</i>	6	7	0.08	0.10
<i>Blastocatella</i>	70	67	0.92	0.93
<i>Blastopirellula</i>	3	1	0.04	0.01
<i>Bosea</i>	3	4	0.04	0.06
<i>Brasilonema</i>	77	1	1.02	0.01
<i>Brevundimonas</i>	87	60	1.15	0.83
<i>Bryobacter</i>	11	17	0.15	0.24
<i>Caenimonas</i>	0	4	0.00	0.05
<i>Calothrix</i>	13	0	0.17	0.00
<i>Candidatus Accumulibacter</i>	1	0	0.01	0.00
<i>Candidatus Alysiosphaera</i>	1	1	0.01	0.01
<i>Candidatus Amoebophilus</i>	10	7	0.13	0.10
<i>Candidatus Captivus</i>	0	1	0.00	0.01
<i>Candidatus Methylocidiphilum</i>	4	0	0.05	0.00
<i>Candidatus Microthrix</i>	1	3	0.01	0.04
<i>Candidatus Nostocoida</i>	1	1	0.01	0.01
<i>Candidatus Solibacter</i>	2	0	0.03	0.00
<i>Candidatus Xiphinematobacter</i>	1	0	0.01	0.00
<i>Chitinimonas</i>	3	0	0.04	0.00
<i>Chitinophaga</i>	7	15	0.09	0.21
<i>Christensenella</i>	1	0	0.01	0.00
<i>Chroococcidiopsis</i>	2	1	0.03	0.01
<i>Chryseolinea</i>	61	43	0.81	0.59
<i>Chthoniobacter</i>	1	3	0.01	0.04
<i>Chthonomonas</i>	1	1	0.01	0.01

CL500-29 marine group	13	16	0.17	0.22
CL500-3	2	2	0.03	0.03
<i>Clostridium sensu stricto</i> 1	1	2	0.01	0.03
<i>Coxiella</i>	0	1	0.00	0.01
<i>Crocinitomix</i>	1	5	0.01	0.07
<i>Cyanobium</i>	0	1	0.00	0.01
<i>Cytophaga</i>	1	1	0.01	0.01
<i>Dechloromonas</i>	1	0	0.01	0.00
<i>Deefgea</i>	0	1	0.00	0.01
<i>Defluviicoccus</i>	2	0	0.03	0.00
<i>Defluviimonas</i>	7	1	0.09	0.01
<i>Desulfatirhabdium</i>	1	1	0.01	0.01
<i>Desulfocapsa</i>	0	3	0.00	0.04
<i>Devosia</i>	3	7	0.04	0.10
<i>Dokdonella</i>	1	0	0.01	0.00
<i>Dongia</i>	2	0	0.03	0.00
<i>Dyadobacter</i>	1	5	0.01	0.07
<i>Elstera</i>	3	0	0.04	0.00
<i>Emticicia</i>	12	4	0.16	0.06
<i>Exiguobacterium</i>	1	0	0.01	0.00
<i>Falsirhodobacter</i>	2	3	0.03	0.04
<i>Ferrithrix</i>	1	1	0.01	0.01
<i>Ferruginibacter</i>	35	33	0.46	0.46
<i>Fibrella</i>	2	1	0.03	0.01
<i>Filomicrobium</i>	34	62	0.45	0.86
<i>Flaviramulus</i>	0	1	0.00	0.01
<i>Flavisolibacter</i>	1	1	0.01	0.01
<i>Flavitalea</i>	0	1	0.00	0.01
<i>Flavobacterium</i>	185	51	2.44	0.71

<i>Flectobacillus</i>	0	2	0.00	0.03
<i>Flexibacter</i>	1	0	0.01	0.00
<i>Fluviicola</i>	1	0	0.01	0.00
<i>Friedmanniella</i>	1	0	0.01	0.00
<i>Gaiella</i>	11	7	0.15	0.10
<i>Geitlerinema</i>	1	0	0.01	0.00
<i>Gemmata</i>	24	14	0.32	0.19
<i>Gemmatimonas</i>	31	18	0.41	0.25
<i>Gemmobacter</i>	250	180	3.30	2.49
<i>Giesbergeria</i>	1	0	0.01	0.00
<i>Gleocapsa</i>	0	2	0.00	0.03
<i>Granulicella</i>	1	1	0.01	0.01
<i>Haliangium</i>	5	13	0.07	0.18
<i>Haliscomenobacter</i>	100	45	1.32	0.62
<i>Haloferula</i>	8	1	0.11	0.01
<i>Hirschia</i>	26	36	0.34	0.50
<i>Hyalangium</i>	1	2	0.01	0.03
<i>Hydrogenophaga</i>	114	30	1.50	0.41
<i>Hymenobacter</i>	0	1	0.00	0.01
<i>Hyphomicrobium</i>	63	105	0.83	1.45
<i>Hyphomonas</i>	12	22	0.16	0.30
<i>Iamia</i>	2	0	0.03	0.00
<i>Ideonella</i>	3	1	0.04	0.01
<i>Ilumatobacter</i>	16	24	0.21	0.33
<i>Incertae Sedis</i>	1	3	0.01	0.04
<i>Inhella</i>	1	0	0.01	0.00
<i>Iodobacter</i>	1	2	0.01	0.03
<i>Leadbetterella</i>	13	1	0.17	0.01
<i>Leeia</i>	1	0	0.01	0.00

<i>Legionella</i>	7	10	0.09	0.14
<i>Leptolinea</i>	1	1	0.01	0.01
<i>Leptolyngbya</i>	338	101	4.46	1.40
<i>Leptospira</i>	6	9	0.08	0.12
<i>Leuconostoc</i>	1	0	0.01	0.00
<i>Lewinella</i>	115	96	1.52	1.33
<i>Litorilinea</i>	1	0	0.01	0.00
<i>Lysobacter</i>	2	0	0.03	0.00
<i>Mangroviflexus</i>	1	0	0.01	0.00
<i>Marmoricola</i>	0	1	0.00	0.01
<i>Megamonas</i>	0	1	0.00	0.01
<i>Meganema</i>	3	1	0.04	0.01
<i>Methylibium</i>	15	2	0.20	0.03
<i>Methylorosula</i>	0	1	0.00	0.01
<i>Microcoleus</i>	9	0	0.12	0.00
<i>Mycobacterium</i>	1	1	0.01	0.01
<i>Nakamurella</i>	0	4	0.00	0.06
<i>Nevskia</i>	2	6	0.03	0.08
<i>Niabella</i>	3	0	0.04	0.00
<i>Nitrospira</i>	21	23	0.28	0.32
<i>Nocardioides</i>	9	2	0.12	0.03
<i>Nodularia</i>	0	1	0.00	0.01
<i>Nordella</i>	10	8	0.13	0.11
<i>Nostoc</i>	113	2	1.49	0.03
<i>Novosphingobium</i>	1	1	0.01	0.01
<i>Oceanicella</i>	1	1	0.01	0.01
<i>Ohtaekwangia</i>	91	88	1.20	1.22
OM27 clade	25	43	0.33	0.59
<i>Opitutus</i>	7	0	0.09	0.00

<i>Paludibacter</i>	1	0	0.01	0.00
<i>Parasegetibacter</i>	2	0	0.03	0.00
<i>Parvularcula</i>	16	17	0.21	0.24
<i>Paucibacter</i>	2	0	0.03	0.00
<i>Pedobacter</i>	0	1	0.00	0.01
<i>Pedomicrobium</i>	10	2	0.13	0.03
<i>Pedosphaera</i>	2	1	0.03	0.01
<i>Peredibacter</i>	0	1	0.00	0.01
<i>Phormidium</i>	6	38	0.08	0.53
<i>Phycisphaera</i>	0	4	0.00	0.06
Pir4 lineage	16	17	0.21	0.24
<i>Pirellula</i>	12	16	0.16	0.22
<i>Piscinibacter</i>	1	0	0.01	0.00
<i>Planctomyces</i>	15	15	0.20	0.21
<i>Planktothrix</i>	0	2	0.00	0.03
<i>Polaromonas</i>	9	3	0.12	0.04
<i>Porphyrobacter</i>	7	3	0.09	0.04
<i>Portibacter</i>	4	7	0.05	0.10
<i>Prochlorothrix</i>	5	0	0.07	0.00
<i>Pseudanabaena</i>	32	33	0.42	0.46
<i>Pseudochrobactrum</i>	1	6	0.01	0.08
<i>Pseudofulvimonas</i>	5	3	0.07	0.04
<i>Pseudolabrys</i>	2	1	0.03	0.01
<i>Pseudomonas</i>	2	0	0.03	0.00
<i>Pseudonocardia</i>	4	1	0.05	0.01
<i>Pseudorhodoferax</i>	3	2	0.04	0.03
<i>Pseudospirillum</i>	1	0	0.01	0.00
<i>Pseudoxanthomonas</i>	7	1	0.09	0.01
<i>Reichenbachiella</i>	4	1	0.05	0.01



<i>Reyranela</i>	8	7	0.11	0.10
<i>Rhizobacter</i>	55	46	0.73	0.64
<i>Rhizobium</i>	30	6	0.40	0.08
<i>Rhodobium</i>	0	3	0.00	0.04
<i>Rhodopirellula</i>	3	3	0.04	0.04
<i>Rickettsia</i>	3	3	0.04	0.04
<i>Roseiflexus</i>	3	5	0.04	0.07
<i>Roseomonas</i>	25	11	0.33	0.15
<i>Rubellimicrobium</i>	1	0	0.01	0.00
<i>Rubribacterium</i>	7	7	0.09	0.10
<i>Rubrivirga</i>	1	0	0.01	0.00
<i>Rudanella</i>	1	0	0.01	0.00
<i>Runella</i>	2	0	0.03	0.00
<i>Sandaracinus</i>	1	3	0.01	0.04
<i>Sandarakinorhabdus</i>	93	50	1.23	0.69
<i>Sediminibacterium</i>	20	3	0.26	0.04
<i>Sideroxydans</i>	2	0	0.03	0.00
<i>Silanimonas</i>	5	4	0.07	0.06
<i>Singulisphaera</i>	1	0	0.01	0.00
<i>Siphonobacter</i>	2	0	0.03	0.00
SM1A02	35	33	0.46	0.46
<i>Solibacillus</i>	1	0	0.01	0.00
<i>Solirubrobacter</i>	0	2	0.00	0.03
<i>Spirosoma</i>	5	1	0.07	0.01
<i>Sporocytophaga</i>	1	0	0.01	0.00
<i>Stenotrophomonas</i>	0	1	0.00	0.01
<i>Steroidobacter</i>	4	3	0.05	0.04
<i>Subdoligranulum</i>	0	1	0.00	0.01
<i>Sulfuricella</i>	1	0	0.01	0.00

<i>Sulfuricurvum</i>	1	3	0.01	0.04
<i>Sulfuritalea</i>	0	1	0.00	0.01
<i>Sulfurospirillum</i>	3	0	0.04	0.00
<i>Sulfurovum</i>	106	124	1.40	1.71
<i>Tabrizicola</i>	21	11	0.28	0.15
<i>Taibaiella</i>	1	1	0.01	0.01
<i>Terrimonas</i>	50	33	0.66	0.46
<i>Thermomonas</i>	5	6	0.07	0.08
<i>Thiobacillus</i>	314	428	4.14	5.92
<i>Thiothrix</i>	1063	1241	14.03	17.16
<i>Turneriella</i>	0	6	0.00	0.08
Unclassified	3113	3480	41.09	48.13
<i>Undibacterium</i>	1	2	0.01	0.03
<i>Woodsholea</i>	17	20	0.22	0.28
<i>Xanthomonas</i>	1	0	0.01	0.00
<i>Zavarzinella</i>	4	0	0.05	0.00

---

**Table S7:** Richness estimators, diversity indices and observed OTU numbers of bacterial community in pond and creek sediment samples based on OTU clustering at a genetic distance of 3%.

	No. of sequences		OTUs	Richness		Diversity	
	Raw	Quality-filtered		Chao	ACE	Shannon	Simpson
<b>Pond</b>	13351	7576	1111	1954	2908	5.16	0.03
<b>Creek</b>	13049	7231	965	1519	2122	4.88	0.04

## REFERENCES

Widdel F, Pfennig N (1981) Studies on dissimilatory sulfate-reducing bacteria that decompose fatty acids. *Archives of Microbiology*, **129**, 396-400.

Widdel F, Kohring GW, Mayer F (1983) Studies on dissimilatory sulfate-reducing bacteria that decompose fatty acids. *Archives of Microbiology*, **134**, 286-294.

# CHAPTER 3

## Formation of green rust and elemental sulfur in a Fe- and S-rich late Archean and Proterozoic ocean analog

E. Koeksoy<sup>†1</sup>, A. Sundman<sup>†1</sup>, J. M. Byrne<sup>1</sup>, R. Lohmayer<sup>2</sup>, B. Planer-Friedrich<sup>2</sup>, I. Halevy<sup>3</sup>, K. O. Konhauser<sup>4</sup> and A. Kappler<sup>1,5\*</sup>

<sup>†</sup> These authors contributed equally

<sup>1</sup> Geomicrobiology, Center for Applied Geoscience, University of Tuebingen, Sigwartstrasse 10, 72076 Tuebingen, Germany

<sup>2</sup> Environmental Geochemistry, University Bayreuth, Universitaetsstrasse 30, 95440 Bayreuth, Germany

<sup>3</sup> Department of Earth and Planetary Sciences, Weizmann Institute of Science, Rehovot 76100 Israel

<sup>4</sup> Department of Earth and Atmospheric Sciences, University of Alberta, Edmonton, Alberta, T6G 2E3 Canada

<sup>5</sup> Center for Geomicrobiology, Department of Bioscience, Aarhus University, Ny Munkegade 114, 8000 Aarhus, Denmark

Submitted to: *Geology*

## **Abstract**

For much of the Proterozoic Eon, bulk seawater was ferruginous (iron(II)-rich), while neritic waters with high primary productivity were either oxygenated or euxinic (sulfide-rich). Sedimentation on the continental shelves was therefore dominated by ferric oxyhydroxides leading to banded iron formations (BIF) or iron sulfides leading to black shales. Transition zones between ferruginous, euxinic and oxic ocean waters presumably played a key role in shaping the depositional environment along the oceanic redoxclines but little is reported about the primary iron and sulfur mineralogy in these settings. Here we present spectroscopic data on the iron- and sulfur-mineralogy in the Arvadi Spring, a proposed analogue for ferro-euxinic transitional zones in the Proterozoic. Our study reveals that green rust is the main iron mineral in low oxygenated waters together with ferrihydrite and lepidocrocite, while we found elemental sulfur to constitute the main sulfur precipitate. Given that green rust and elemental sulfur have reactivities and diagenetic histories that differ from ferric hydroxides and iron sulfides, their roles in the transfer of solutes from the marine mixed layer to sediments are important to understand, if we wish to use these sediments as sources of information on past conditions at Earth's surface.

## Introduction

The chemical, mineralogical and isotopic composition of banded iron formations (BIFs) and black shales have been successfully used as archives for Precambrian seawater composition. Their deposition was a consequence of marine Fe precipitation, either as Fe(III) (oxyhydr)oxides to form BIFs (Cloud, 1972) or as Fe(II) sulfides in black shales (Canfield, 1998; Werne et al., 2002), respectively. An end to abundant BIF deposition, and an accompanying shift to increased black shale formation by around 1.8 Ga (Poulton et al., 2004), reflects a major transition in seawater composition in the wake of an earlier atmospheric oxygenation pulse during the 2.3-2.0 Ga Lomagundi Event (Bekker and Holland, 2012; Planavsky et al., 2012). Specifically, increased oxidative weathering of continental pyrite delivered substantial amounts of mobilized sulfate to ocean shores during the Archean-Proterozoic boundary and thereafter (Canfield, 1998; Reinhard et al., 2009). Enhancing sulfate reduction rates along the highly productive paleo-shoreline (Canfield, 1998), the oceanic sulfide pool in respective zones became enlarged and presumably expanded into mid-depths of the ocean (Dahl et al., 2011; Reinhard et al., 2009) where Fe(II) was removed in the form of Fe(II) sulfides.

Although knowledge of Proterozoic ocean redox chemistry has advanced significantly over the past decade, there remains no consensus on the primary mineral precipitates comprising the precursor sediments to BIF and black shales (Klein, 1983; Posth et al., 2014). Even more, despite the transition zones between ferruginous and euxinic conditions (referred to herein as ferro-euxinic) likely being a prominent feature on the Proterozoic shelves, their areal scope, biogeochemical composition and the composition of the chemical sediments precipitating from their respective water columns remain unknown. The rock record itself is particularly problematic in this regard because unlike BIF and black shales, it is unclear what lithologies would mark the ferro-euxinic environments.

The analyses of modern habitats that resemble ancient ocean settings, such as Lake Matano (Crowe et al., 2008), Lake Pavin (Busigny et al., 2014; Cosmidis et al., 2014), Lake Cadagno (Canfield et al., 2010) and Lake La Cruz (Walter et al., 2014), is an emerging alternative

approach to reconstructing paleo-seawater composition and the identity of primary mineral phases (Koeksoy et al., 2016). Here we present spectroscopic data of Fe- and S-rich precipitates that formed by biogeochemical processes in an Fe- and S-rich proposed modern analogue for ferro-euxinic Proterozoic ocean waters, i.e., the Arvadi Spring (Koeksoy et al., in press). By integrating our results into current models of BIF and black shale deposition, we aim to reconstruct (1) the primary Fe- and S-mineral phases that precipitated in ferro-euxinic transition zones of the Proterozoic ocean and (2) depending on the mineral identity, the major consequences for nutrient and trace metal bioavailability due to their sorption to mineral surfaces in ancient settings that the Arvadi Spring represents.

## Material and Methods

All samples were collected in the Fe(II)- and sulfide-containing Arvadi Spring, Switzerland (46°40'17.4" N 9°39'18.8"E). The Fe(II) likely originates from corrosion of metal pipes through which water is transported until it emerges at the spring outlet (location 1, L1), whereas the water sulfide originates from reduction of sulfate in the sediment from evaporitic gypsum of the alpine orogeny (Strauss et al., 2016). Mineral precipitates of red and white color, referred to as 'red flocs' and 'white flocs' respectively, were collected from the sediment top layer at L1 and the pond side (location 2, L2) and from a deeper sediment layer at L2 (L2-D; Fig. A1 in the GSA Data Repository<sup>1</sup>). Samples were collected anoxically and transported on ice and in the dark to the geomicrobiology laboratory at Tuebingen where they were immediately frozen at -80°C, freeze-dried and stored anoxically in the dark.

Freeze-dried samples were analyzed using synchrotron-based X-ray absorption spectroscopy (XAS), which provides spectroscopic information about both, amorphous and crystalline mineral phases (in contrast to XRD which only provides information about the crystalline phases), on the Fe and S K-edges at the SUL-X beamline at ANKA, Karlsruhe Institute of Technology, Germany. To determine detailed Fe speciation in red flocs, <sup>57</sup>Fe Mössbauer spectra of the freeze-dried samples were collected at 140 K. Spectra were fitted

using Recoil (University of Ottawa) with the Voigt based fitting routine (Rancourt and Ping, 1991). White flocs were further subjected to elemental sulfur, sulfide and polysulfide analysis following the protocol of Wan et al. (2014), the methylene blue assay after Cline (1969) and the protocol of Kamyshny et al. (2006).

## Results and Discussion

**Water geochemistry.** The Arvadi Spring water at L1 had a pH of 7.8, a temperature of 7.5°C and dissolved O<sub>2</sub> concentration of 11.01 mg l<sup>-1</sup> (i.e., saturated with respect to atmospheric O<sub>2</sub>), whereas at L2 the water had a pH of 8.0, a temperature of 7.5°C and a dissolved O<sub>2</sub> concentration of 10.9 mg l<sup>-1</sup>. Dissolved Fe(II) was quantified at 15.6±2.3 μM and 13.7±3.8 μM (n=3) and sulfide at 1.8±0.1 μM and 1.4±0.5 μM (n=4) at L1 and L2 respectively, whereas no dissolved Fe(III) was detected. Sulfate (8.4±0.0 and 7.1±1.4 mM at L1 and L2, respectively (n=3)), bicarbonate (4.5±0.0 mM at L2 (n=3)), magnesium (3.3±0.0 and 3.3±0.0 mM at L1 and L2, respectively (n=3)) and calcium (7.0±0.4 mM and 7.3±0.4 mM at L1 and L2, respectively (n=3)) constituted the dominating anions and cations. Dissolved organic carbon was detected at 1.12±0.03 mg l<sup>-1</sup> at L2.

**Bulk Fe speciation in red flocs** Bulk Fe speciation in red flocs. Linear combination fitting (LCF) and shell-by-shell fitting of the Fe bulk spectra (Fig. 1A-D, Tab. A1 and Fig. A2) together with shell-by-shell EXAFS data fitting of all triplicate samples from L1, L2 and the deeper L2 sediment (L2-D) revealed red flocs to consist largely of octahedrally coordinated Fe(III) minerals. Generally, the speciation was identified to be very heterogeneous, even within bulk spectra (Fig. 1A-D). The EXAFS data fitting corresponded to first shell oxygen-neighbors and second shell Fe-neighbors at distances typical for ferrihydrite and goethite, i.e. around 3.0 and 3.4 Å, respectively (Tab. A1, Fig. A2). According to the LCF, the Fe(II)-Fe(III) mixed-valent mineral green rust ([Fe(II)<sub>1-x</sub>Fe(III)<sub>x</sub>(OH)<sub>2</sub>]<sup>x+</sup>. [(x/n) A<sup>n-</sup>, m H<sub>2</sub>O]<sup>x-</sup>, where A<sup>n-</sup> denotes either Cl<sup>-</sup>, SO<sub>4</sub><sup>2-</sup>, or CO<sub>3</sub><sup>2-</sup>, together with the Fe(III) oxyhydroxides lepidocrocite and



ferrihydrite are the dominating Fe mineral species, with minor contributions from goethite, magnetite and organically complexed Fe (Fig. 1A, C & D). While the red color of the red flocs already suggested ferric iron to be abundant, the identification of the Fe(II)-Fe(III) mixed-valent and highly reactive mineral green rust as a major fraction in these samples was unexpected. The LCF showed almost no Fe(II) sulfides, including pyrite and mackinawite, in red flocs, as expected based on a calculated saturation index of -7.42 of the Arvadi water with respect to amorphous Fe(II) sulfide. Calculations further predicted  $\text{FeCO}_3$  to precipitate from the Arvadi Spring water at a saturation index of 2.67, which we however could not identify in our samples. Pre-edge intensities and centroid positions within a detailed pre-edge analysis of red flocs according to Wilke et al. (2001) indicate results similar to the LCF with mixtures of octahedrally coordinated goethite, ferrihydrite and lepidocrocite, as well as Fe(II)-species in mostly octahedral coordination as green rust or in cubic coordination as pyrite (Fig. A3).

Mössbauer spectroscopy data on the red floc sample from L1 were fitted with a wide paramagnetic doublet ( $\delta$  (chemical shift) = 1.27 mm/s,  $\Delta E_Q$  (quadrupole splitting) = 2.74 mm/s) that is characteristic of a Fe(II) mineral phase and accounts for 55.6% of the total spectral area. The parameters of this doublet were consistent with Fe(II) present in green rust, as reported by Génin et al. (1998), thus providing additional support to the LCF and EXAFS data fitting. Due to masking by Fe(III) (oxy)hydroxides present in the samples it is difficult to say whether or not the corresponding Fe(III) doublet of green rust, which is necessary for its conclusive identification, is present in the spectra. Nevertheless, the abundance of green rust as determined by Mössbauer analysis, is in agreement with XANES and EXAFS spectra, in which green rust was also identified (Fig. A4).

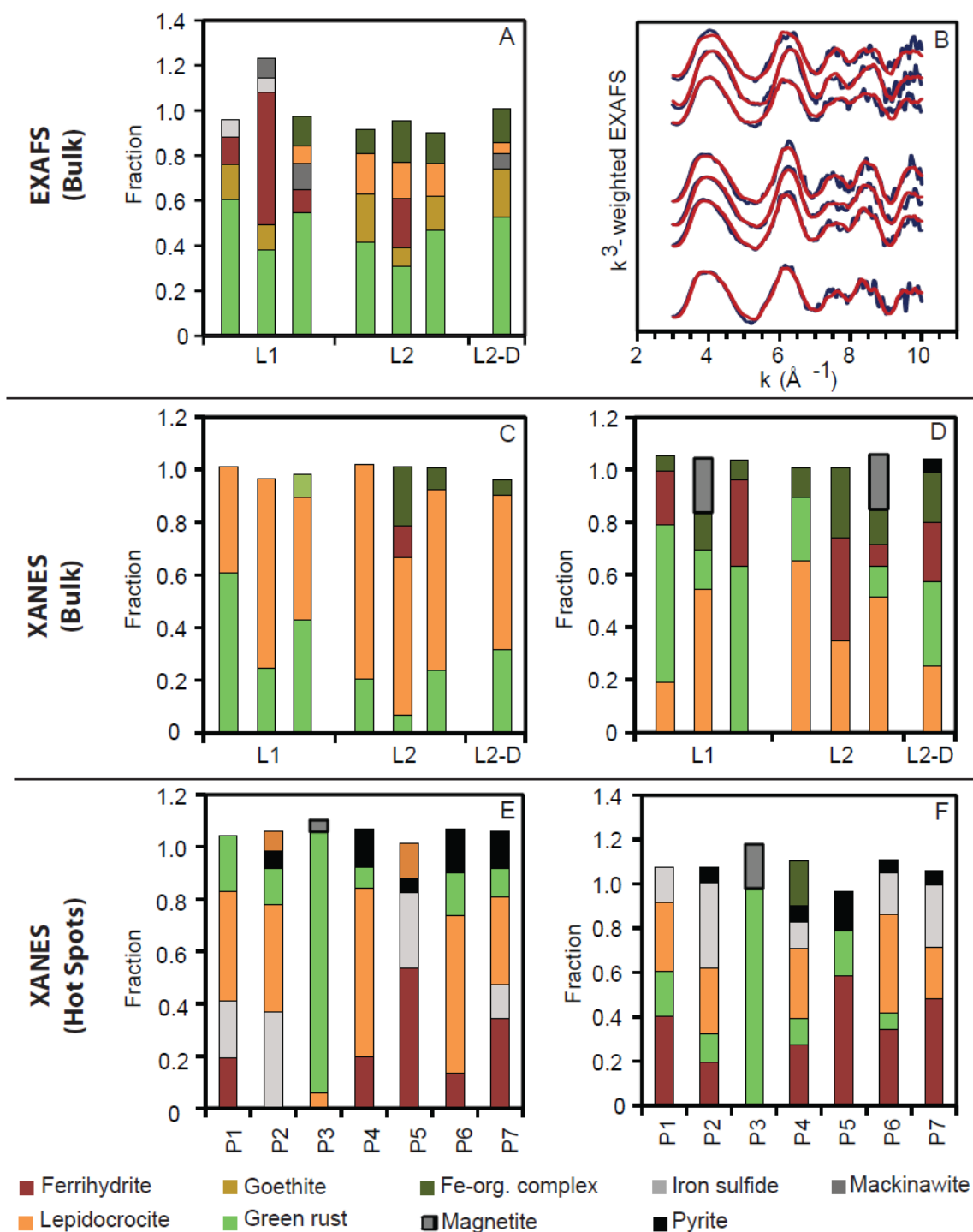


**Figure 1.** Results of Fe K-edge LCF of the EXAFS (A and B) and XANES (C-F) region in the red floc bulk (A-D) and  $\mu$ -XANES points P1-P7 (E and F) spectra of white floc samples from L1. A) LCF of L1 and L2 samples, B) LCF fits of L1 triplicates (a-c) and g) deeper sediment from L2 (L2-D), C) LCF of normalized bulk XANES spectra of L1 and L2 samples, D) LCF of first

derivative XANES spectra of L1 and L2 samples, E) LCF of normalized  $\mu$ -XANES of P1-P7 in the white floc sample from L1 and F) LCF of first derivative  $\mu$ -XANES of P1-P7 in the white floc sample from L1. Blue lines represent experimental data and red lines are fits.

The Fe(II)/Fe(III) ratios of red flocs were calculated from Mössbauer data to be  $1.51 \pm 0.34$  and  $0.21 \pm 0.04$  for samples from L1 and L2, respectively, revealing the L2 sample to be much more oxidized (Table A2). This is also clear from differences between the two spectra, with L1 dominated by a wide paramagnetic Fe(II) phase compared to the L2 spectrum which is dominated by a narrow paramagnetic doublet with a low center shift and quadrupole splitting ( $\delta = 0.47$  mm/s,  $\Delta E_0 = 0.83$  mm/s) that corresponds to an Fe(III) phase.

Our data identified red flocs to be extremely heterogeneous in their Fe-mineral speciation, but green rust, lepidocrocite and ferrihydrite clearly play a major role in the overall Fe-biogeochemistry in the Arvadi spring. Red flocs were found to be colonized by phototrophic, nitrate-reducing and microaerophilic Fe(II)-oxidizers as well as by Fe(III)-reducing microorganisms in a recent study of Koeksoy et al. (in press), that, in combination with the Fe-mineralogy data in the present study, implies red flocs to be the direct products of biotic and abiotic Fe(II) oxidation and Fe(III) reduction. We suggest that the apparent heterogeneity in Fe-mineralogy is a result of geochemically distinct microenvironments in the flocs and cell-mineral aggregates leading to a complex network of redox reactions and mineral transformation processes (summarized in Fig. 3).

As green rust can be formed by direct precipitation of Fe(II) upon partial microbial and abiotic oxidation as well as by reduction of Fe(III) oxyhydroxides, mainly as lepidocrocite and ferrihydrite (Bhave and Shejwalkar, 2017; Guilbaud et al., 2013; Ona-Nguema et al., 2002; Pantke et al., 2012; Parmar, 2001), we suggest both pathways to be possible sources for the Arvadi Spring green rust.

**Fe and S bulk and spatially resolved speciation in white flocs.** According to the peak fit of the S K-edge bulk spectra following similar approaches as outlined in references (Prietz et al., 2007; ThomasArrigo et al., 2016), the sulfur speciation in the freeze-dried white flocs was dominated by elemental sulfur ( $S^0$ ;  $\sim 2472$  eV) and sulfate ( $SO_4^{2-}$ ;  $\sim 2481$  eV) (Fig. 2A). The sulfate most likely originates from the high concentrations of dissolved sulfate originally present in the pond water. Upon freeze-drying, the concentrations of  $Mg^{2+}$ ,  $Ca^{2+}$  and  $SO_4^{2-}$  in the co-sampled original pond water overlying white floc samples may reach saturation, resulting in  $MgSO_4$  or  $CaSO_4$  precipitation. Interestingly, the speciation varied depending on local conditions (Fig. 2B), with  $S^0$  being dominant under high S concentrations (hotspots P1, P2, P4, P6 and P7), whereas more sulfate was detected in samples with low or very low S concentrations (P3 and P5; Fig. 2B).  $S^0$  concentrations were quantified by HPLC at  $185 \pm 41$  and  $229 \pm 36$  mg  $g^{-1}$  dry flocs in the L1 and L2 samples, making up 18.5 and 22.9% of the white floc dry weight, respectively. Polysulfides in form of  $S_5^{2-}$  were detected at much lower concentrations of only  $186 \pm 72$  and  $356 \pm 6$   $\mu g$   $g^{-1}$  dry flocs in unfiltered samples from L1 and L2, respectively.

The fact that  $S_5^{2-}$ , hydrogen sulfide and other polysulfides were below detection limits in the Arvadi water (2-5  $\mu M$  for polysulfides, 1  $\mu M$  for hydrogen sulfide), supports their quick turnover to more oxidized  $S^0$  and sulfate. Additional support for a major microbial contribution comes from Koeksoy et al. (in press) who showed that *Thiothrix spec.*, i.e., aerobic sulfide-oxidizing microorganisms (Nielsen et al., 2000), dominate the Arvadi Spring microbial community and are highly abundant in white floc samples from L1 and L2.

Apart from sulfur, white flocs also contained a minor fraction of Fe at ca.  $837.8$   $\mu g$   $g^{-1}$  and  $893.6$   $\mu g$   $g^{-1}$  dry flocs in L1 and L2 samples, respectively, constituting 0.0838 and 0.0894 wt% of the white flocs, respectively. LCF of the XANES region together with  $\mu$ XANES analysis performed at hot-spots in white flocs from L1 (Fig. 1 E & F) reflected a high heterogeneity in Fe-mineral speciation, with the fitting corresponding mainly to green rust, ferrihydrite and lepidocrocite similar to red flocs, but interestingly, also to Fe(II) sulfides (pyrite and mackinawite, Fig. 1 E & F). We found the mineralogy to vary among hot spots depending on the prevailing Fe and S concentrations. For instance, about 50% of the mineral species at

hotspot P2, which has relatively high S and low Fe concentrations, corresponded to green rust, mackinawite and pyrite. In contrast, hotspots P1, P4, P6 and P7 that contained high Fe and S concentrations, were dominated by ferrihydrite and lepidocrocite which constituted about 60-70% of the Fe-species. These samples also contained some green rust, pyrite, mackinawite and potentially some Fe-organic complexes (Fig. 1 E & F).

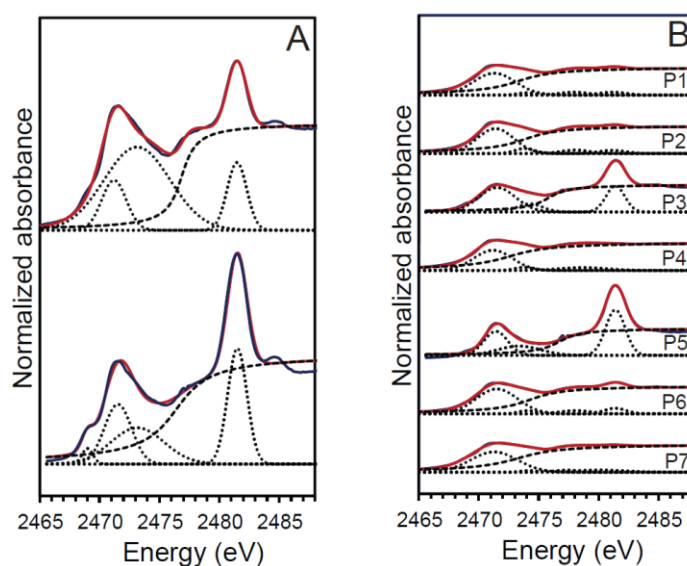
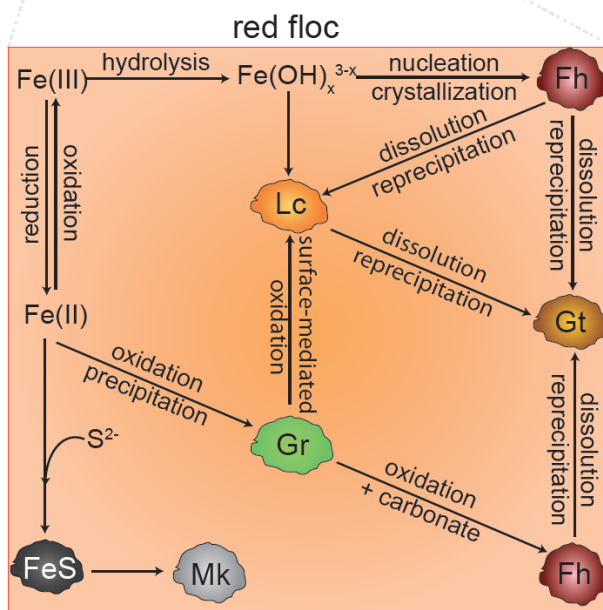
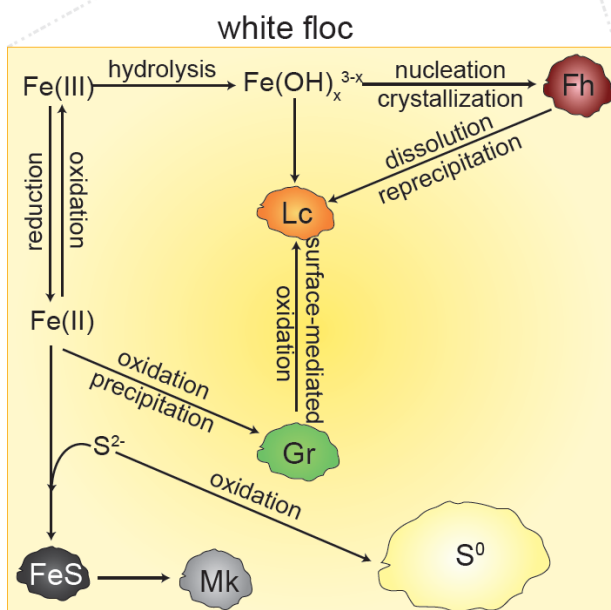
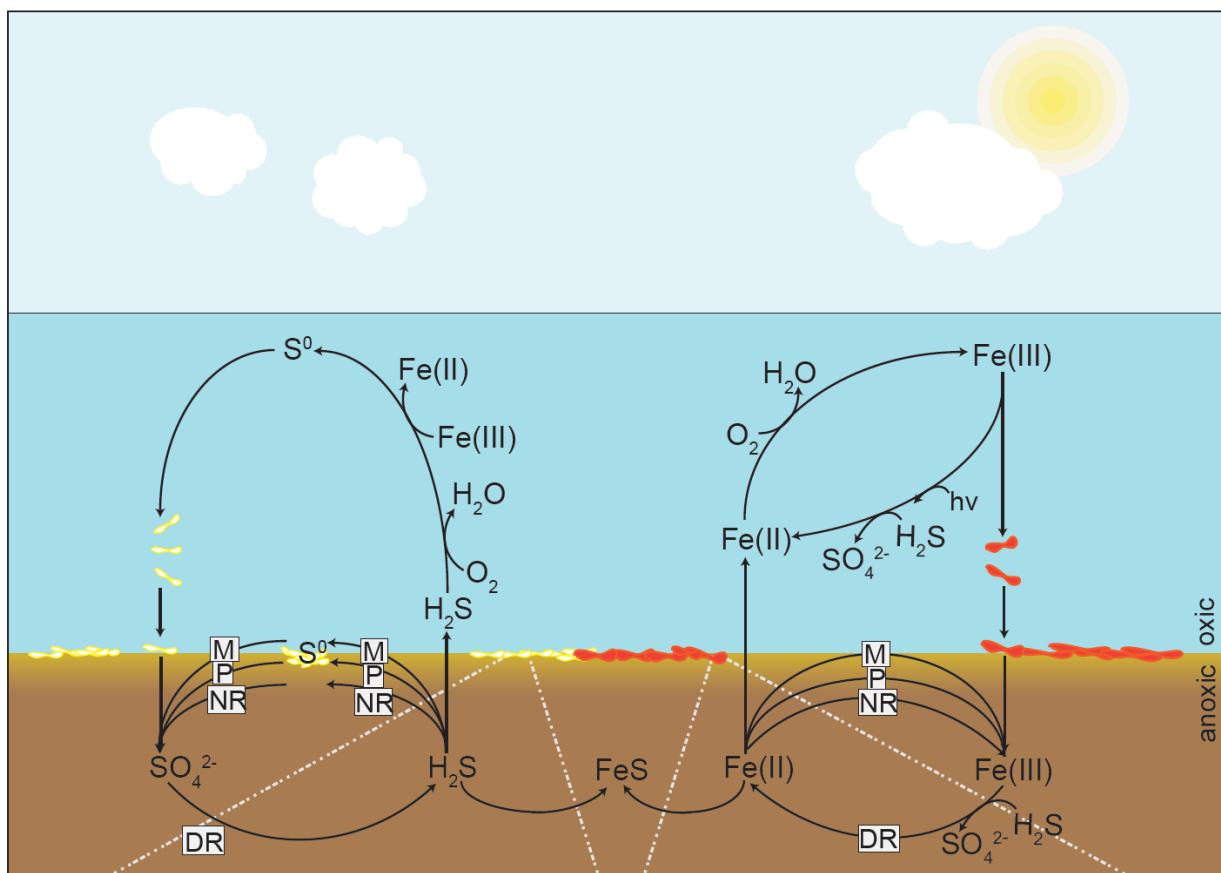


**Figure 2.** Results of peak fits of S K-edge XANES spectra of A) white floc samples from L1 (top) and L2 (bottom) and B) hot spots P1-P7 in white floc sample from L1. The black lines correspond to experimental data, red lines to fits and dashed lines to the individual peak and step functions used in the fitting.

☁ = white flocculent      🌸 = red flocculent

NR = coupled to nitrate reduction    P = phototrophic    M = microaerophilic    DR = dissimilatory reduction



**Fh** = Ferrihydrite  
**Mk** = Mackinawite

**Gt** = Goethite  
**FeS** = Iron(II) sulfide

**Lc** = Lepidocrocite

**Gr** = Green rust

**Figure 3.** Connection of Fe- and S-cycles in the Arvadi Spring water column and sediment and proposed mineral formation & transformation processes in white and red flocs (adapted from Koeksoy et. al, in review).

Despite their overall lower abundance compared to lepidocrocite, ferrihydrite and green rust, the higher prevalence of FeS, mackinawite and pyrite at white floc hot spots compared to their near absence in red flocs indicates FeS formation to be highly dependent on the local availability of  $S^0$  and polysulfides. Generally, we suggest sulfate reduction to be an ongoing process in white flocs based on S-isotope data (Strauss et al., 2016) and as Koeksoy et al. (in press) showed sulfate-reducing microorganisms to be fairly abundant in white flocs. We therefore suggest sulfate reduction in white flocs to produce locally high concentrations of sulfide that can reduce Fe(III) abiotically to Fe(II), which in turn can precipitate with the sulfide in form of amorphous FeS. The more reduced average Fe oxidation state at white floc hot spots compared to red floc samples (Fig. A3 and A5) supports our assumption of sulfide-dependent Fe(III) reduction in respective samples (Yao and Millero, 1996). The prevalence of  $S^0$  and polysulfides in white flocs explains the appearance of higher crystalline pyrite and mackinawite, as both S-compounds are known to trigger FeS to transform into more crystalline forms (Hunger and Benning, 2007; Rickard, 1997).

## **Implications for Fe-S-mineralogy and nutrient cycling in ferro-euxinic intermixed waters of late Archean and Proterozoic Oceans**

Our study provides unique insights into the potential identity and composition of Fe- and S-rich mineral precipitates that settled on the topmost seafloor layer underlying ferro-euxinic transition waters of late Archean and Proterozoic oceans during intervals of atmospheric oxygenation. More generally, our data provide a glimpse into the diversity and complexity of the primary mineral assemblage formed within the water column, at the sediment-water interface, and during the earliest stages of diagenesis. In Archean and Proterozoic

sedimentary rocks this complexity is obliterated by later diagenesis, and by metamorphism under increasing burial pressures and temperatures, making it difficult to constrain the initial mineral assemblage and extract environmental information.

Our observations support previous studies suggesting ferrihydrite and lepidocrocite as important precursors to preserved Fe-mineral phases in geologic rock formations (Klein, 2005). Most notably however, our data strongly support the recent suggestion of green rust as a highly reactive BIF precursor (Halevy et al., 2017), and shows that green rust might not only have played a role in Archean ocean settings with a dominantly anoxic and ferruginous water column (Zegeye et al., 2012) but presumably also precipitated from oxygenated ferro-euxinic intermixing waters in surface layers of the ocean during the late Archean and throughout the Proterozoic. Given the higher reactivity of green rust (relative to Fe(III) oxides and hydroxides) towards silica, phosphate and trace metals (Hansen and Poulsen, 1999; Kwon et al., 2007; Parmar, 2001), our findings may have important implications for nutrient and trace metal cycling in paleo-seawater. The fate of nutrients and metals upon diagenetic transformation of green rust to thermodynamically stable phases is uncertain and requires further research.

Our study further highlights a previously neglected role of  $S^0$  in the overall geochemistry of ferro-euxinic oxygenated shallow ocean waters, as it appears to be the dominating solid S-mineral in the Arvadi Spring. Being labile and highly reactive, mostly due to its electron donating and accepting capacities that are preferred not only by S- but also Fe-metabolizing microorganisms (Holmes et al., 2004),  $S^0$  was not preserved in ancient settings and hence cannot be tracked in the rock record (Cosmidis and Templeton, 2016). However, evidence for Precambrian  $S^0$ -metabolism, including its disproportionation, come from S-isotope data already for the Archean (Farquhar et al., 2013; Havig et al., 2017; Philippot et al., 2007), and our data support a role for  $S^0$  in the subsequent Proterozoic era.  $S^0$  can chelate trace metals such as Cu, Hg, and As and is thought to limit their bioavailability (Helz, 2014) and hence,  $S^0$  may have additionally affected mid-Proterozoic evolutionary stasis, similar to green rust.



In summary, we suggest green rust and  $S^0$  as key early precipitates in the late Archean and Proterozoic oceans, which contributed to the formation of the mineral assemblages observed in sedimentary rocks of these ages. Both green rust and  $S^0$  may have exacerbated trace metal limitation and hence impacted evolutionary stasis during the mid-Proterozoic. We emphasize the requirement for the consideration of both compounds as major contributors to biogeochemical Fe-S-cycling in respective modern and ancient environmental settings and to the observed rock record mineralogy by evaluating possible transformations through diagenesis.

### **Acknowledgements**

This work was supported by the German Research Foundation (DFG) grant KA 1736/27-1. We thank Joerg Goettlicher and Ralph Steininger from the KIT ANKA facilities and Cindy Lockwood for assistance during the data collection process.

## REFERENCES

- Bekker, A., and Holland, H., 2012, Oxygen overshoot and recovery during the early Paleoproterozoic: *Earth and Planetary Science Letters*, v. 317, p. 295-304.
- Bhave, C., and Shejwalkar, S., 2017, A review on the synthesis and applications of green rust for environmental pollutant remediation: *International Journal of Environmental Science and Technology*, pp. 1-6.
- Busigny, V., Planavsky, N. J., Jézéquel, D., Crowe, S., Louvat, P., Moureau, J., Viollier, E., and Lyons, T. W., 2014, Iron isotopes in an Archean ocean analogue: *Geochimica et Cosmochimica Acta*, v. 133, p. 443-462.
- Canfield, D. E., 1998, A new model for Proterozoic ocean chemistry: *Nature*, v. 396, no. 6710, p. 450-453.
- Canfield, D. E., Farquhar, J., and Zerkle, A. L., 2010, High isotope fractionations during sulfate reduction in a low-sulfate euxinic ocean analog: *Geology*, v. 38, no. 5, p. 415-418.
- Cloud, P., 1972, A working model of the primitive Earth: *American Journal of Science*, v. 272, no. 6, p. 537-548.
- Cosmidis, J., Benzerara, K., Morin, G., Busigny, V., Lebeau, O., Jezequel, D., Noel, V., Dublet, G., and Othmane, G., 2014, Biomineralization of iron-phosphates in the water column of Lake Pavin (Massif Central, France): *Geochimica et Cosmochimica Acta*, v. 126, p. 78-96.
- Cosmidis, J., and Templeton, A. S., 2016, Self-assembly of biomorphic carbon/sulfur microstructures in sulfidic environments, v. 7, p. 12812.
- Crowe, S. A., Jones, C., Katsev, S., Magen, C., O'Neill, A. H., Sturm, A., Canfield, D. E., Haffner, G. D., Mucci, A., and Sundby, B., 2008, Photoferrotrophs thrive in an Archean Ocean analogue: *Proceedings of the National Academy of Sciences*, v. 105, no. 41, p. 15938-15943.
- Dahl, T. W., Canfield, D. E., Rosing, M. T., Frei, R. E., Gordon, G. W., Knoll, A. H., and Anbar, A. D., 2011, Molybdenum evidence for expansive sulfidic water masses in similar to 750 Ma oceans: *Earth and Planetary Science Letters*, v. 311, no. 3-4, p. 264-274.
- Farquhar, J., Cliff, J., Zerkle, A. L., Kamyshny, A., Poulton, S. W., Claire, M., Adams, D., and Harms, B., 2013, Pathways for Neoproterozoic pyrite formation constrained by mass-independent sulfur isotopes: *Proceedings of the National Academy of Sciences*, v. 110, no. 44, p. 17638-17643.
- Génin, J.-M. R., Bourrié, G., Trolard, F., Abdelmoula, M., Jaffrezic, A., Refait, P., Maitre, V., Humbert, B., and Herbillon, A., 1998, Thermodynamic Equilibria in Aqueous Suspensions of Synthetic and Natural Fe(II)-Fe(III) Green Rusts: Occurrences of the Mineral in

- Hydromorphic Soils: Environmental Science & Technology, v. 32, no. 8, p. 1058-1068.
- Guilbaud, R., White, M. L., and Poulton, S. W., 2013, Surface charge and growth of sulphate and carbonate green rust in aqueous media: *Geochimica et Cosmochimica Acta*, v. 108, p. 141-153.
- Halevy, I., Alesker, M., Schuster, E., Popovitz-Biro, R., and Feldman, Y., 2017, A key role for green rust in the Precambrian oceans and the genesis of iron formations: *Nature Geoscience*, v. 10, p. 135-139.
- Hansen, H. C. B., and Poulsen, I. F., 1999, Interaction of synthetic sulphate "green rust" with phosphate and the crystallization of vivianite: *Clays and Clay Minerals*, v. 47, p. 312-318.
- Havig, J. R., Hamilton, T. L., Bachan, A., and Kump, L. R., 2017, Sulfur and carbon isotopic evidence for metabolic pathway evolution and a four-stepped Earth system progression across the Archean and Paleoproterozoic: *Earth-Science Reviews*, v. 174, p. 1-21.
- Helz, G. R., 2014, Activity of zero-valent sulfur in sulfidic natural waters: *Geochemical Transactions*, v. 15, no. 1, p. 13.
- Holmes, D. E., Bond, D. R., and Lovley, D. R., 2004, Electron transfer by *Desulfobulbus propionicus* to Fe (III) and graphite electrodes: *Applied and Environmental Microbiology*, v. 70, no. 2, p. 1234-1237.
- Hunger, S., and Benning, L. G., 2007, Greigite: a true intermediate on the polysulfide pathway to pyrite: *Geochemical Transactions*, v. 8, no. 1, p. 1.
- Cline, J.D., 1969, Spectrophotometric determination of hydrogen sulfide in natural waters: *Limnology and Oceanography*, v. 14, p. 454-458.
- Kamyshny, A., Ekeltchik, I., Gun, J., and Lev, O., 2006, Method for the Determination of Inorganic Polysulfide Distribution in Aquatic Systems: *Analytical Chemistry*, v. 78, no. 8, p. 2631-2639.
- Klein, C., 1983, Diagenesis and metamorphism of Precambrian Banded Iron-Formations: Developments in Precambrian Geology, v. 6, p. 417-469.
- Klein, C., 2005, Some Precambrian Banded Iron Formations (BIFs) from around the world: Their age, geologic setting, mineralogy, metamorphism, geochemistry, and origins: *American Mineralogist*, v. 90, no. 10, p. 1473-1499.
- Koeksoy, E., Halama, M., Konhauser, K. O., and Kappler, A., 2016, Using modern ferruginous habitats to interpret Precambrian banded iron formation deposition: *International Journal of Astrobiology*, v. 15, no. 3, p. 205-217.
- Koeksoy, E., Halama, M., Hagemann, N., Weigold, P.R., Laufer, K., Kleindienst, S., Byrne, J.M., Sundman, A., Hanselmann, K., Halevy, I., Schoenberg, R., Konhauser, K.O. and Kappler, A., in press, A case study for late Archean and Proterozoic biogeochemical iron- and sulphur-cycling in a modern habitat – the Arvadi Spring: *Geobiology*.

- Kwon, S.-K., Kimijima, K. i., Kanie, K., Suzuki, S., Muramatsu, A., Saito, M., Shinoda, K., and Waseda, Y., 2007, Influence of silicate ions on the formation of goethite from green rust in aqueous solution: *Corrosion science*, v. 49, no. 7, p. 2946-2961.
- Nielsen, P. H., De Muro, M. A., and Nielsen, J. L., 2000, Studies on the in situ physiology of *Thiothrix* spp. present in activated sludge: *Environmental microbiology*, v. 2, no. 4, p. 389-398.
- Ona-Nguema, G., Abdelmoula, M., Jorand, F., Benali, O., Géhin, A., Block, J.-C., and Génin, J.-M. R., 2002, Microbial Reduction of Lepidocrocite  $\gamma$ -FeOOH by *Shewanella putrefaciens*; The Formation of Green Rust: *Hyperfine Interactions*, v. 139, no. 1, p. 231-237.
- Pantke, C., Obst, M., Benzerara, K., Morin, G., Ona-Nguema, G., Dippon, U., and Kappler, A., 2012, Green Rust Formation during Fe(II) Oxidation by the Nitrate-Reducing *Acidovorax* sp. Strain BoFeN1: *Environmental Science & Technology*, v. 46, no. 3, p. 1439-1446.
- Parmar, N., Gorby, Y.A., Beveridge, T.J. and Ferris, F.G., 2001, Formation of Green Rust and Immobilization of Nickel in Response to Bacterial Reduction of Hydrous Ferric Oxide: *Geomicrobiology Journal*, v. 18, no. 4, p. 375-385.
- Philippot, P., Van Zuilen, M., Lepot, K., Thomazo, C., Farquhar, J., and Van Kranendonk, M. J., 2007, Early Archaean Microorganisms Preferred Elemental Sulfur, Not Sulfate: *Science*, v. 317, no. 5844, p. 1534-1537.
- Planavsky, N. J., Bekker, A., Hofmann, A., Owens, J. D., and Lyons, T. W., 2012, Sulfur record of rising and falling marine oxygen and sulfate levels during the Lomagundi event: *Proceedings of the National Academy of Sciences*, v. 109, no. 45, p. 18300-18305.
- Posth, N. R., Canfield, D. E., and Kappler, A., 2014, Biogenic Fe(III) minerals: From formation to diagenesis and preservation in the rock record: *Earth-Science Reviews*, v. 135, p. 103-121.
- Poulton, S. W., Fralick, P. W., and Canfield, D. E., 2004, The transition to a sulphidic ocean ~1.84 billion years ago: *Nature*, v. 431, no. 7005, p. 173-177.
- Prietzl, J., Thieme, J., Salomé, M., and Knicker, H., 2007, Sulfur K-edge XANES spectroscopy reveals differences in sulfur speciation of bulk soils, humic acid, fulvic acid, and particle size separates: *Soil Biology and Biochemistry*, v. 39, no. 4, p. 877-890.
- Rancourt, D. G., and Ping, J. Y., 1991, Voigt-based methods for arbitrary-shape static hyperfine parameter distributions in Mössbauer spectroscopy: *Nuclear Instruments and Methods in Physics Research Section B: Beam Interactions with Materials and Atoms*, v. 58, no. 1, p. 85-97.
- Reinhard, C. T., Raiswell, R., Scott, C., Anbar, A. D., and Lyons, T. W., 2009, A Late Archean Sulfidic Sea Stimulated by Early Oxidative Weathering of the

- Continents: Science, v. 326, no. 5953, p. 713-716.
- Rickard, D., 1997, Kinetics of pyrite formation by the H<sub>2</sub>S oxidation of iron (II) monosulfide in aqueous solutions between 25 and 125°C: The rate equation: *Geochimica et Cosmochimica Acta*, v. 61, no. 1, p. 115-134.
- Strauss, H., Chmiel, H., Christ, A., Fugmann, A., Hanselmann, K., Kappler, A., Königer, P., Lutter, A., Siedenberg, K., and Teichert, B. M., 2016, Multiple sulphur and oxygen isotopes reveal microbial sulphur cycling in spring waters in the Lower Engadin, Switzerland: *Isotopes in environmental and health studies*, v. 52, no. 1-2, p. 75-93.
- ThomasArrigo, L. K., Mikutta, C., Lohmayer, R., Planer-Friedrich, B., and Kretzschmar, R., 2016, Sulfidization of Organic Freshwater Floccs from a Minerotrophic Peatland: Speciation Changes of Iron, Sulfur, and Arsenic: *Environmental Science & Technology*, v. 50, no. 7, p. 3607-3616.
- Walter, X. A., Picazo, A., Miracle, M. R., Vicente, E., Camacho, A., Aragno, M., and Zopfi, J., 2014, Phototrophic Fe(II)-oxidation in the chemocline of a ferruginous meromictic lake: *Frontiers in Microbiology*, v. 5, p. 713.
- Wan, M., Shchukarev, A., Lohmayer, R., Planer-Friedrich, B., and Peiffer, S., 2014, Occurrence of Surface Polysulfides during the Interaction between Ferric (Hydr)Oxides and Aqueous Sulfide: *Environmental Science & Technology*, v. 48, no. 9, p. 5076-5084.
- Werne, J. P., Sageman, B. B., Lyons, T. W., and Hollander, D. J., 2002, An integrated assessment of a "type euxinic" deposit: evidence for multiple controls on black shale deposition in the Middle Devonian Oatka Creek Formation: *American Journal of Science*, v. 302, no. 2, p. 110-143.
- Wilke, M., Farges, F., Petit, P.-E., Brown, G. E., and Martin, F., 2001, Oxidation state and coordination of Fe in minerals: An Fe K-XANES spectroscopic study: *American Mineralogist*, v. 86, no. 5-6, p. 714.
- Yao, W. S., and Millero, F. J., 1996, Oxidation of hydrogen sulfide by hydrous Fe(III) oxides in seawater: *Marine Chemistry*, v. 52, no. 1, p. 1-16.
- Zegeye, A., Bonneville, S., Benning, L. G., Sturm, A., Fowle, D. A., Jones, C., Canfield, D. E., Ruby, C., MacLean, L. C., Nomosatryo, S., Crowe, S. A., and Poulton, S. W., 2012, Green rust formation controls nutrient availability in a ferruginous water column: *Geology*, v. 40, no. 7, p. 599-602.

## SUPPLEMENTAL INFORMATION FOR

### **Formation of green rust and elemental sulfur in a Fe- and S-rich late Archean and Proterozoic ocean analog**

E. Koeksoy<sup>†1</sup>, A. Sundman<sup>†1</sup>, J. M. Byrne<sup>1</sup>, R. Lohmayer<sup>2</sup>, B. Planer-Friedrich<sup>2</sup>, I. Halevy<sup>3</sup>, K. O. Konhauser<sup>4</sup> and A. Kappler<sup>1,5\*</sup>

<sup>†</sup> These authors contributed equally

<sup>1</sup>Geomicrobiology, Center for Applied Geoscience, University of Tuebingen, Sigwartstrasse 10, 72076 Tuebingen, Germany

<sup>2</sup>Environmental Geochemistry, University Bayreuth, Universitaetsstrasse 30, 95440 Bayreuth, Germany

<sup>3</sup>Department of Earth and Planetary Sciences, Weizmann Institute of Science, Rehovot 76100 Israel

<sup>4</sup>Department of Earth and Atmospheric Sciences, University of Alberta, Edmonton, Alberta, T6G 2E3 Canada

<sup>5</sup>Center for Geomicrobiology, Department of Bioscience, Aarhus University, Ny Munkegade 114, 8000 Aarhus, Denmark

Submitted to: *Geology*

**SI. 1: Collection of flocs samples.** White precipitate flocs from L1 and L2 were collected in acid-washed Schott bottles that were filled to the brim with pond water and then closed with oxygen-tight butyl stoppers for transport on ice and in the dark to the lab. The samples were immediately treated upon return to the lab. They were flushed with N<sub>2</sub> and most of the supernatant was pipetted out (the flocs sedimented to the bottom of the bottle). These more concentrated floc samples were then brought into an anoxic glovebox, transferred into weighted plastic tubes and centrifuged. The supernatant was collected in acid-washed Schott bottles, the mass of the wet floc samples was determined. When necessary, the samples were diluted with the collected Arvadi pond water.

**SI. 2: Elemental sulfur analysis.** 125  $\mu$ L anoxic MilliQ and 125  $\mu$ L of 2% (w/v) ZnAc were added to 500  $\mu$ L of unfiltered sample. The samples were stored dark and at 4°C for 8 days. Six mL of methanol were added to the refrigerated samples, which were placed on a rolling shaker for 3 h with occasional shaking. The samples were then centrifuged for 5 minutes at 4000 rpm. Liquid samples were subsequently analyzed for elemental sulfur by HPLC on an Ultrasphere ODS column, operated with an isocratic mixture of 98% methanol and 2% H<sub>2</sub>O run with a flow rate of 0.8 mL/min and detection at 265  $\mu$ m.

**SI. 3: Polysulfide analysis.** Triplicate samples from locations L1 and L2 (see Fig. A1) were prepared for unfiltered and 0.45- $\mu$ m-filtered samples to distinguish between total and aqueous polysulfides. Obviously, this separation is hampered by the earlier centrifugation, but concentration of the flocks via e.g. flash-freezing in the field, using liquid nitrogen was not possible due to safety reasons as the sampling involved long-distance driving in a vehicle that did not allow transport of gas. For the unfiltered samples, 1067  $\mu$ L anoxic methanol was pipetted to plastic tubes; 267  $\mu$ L sample and 8  $\mu$ L methyl trifluoromethanesulfonate were added simultaneously. The samples were then stored in the dark and at 4°C for ca. 36 h. The samples were then filtered in the glovebox using 0.45  $\mu$ m filters and put back into the freezer. For the filtered samples, 800  $\mu$ L anoxic methanol was pipetted into the plastic tubes, then

200  $\mu\text{L}$  sample and 6  $\mu\text{L}$  methyl-triflate was added. These samples were also stored dark and frozen until analysis. Finally, the samples were analyzed for polysulfides on a HPLC (Merck Hitachi, L-2130 pump, L-2200 autosampler, L-2420 UV-vis detector) using a C18 column (Waters-Spherisorb, ODS2) as previously described in Wan et al. (2014).

**SI. 4: Mössbauer spectroscopy.** The Mössbauer spectrometer instrument was calibrated with a 7  $\mu\text{m}$  thick  $\alpha\text{-}^{57}\text{Fe}$  foil measured at room temperature, which was also used to determine the half width at half maximum (fixed to 0.128 mm/s during fitting). Fitting was carried out using Recoil (University of Ottawa) with the Voigt based fitting routine (VBF) (Rancourt et al., 1991). The purpose of these  $^{57}\text{Fe}$  Mössbauer measurements was to determine Fe(II)/Fe(III) ratio and mineral composition as a complementary analysis to the synchrotron-based Fe K-edge X-ray absorption spectroscopy analysis.



**Table A1.** Fe K-Edge EXAFS shell-by-shell fit results of the red floc samples.

Sample	Path	Coordination number	$\sigma^{2*}$ ( $\text{\AA}^2$ )	Bond distance ( $\text{\AA}$ )	$\Delta E_0^\dagger$	$F_i^\S$
L1-1	Fe-O	5.8	0.0158	2.02	0.2	6.75
	Fe-Fe	1.6	0.0100 <sup>#</sup>	3.05		
	Fe-Fe	0.9	0.0100 <sup>#</sup>	3.37		
L1-2	Fe-O	6.1	0.0144	2.00	-0.85	6.47
	Fe-Fe	1.8	0.0100 <sup>#</sup>	3.03		
	Fe-Fe	1.0	0.0100 <sup>#</sup>	3.42		
L1-3	Fe-O	5.6	0.015	2.02	0.36	6.55
	Fe-Fe	1.3	0.0100 <sup>#</sup>	3.06		
	Fe-Fe	0.7	0.0100 <sup>#</sup>	3.41		
L2-1	Fe-O	6.4	0.0145	2.00	-1.62	6.18
	Fe-Fe	2.2	0.0100 <sup>#</sup>	3.00		
	Fe-Fe	1.7	0.0100 <sup>#</sup>	3.38		
L2-2	Fe-O	5.9	0.0122	1.98	-2.03	3.96
	Fe-Fe	2.1	0.0100 <sup>#</sup>	3.02		
	Fe-Fe	1.0	0.0100 <sup>#</sup>	3.41		
L2-3	Fe-O	5.7	0.013	1.99	-1.58	4.41
	Fe-Fe	1.8	0.0100 <sup>#</sup>	3.03		
	Fe-Fe	1.2	0.0100 <sup>#</sup>	3.42		
L2-D	Fe-O	5.9	0.0135	2.01	0.37	7.81
	Fe-Fe	1.7	0.0100 <sup>#</sup>	3.05		
	Fe-Fe	0.6	0.0100 <sup>#</sup>	3.38		

The amplitude reduction factor was set to 0.75.

\*Debye-Waller factor

<sup>†</sup> $E_0$  was assumed to be identical for all shells.

<sup>§</sup> $F_i$  is defined as  $(\sum(k^3\chi_{\text{exp}}-k^3\chi_{\text{fit}})^2/\sum(k^3\chi_{\text{exp}})^2)\times 100$ , where  $\chi_{\text{exp}}$  and  $\chi_{\text{fit}}$  represent experimental and fitted data points, respectively.

<sup>#</sup>Fixed to 0.0100 according to Maillot et al. (2011).

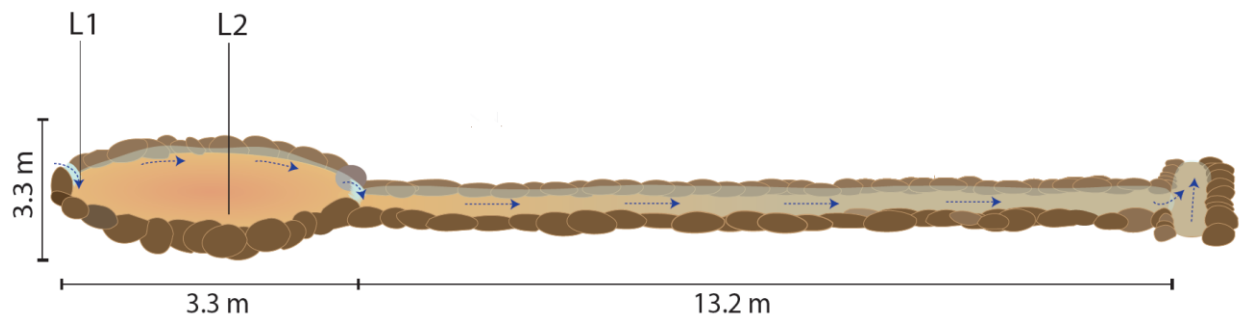


**Figure A1.** Schematic overview of the Arvadi Spring. Locations L1 and L2 are situated within the spring pond. The spring discharge is at L1. This figure is modified from Koeksoy et al. (in press).

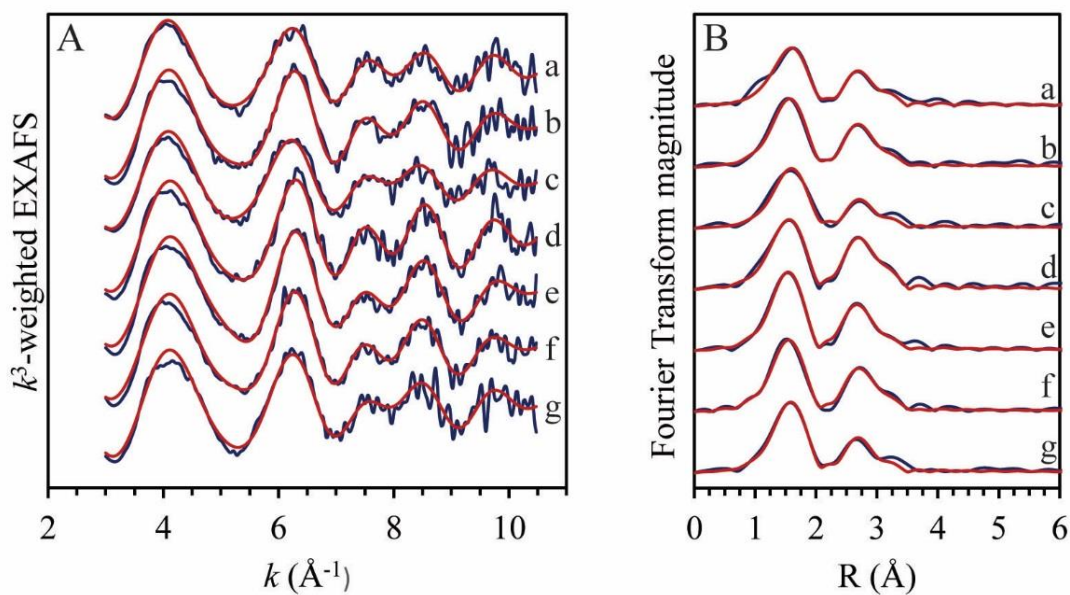


**Figure A2.**  $k^3$ -weighted (A) and Fourier Transformed (B) Fe K-edge EXAFS for Fe-rich floccs from location L1 (a, b, c), location L2 (d, e, f) and from deeper sediment at L2 (g) in the Arvadi Spring. Blue lines represent experimental data and red lines fit results.

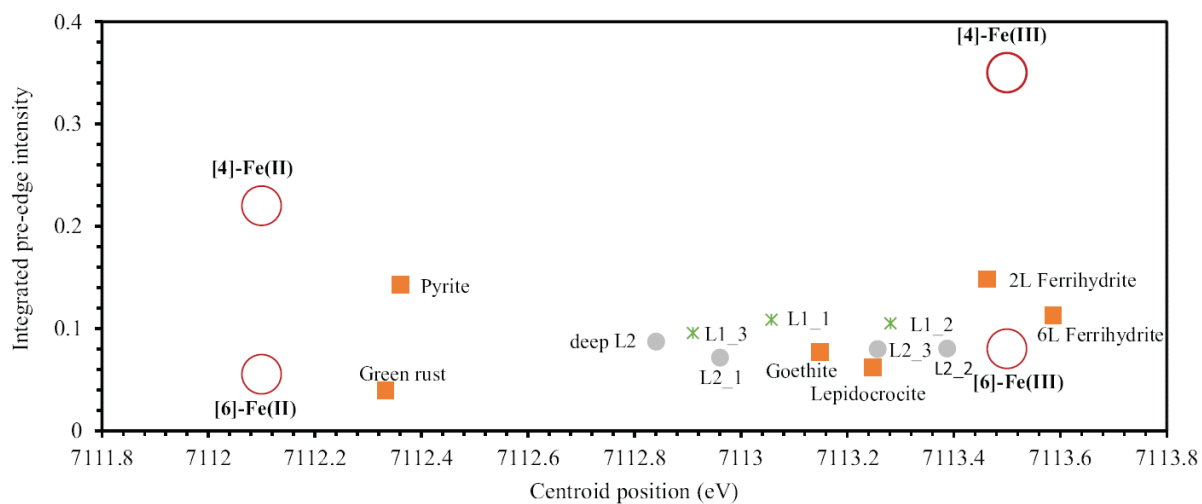


**Figure A3.** Pre-edge analysis following Wilke et al. (2001) comparing centroid energies and integrated pre-edge intensity of model compounds (orange filled squares), L1 samples (green stars) and L2 top sediment and deeper sediment samples (grey filled circles) of red flocs. The open circles represent pure Fe(II) and Fe(III) compounds in tetrahedral and octahedral configuration.

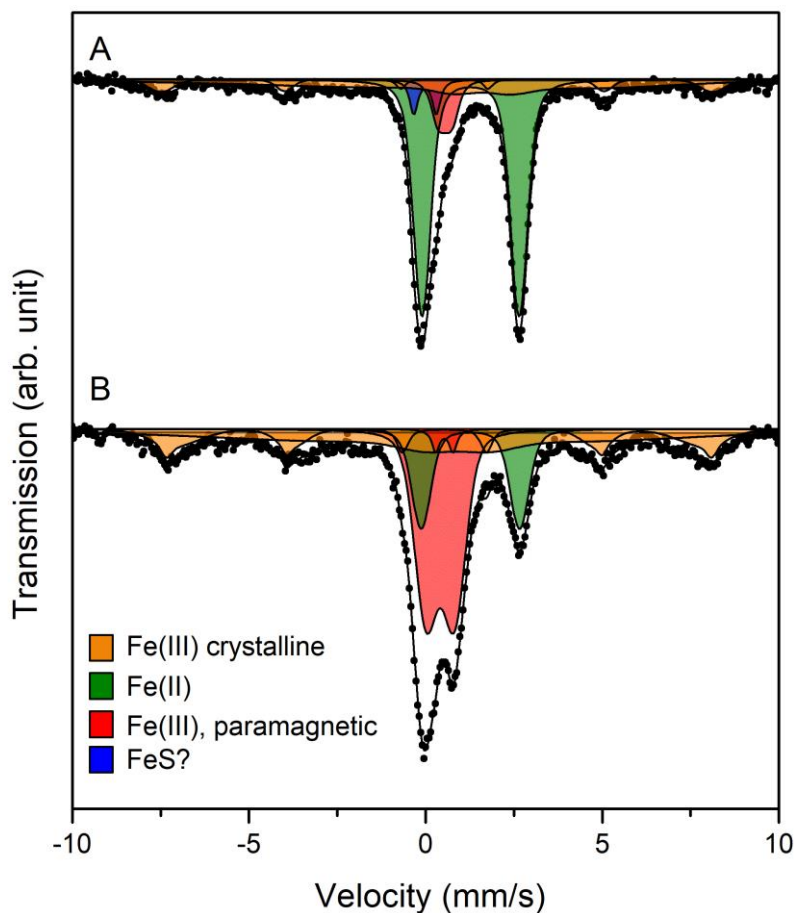


**Figure A4.**  $^{57}\text{Fe}$  Mössbauer spectra collected at 77 K for red flocs from L1 (A) and red flocs from L2 (B). Fe(III) crystalline phases likely correspond to ordered Fe(III) phases such as goethite. The Fe(II) phase is best fitted with parameters that show close similarity to green rust. Fe(III) paramagnetic phase likely corresponds to poorly crystalline phases such as ferrihydrite or lepidocrocite. A minor FeS phase appears to be present in sample L1.

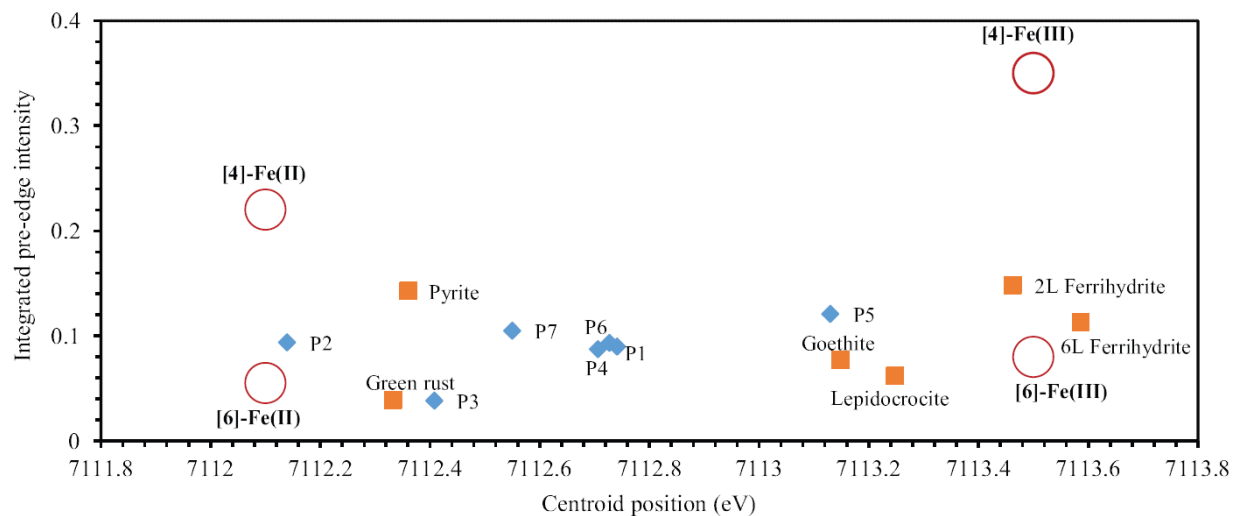


**Figure A5.** Pre-edge analysis following Wilke et al. (2001) comparing centroid energies and integrated pre-edge intensity of model compounds (orange filled squares). Blue diamonds correspond to the sample points in the white floc sample from L1 analyzed by  $\mu$ XANES. The open circles represent pure Fe(II) and Fe(III) compounds in tetrahedral and octahedral configuration.

## REFERENCES

- Koeksoy, E., Halama, M., Hagemann, N., Weigold, P.R., Laufer, K., Kleindienst, S., Byrne, J.M., Sundman, A., Hanselmann, K., Halevy, I., Schoenberg, R., Konhauser, K.O. and Kappler, A., in press, A case study for late Archean and Proterozoic biogeochemical iron- and sulphur-cycling in a modern habitat – the Arvadi Spring: *Geobiology*.
- Maillot, F., Morain, G., Wang, Y., Bonnin, D., Ildefonse, P., Chaneac, C. and Calas, G., 2011, New insight into the structure of nanocrystalline ferrihydrite: EXAFS evidence for tetrahedrally coordinated iron(III): *Geochimica et Cosmochimica Acta*, v. 75, p. 2708-2720.
- Rancourt, D.G. and J.Y. Ping, 1991, Voigt-based methods for arbitrary-shape static hyperfine parameter distributions in Mössbauer spectroscopy: *Nuclear Instruments and Methods in Physics Research Section B: Beam Interactions with Materials and Atoms*, v. 58, p. 85-97.
- Wan, M., Schukarev, A., Lohmayer, R., Planer-Friedrich, B. and Pfeiffer, S., 2014, Occurrence of Surface Polysulfides during the Interaction between Ferric (Hydr)Oxides and Aqueous Sulfide: *Environmental Science & Technology*, v. 48, p. 5076-5084.
- Wilke, M., Farge, F., Petit, P.E., Borwn, G.E. Jr. and Martin, F., 2001, Oxidation state and coordination of Fe in minerals: An Fe K-XANES spectroscopic study: *American Mineralogist*, v. 86, p. 714.

# CHAPTER 4

## Microbial Fe-cycling in a late Archean and Proterozoic Ocean Analogue

E. Koeksoy<sup>1</sup>, F. Schaedler<sup>1</sup>, V. Nickeleit<sup>1</sup>, C. Schmidt<sup>1</sup>, I. Halevy<sup>2</sup>, R. Schoenberg<sup>3</sup> and A. Kappler<sup>1,4\*</sup>

<sup>1</sup> Geomicrobiology, Center for Applied Geoscience, University of Tuebingen, Sigwartstrasse 10, 72076 Tuebingen, Germany

<sup>2</sup> Department of Earth and Planetary Sciences, Weizmann Institute of Science, Rehovot 76100 Israel

<sup>3</sup> Isotope Geochemistry, University of Tuebingen, Wilhelmstrasse 56, 72074 Tuebingen

<sup>4</sup> Center for Geomicrobiology, Department of Bioscience, Aarhus University, Ny Munkegade 114, 8000 Aarhus, Denmark

Unpublished manuscript



## Abstract

Fe was an abundant constituent of ancient seawater throughout much of the Precambrian, but the rise of atmospheric oxygen across the Archean-Proterozoic boundary came along with a partial transition of seawater composition towards more sulfidic conditions in ocean neritic zones. While ferruginous conditions are thought to still have persisted in the open deep ocean, the actual extent of sulfidic vs. ferruginous waters and controlling factors on their relative prevalence remain poorly constrained. Evidence from the rock record suggests a major role for Fe(II)-oxidizing and Fe(III)-reducing microorganisms in shaping the ancient ocean environment, but their actual contribution requires to be deciphered. Here we present Fe(II) oxidation and Fe(III) reduction data from controlled microcosm experiments with sediment from the Arvadi Spring, a model habitat for ferro-euxinic transition zones of late Archean and Proterozoic oceans. Fe(II) oxidation was demonstrated not to take place under anoxic conditions, whereas a clear increase in Fe(III) was observed in microoxic microcosms with 0.5%, 1% and 3% headspace oxygen. Fe(III) reduction was identified to be intensely proceeding under anoxic conditions, with a full reduction of the available Fe(III) within 9 days in organic-spiked microcosms. We demonstrated Fe(III) reduction to be limited by the organic carbon availability in the Arvadi Spring and to be accelerated under the contemporaneous presence of active sulfate reduction and sufficient organic carbon. Our results imply a spatial separation of Fe(II) oxidation and Fe(III) reduction into oxic and anoxic parts of the ferro-euxinic ocean transition zones. Furthermore, we suggest Fe(II) accumulation and hence the development of ferruginous conditions to have been elevated under high organic carbon availability and contemporaneous dissimilatory sulfate reduction.

## Introduction

Ancient Earth's atmosphere, hydrosphere and biosphere differed much from today, and the majority of past conditions is reconstructed with information from the geologic record. Banded Iron Formations (BIFs), sedimentary rocks that deposited between the Eoarchean (3.8 Ga) and Paleoproterozoic (1.8 Ga), consist of up to 40 wt% Fe, implying their depositional settings to have been ferruginous (Fe(II)-enriched) [1, 2]. Fe-speciation data from a variety of mid-Proterozoic marine mudstones [3] and Neoproterozoic geologic formations [4] revealed the open deep ocean to have persisted dominantly ferruginous even throughout much of the Proterozoic, with Fe(II) concentrations ranging between 40 to 120  $\mu\text{mol liter}^{-1}$  [5]. The direct consequence of these assumptions on ancient ocean chemistry is that biotic and abiotic Fe-cycling must have played a major role early in Earth's history.

Evidence for the existence of Precambrian Fe-metabolizers most notably comes in form of microfossil [6-8] and Fe-isotope data [9-13]. For instance, Fe-isotopes combined with Nd-isotope and rare earth element (REE) data from the late Archean Brockman Iron Formation (Hamersley Basin, Australia) revealed dissimilatory Fe(III) reduction to have mobilized continental Fe from riverine runoff in coastal margin sediments [11]. Dissimilatory Fe(III) reduction therefore is suggested to have contributed significantly to the late Archean oceanic Fe(II) budget in addition to the hydrothermal Fe(II) source [14, 15]. Furthermore, Fe-isotope and REE data from the Paleoproterozoic Gunflint and Biwabik Iron Formations (Lake Superior, Canada & USA) unveiled the presence of Fe(II)-oxidizing ecosystems in respective depositional settings [7]. Microfossil data from the Paleoproterozoic Jhamarkotra Iron Formation (Rajasthan, India, [6]) indicate a similar scenario, with an emphasis on the role of microaerophilic Fe(II)-oxidizers in the Fe-metabolizer community. Respective microfossils resembled the morphology of twisted stalks, Fe(II) oxidation products with characteristic shapes that are typically formed by certain extant microaerophilic Fe(II)-oxidizers [16-18]. In addition to evidence from the rock record, laboratory simulation of past ocean conditions together with theoretical calculations suggest anaerobic phototrophic Fe(II)-oxidizers to have played a crucial role in the deposition of Banded Iron Formations [19]. Most recently, a

study of Kabuno Bay of Lake Kivu (Rwanda and Dem. Rep. of Congo) showed nitrate-reducing Fe(II) oxidation to be a significant process in ferruginous water columns, suggesting a similar scenario for corresponding ancient ocean settings [20].

Despite the evident presence of Fe-metabolizers early in Earth's history, little is known about their relative activity and response to challenging environmental conditions. The advent of oxygenic photosynthesis [21, 22] and the therein involved oxygen overshoot and recovery during the Paleoproterozoic Lomagundi Event [23, 24] caused drastic geochemical changes in surface seawater and in intermediate depths of the ocean during the late Archean [25] and Paleoproterozoic [26-28]. Fe(II) levels in respective settings are assumed to have decreased substantially as a consequence of (1) Fe(II) oxidation by molecular oxygen and therewith associated precipitation of poorly soluble Fe(III) (oxyhydr)oxides, and (2) Fe(II) precipitation as Fe(II) sulfides in euxinic (anoxic and sulfide-rich) seawater. The latter accumulated in intermediate depths of neritic ocean zones in form of 'sulfide wedges' as a result of increased oxidative weathering of terrestrial pyrite and an accompanying elevation of oceanic sulfate levels in ocean neritic zones, stimulating dissimilatory sulfate reduction [29]. The transition from ferruginous to euxinic conditions in respective ocean zones remains vague, and especially the relative extent of ferruginous versus euxinic conditions and factors controlling their expansion require to be deciphered [30, 31].

Our knowledge gaps on the relative extent of ferrous and euxinic conditions and the impact of this drastic transition on the activity of Fe-metabolizers but also the contribution of Fe-metabolizers on shaping ocean geochemistry are mostly due to the metamorphosed and incomplete rock record that impedes interpreting observed biogeochemical signatures. An alternative way to study ancient ocean composition and microbial community structure and activity is the analyses of modern model habitats, i.e. environments that resemble conditions of the ancient ocean [32]. This type approach was the basis for studies with Kabuno Bay [20], Lake Matano (Indonesia) [33, 34], Lake Pavin (France) [35] and Lake Cadagno (Switzerland) [36] that all represent either ferruginous or euxinic ancient seawater conditions. A recent study by Koeksoy et al. (in press) on a modern model habitat for ferro-euxinic transition zones of late Archean and Proterozoic oceans, i.e. the Arvadi Spring

(Switzerland) revealed phototrophic, nitrate-reducing and microaerophilic Fe(II)-oxidizers and Fe(III)- and sulfate-reducers to be part of the microbial community, with microaerophiles being the dominant Fe- and S-metabolizers. Koeksoy et al. suggested a similar scenario for oxygenated, ferro-euxinic transition zones of late Archean and Proterozoic oceans, but have not addressed the relative metabolic activity of respective Fe- and S-metabolizers in the Arvadi Spring, and hence conclusions on their relative contribution on the Fe- and S-rich water geochemistry prevail uncertain.

In this study, we examined the activity of Fe(III)-reducers and Fe(II)-oxidizers in the Arvadi Spring sediment under controlled anoxic and microoxic conditions in microcosms with specific amendments. By testing different conditions, we followed the ultimate goal to understand limiting factors on biogeochemical Fe-cycling and on the formation of ferruginous versus euxinic waters in late Archean and Proterozoic oceans.

## Methods

**Sampling and Arvadi water processing.** Major physical and chemical parameters (pH, temperature, O<sub>2</sub> saturation, salinity) were measured in the Arvadi Spring pond water with a field multimeter (WTW, Multi 3430) containing an oxygen sensor (FDO@925), a conductivity electrode (TetraCon@925) and a pH sensor (SenTix®) with an additional temperature sensor. Water samples for Fe(II) and sulfide quantification were fixed in 1 M HCl and 2% (w/v) Zn-acetate. Sediment and water samples for the microcosm setup were collected from the spring pond and were transported and stored in the lab at 4°C and in the dark until their use. The Arvadi water was flushed with N<sub>2</sub> for 1 h liter<sup>-1</sup> prior to filter-sterilization (0.22µm, steritop) in the glovebox under a 100% N<sub>2</sub> atmosphere. Afterwards, the water headspace was exchanged with N<sub>2</sub>:CO<sub>2</sub> (90:10) before 30 mM bicarbonate buffer was added. The buffered water was further supplemented with 1 mL liter<sup>-1</sup> 7-vitamine solution [37], 1 mL liter<sup>-1</sup> selenite tungstate solution and 1 mL liter<sup>-1</sup> SL10 solution [38].

Additional supplements were added to the Arvadi water according to the conditions to be tested. Arvadi water for phototrophic Fe(II) oxidation microcosms was supplemented with 10 mM FeCl<sub>2</sub> only. Arvadi water for nitrate-reducing Fe(II) oxidation microcosms was amended with 10 mM FeCl<sub>2</sub>, 10 mM NaNO<sub>3</sub> and 10 mM Na-acetate. Arvadi water for microoxic Fe(II) oxidation microcosms was amended with 10 mM FeCl<sub>2</sub>. Different combinations of supplements were added to Arvadi water for Fe(III) reduction microcosms. Arvadi water for non-amended conditions was not supplemented with any additions. Arvadi water for Fe(III) reduction microcosms with elevated Fe(III) levels were spiked with ~5mM ferrihydrite. Arvadi water for Fe(III) reduction microcosms with additional organic carbon were amended with 5 mM Na-acetate and 5 mM Na-lactate. Arvadi water for Fe(III) reduction microcosms with elevated Fe(III) and organic carbon levels were amended with 5 mM ferrihydrite, 5 mM Na-acetate and 5 mM Na-lactate. Arvadi water for Fe(III) reduction microcosms with inhibited sulfate reduction was amended with 5 mM Na-molybdate. Arvadi water for abiotic microcosms was amended with 164 mM NaN<sub>3</sub>, an inhibitor of respiratory cytochromes [39]. For each experiment, the pH of the Arvadi water was adjusted to 7.2 by 0.5 M Na<sub>2</sub>CO<sub>3</sub> after the addition of the specific supplements.

### **General experimental setup**

**Anoxic microcosms.** Microcosms for the quantification of Fe(II) oxidation and Fe(III) reduction under anoxic conditions were prepared according to a non-sacrificial sampling approach, i.e. all samples at each sampling time point of a replicate were collected from the same microcosm. Each experiment was prepared in triplicates with ca. 5 g of homogenized Arvadi sediment in each replicate that was deoxygenated with N<sub>2</sub>:CO<sub>2</sub> (90:10) prior to the addition of supplemented Arvadi water. Fe(II) oxidation microcosms contained 50 mL of Arvadi water, while Fe(III) reduction microcosms contained 60 mL of Arvadi water due to a higher requirement of sample volume over time in the latter. The microcosm headspace was exchanged with N<sub>2</sub>:CO<sub>2</sub> (90:10) prior to closing the bottle with a butyl stopper via Hungate technique. After the first samples were collected from each replicate, all microcosms were

incubated either in the dark (covered with aluminum foil) or under visible light (40W halogen bulb) over the course of the experiment.

**Microoxic microcosms.** Microcosms for the quantification of Fe(II) oxidation rates under microoxic conditions were prepared according to a sacrificial sampling approach, i.e. each sample from each replicate at each sampling time point was collected from a single microcosm. Each experimental condition was tested in triplicates. Every microcosm contained ca. 1 g of homogenized Arvadi sediment and 2 mL of Arvadi water in 20 mL headspace vials. The microcosms were prepared anoxically first with a headspace of N<sub>2</sub>:CO<sub>2</sub> (90:10), and were amended with defined amounts of sterile-filtered (0.22 μm) air O<sub>2</sub> via Hungate syringe afterwards. The headspace O<sub>2</sub> content thereby either was 0.5%, 1% or 3%. Abiotic control microcosms were incubated for 4 days prior to the first addition of O<sub>2</sub> to ensure all respiratory cytochromes were blocked before the experiment was started. All microcosms were incubated horizontally on rolling shakers at a speed of 40 rpm in the dark upon sampling, in order to increase the surface area of the incubated slurry phase and hence to yield a better diffusion of oxygen.

**Microcosm sampling.** All microcosms with the exception of O<sub>2</sub> monitoring vials for optode measurements during microoxic Fe(II) oxidation analyses were sampled in the glovebox under a 100% N<sub>2</sub> atmosphere. During the sampling process, 1 mL of slurry sample was taken from each microcosm via syringe and with contemporaneous thorough shaking of the microcosm. For subsequent quantification of total Fe in the slurry phase, 100 μL of slurry sample were added to 900 μL of 1 M HCl. In case of Fe samples from nitrate-reducing Fe(II) oxidation microcosms, slurry samples were added to 40 mM sulfamic acid instead of 1 M HCl in order to avoid abiotic Fe(II) oxidation by nitrite [40]. Fe was extracted for 1 h and the extraction was stopped afterwards by centrifugation at 7000 g for 5 minutes and transfer of the supernatants into fresh plastic tubes. The Fe extracts were used for Fe-quantification by the spectrophotometric ferrozine assay after Stookey [41]. The remaining slurry samples

were centrifuged at 7000 g for 10 minutes and the supernatants were transferred into fresh plastic tubes. These samples were used for dissolved Fe quantification by the ferrozine assay and nitrate, nitrite and ammonium quantification by flow injection analyses in case of nitrate-reducing Fe(II) oxidation microcosms.

**Fe quantification.** Total Fe (Fe(tot)) and Fe(II) in the slurry extract and dissolved phase samples were quantified spectrophotometrically by the ferrozine assay after Stookey [41]. For the quantification of Fe(II), 20  $\mu\text{L}$  of sample were added to 80  $\mu\text{L}$  of 1 M HCl. For the quantification of Fe(tot) in the same samples, 20  $\mu\text{L}$  of sample were added to 80  $\mu\text{L}$  of hydroxylamine hydrochloride (10% w/v) in order to reduce all Fe(III) in the sample to Fe(II) during an incubation of 30 minutes. Afterwards, 100  $\mu\text{L}$  of ferrozine were added to each test well and incubated for 5 minutes prior to measuring the absorption at 562 nm with a plate reader (FlashScan 550, Analytic Jena, Germany). Each sample was measured in triplicates.

**Sulfide quantification.** Sulfide in dissolved phase samples was quantified photometrically by the methylene blue method after Cline [42]. Thereby, 50  $\mu\text{L}$  of sample were added to 50  $\mu\text{L}$  of N,N-dimethyl-p-phenyldiamine sulfate, forming an aromatic compound. 50  $\mu\text{L}$  of  $\text{NH}_4\text{Fe(III)SO}_4 \times 12 \text{H}_2\text{O}$  were added to each test well to oxidize the formed aromatic compound to methylene blue prior to measuring its absorption at 664 nm with a plate reader (FlashScan 550, Analytic Jena, Germany). Each sample was measured in triplicates.

**Oxygen quantification.** Oxygen concentrations in microoxic Fe(II) oxidation microcosms were analyzed in the microcosm headspace and slurry phase by optodes (Fibox3, PreSens/OXY-4 Mini, PreSens) that enabled non-invasive quantification. Headspace vials for oxygen measurement were equipped with small patches (ca. 4 x 4 mm) of oxygen sensitive foil that were fixed with silicon glue in the inner glass wall. The optode was calibrated at 19.8°C and a pressure of 1116 hPa. Signals for 0%  $\text{O}_2$  (0.1 M Na-ascorbate in 0.1 M NaOH) and 100%  $\text{O}_2$  (air-saturated Arvadi water) were determined. Based on the measured  $\text{O}_2$  concentration, the

volume of air-oxygen that was required to maintain 0.5%, 1% and 3% headspace oxygen in the microcosms was determined and added through a sterile filter (0.22  $\mu\text{m}$ ) via Hungate syringe to the respective microcosms.

## Results

The pH of the Arvadi water was measured to be 7.9 with a temperature of 7.1, a salinity of 0.7 and an  $\text{O}_2$  saturation of 101.1% (with respect to atmospheric  $\text{O}_2$ ). We could quantify  $16.0 \pm 2.2 \mu\text{M}$  Fe(II),  $8.3 \pm 0.1 \text{ mM}$  sulfate and  $2.7 \pm 0.3 \mu\text{M}$  sulfide in the Arvadi pond water, whereas no dissolved Fe(III) was found to present. The water contained  $3.2 \pm 0.6 \text{ mg liter}^{-1}$  organic carbon and  $4.3 \pm 0.1 \text{ mM}$  bicarbonate.

The pH remained stable in all microcosms over the course of the experiment at the initially adjusted value of 7.2-7.3. Sulfide was below the detection limit of the Cline assay ( $1 \mu\text{M}$ ) in all microcosms throughout the experiment. Based on the heterogeneous nature of the Arvadi Spring sediment, it was not possible to monitor the Fe(II)/Fe(III) development in the slurry phase in molar concentrations, and hence the data is presented in percent Fe(II) and Fe(III) relative to the total Fe content (Fe(tot)).

**Fe(II) oxidation under anoxic conditions.** The initial Fe(II)/Fe(III) ratios were quite similar among biotic phototrophic Fe(II) oxidation microcosms with  $6.2 \pm 1.4$  and  $5.2 \pm 1.1$  in light and dark incubated microcosms, respectively, and were slightly higher in abiotic controls with  $7.1 \pm 1.1$  and  $7.9 \pm 0.8$ . No net increase in the Fe(III) content was observed. Instead, all initially available Fe(III) ( $14.4 \pm 2.4$  and  $16.6 \pm 2.8\%$  in light and dark incubations) was reduced in biotic microcosms within 12 days. In contrast, it took 16 days in abiotic microcosms to reduce nearly all initial Fe(III) ( $12.5 \pm 2.4$  and  $11.3 \pm 1.0\%$  in light and dark incubations, respectively, Fig. 1A).



Comparable results were recorded for the Fe(II)/Fe(III) development in nitrate-reducing Fe(II) oxidation microcosms. The initial Fe(II)/Fe(III) ratios were similar to those in phototrophic Fe(II) oxidation microcosms with  $5.3 \pm 1.0$  and  $6.5 \pm 1.1$  in biotic microcosms and  $6.8 \pm 2.2$  and  $4.9 \pm 0.9$  in abiotic microcosms, respectively. A complete reduction of the initial Fe(III) content was observed in biotic ( $16.2 \pm 2.6$  and  $13.7 \pm 1.9\%$ , light and dark incubations) and abiotic ( $13.6 \pm 3.1$  and  $17.4 \pm 2.3\%$ ) microcosms within 12 days (Fig. 1B). In dark incubated biotic microcosms, a decrease in the Fe(II) content of  $10.8 \pm 2.8\%$  was recorded after 12 days (Fig. 1B). In the same microcosms, the initial nitrate concentrations of  $8.1 \pm 0.1$  mmols liter<sup>-1</sup> decreased to  $3.7 \pm 0.2$  and  $4.0 \pm 0.4$  mmol liter<sup>-1</sup> in biotic microcosms that were incubated in the light and in the dark, respectively (Fig. 2A). An accompanying increase in ammonium concentrations to  $1.8 \pm 1.1$  and  $2.8 \pm 0.1$  mmols liter<sup>-1</sup> was recorded in light and dark incubated microcosms (Fig. 2B). No nitrite could be detected (Fig. 2A). Nitrate, nitrite and ammonium concentrations did not change in abiotic controls, except for a slight increase in nitrate in light and dark incubated microcosms at day 9. (Fig. 2A).

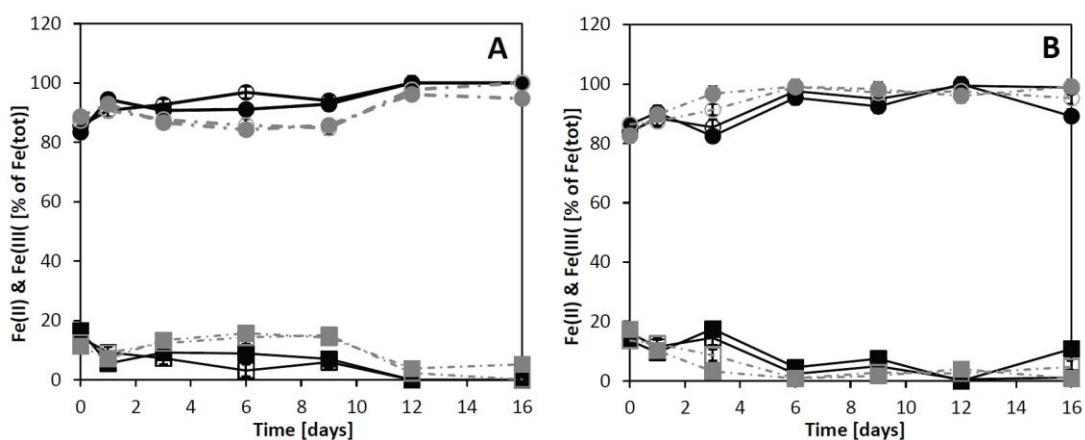


**Fig. 1:** Fe(II) (circles) and Fe(III) (squares) in the slurry phase of phototrophic (A) and nitrate-reducing Fe(II) oxidation (B) microcosms that were incubated in the light (open symbols) and in the dark (filled symbols), respectively. Black graphs show data from biotic microcosms, grey graphs show abiotic controls.

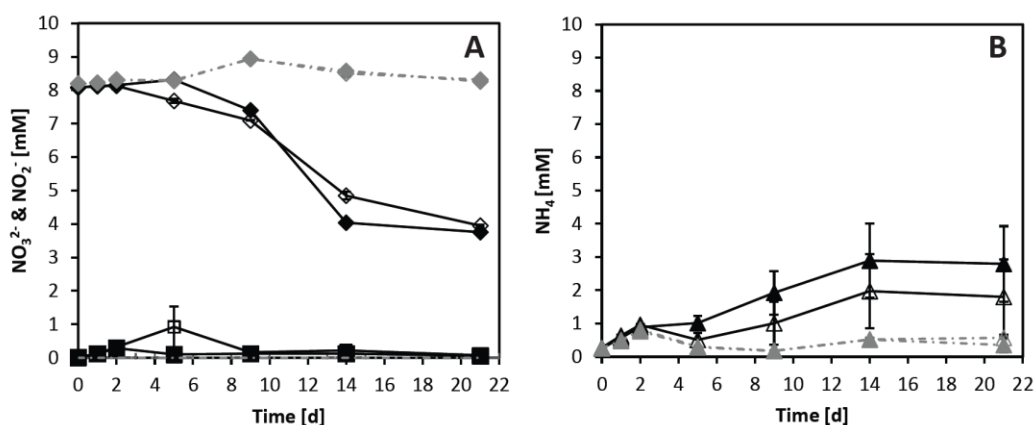


**Fig. 2:** Nitrate (diamonds, A), nitrite (squares, A) and ammonium (triangles, B) concentrations in the dissolved phase of nitrate-reducing Fe(II) oxidation microcosms over time.

**Fe(II) oxidation under microoxic conditions.** Despite thorough homogenization of the sediment during microcosm preparation, the initial Fe(II)/Fe(III) ratio varied among microcosms between 0.4 and 1.5 at the start of the experiment and abiotic microcosms were found to generally have a higher Fe(II) content.

In none of the microcosms, a complete turnover of Fe(II) into Fe(III) could be monitored within the time frame of the experiment (Fig. 3). In biotic microcosms, the lowest Fe(II)/Fe(III) ratio was reached already after 24 hours in 3% headspace O<sub>2</sub> setups ( $0.19 \pm 0.02$ ) and persisted similar until the end of the experiment. Similar Fe(II)/Fe(III) ratios were reached in 1% headspace O<sub>2</sub> microcosms after 96 hours ( $0.17 \pm 0.01$ ). The lowest Fe(II)/Fe(III) ratios in 0.5% headspace O<sub>2</sub> microcosms was  $0.33 \pm 0.02$  and was reached at 96 hours as well.

Generally, the total increase in the slurry phase Fe(III) content between 0 and 196 hours was found not to depend on the headspace O<sub>2</sub> content. An Fe(III) increase of  $17.7 \pm 9.5\%$ ,  $21.2 \pm 5.3\%$  and  $19.0 \pm 3.8\%$  could be recorded for biotic microcosms incubated with 0.5%, 1% and 3% headspace O<sub>2</sub>, whereas a higher increase in Fe(III) of  $26.4 \pm 5.2\%$ ,  $27.6 \pm 7.0\%$  and  $27.9 \pm 3.4\%$  was observed in abiotic microcosms with 0.5%, 1% and 3% headspace O<sub>2</sub>, respectively.

In contrast to the slurry phase, Fe(II) in the dissolved phase was oxidized completely within 24 hours in 3% O<sub>2</sub> microcosms and within 96 hours in 1% headspace O<sub>2</sub> microcosms. Fe(II) was still detectable in the millimolar range (1.7±1.2 mM) at the end of the experiment in biotic and abiotic microcosms with 0.5% O<sub>2</sub> (Fig. 3, bottom left). Fe(III) was not detected in the dissolved phase.

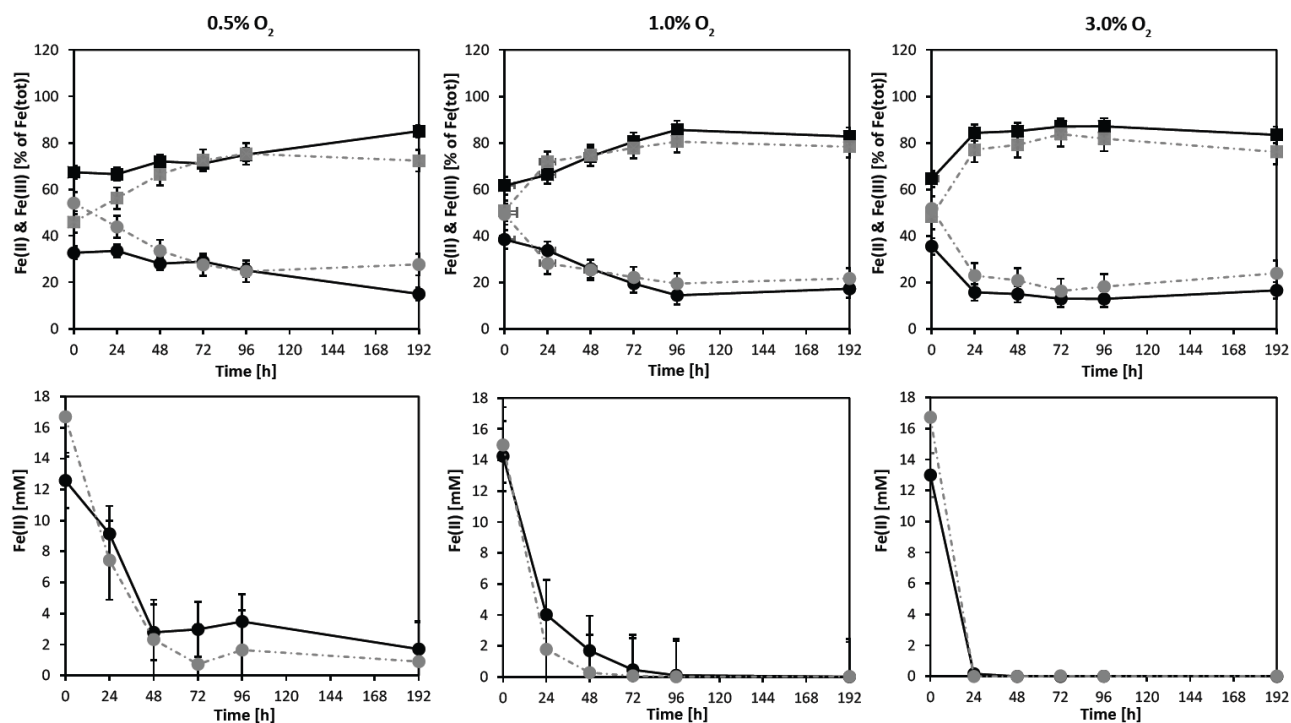


**Fig 3:** Fe(II) (circles) and Fe(III) (squares) in slurry phase (top) and dissolved phase (bottom) over time in microcosms for microaerophilic Fe(II) oxidation at 0.5%, 1% and 3% headspace oxygen. Black graphs show biotic sample data, grey graphs show abiotic controls.

Oxygen concentrations were kept stable in the headspace by spiking with filter-sterilized (0.22  $\mu$ m) air O<sub>2</sub> every 24 h. The headspace O<sub>2</sub> content decreased within 24 hours in all microcosms, but the discrepancy between present O<sub>2</sub> and required headspace O<sub>2</sub> became smaller after each O<sub>2</sub>-spiking event over the course of the experiment (Fig. 4 top). The discrepancy was observed to be overcome fastest in abiotic microcosms, with a near O<sub>2</sub>

saturation in 3% O<sub>2</sub> microcosms already after 24 hours. Furthermore, O<sub>2</sub> was observed to accumulate faster and to higher concentrations in the slurry phase of abiotic microcosms compared to biotic microcosms, reaching maximal concentrations of  $36.3 \pm 1.4 \mu\text{M}$  in 3% O<sub>2</sub> microcosms after 72 hours that remained stable until the end of the experiment at 192 hours. O<sub>2</sub> accumulated to  $10.0 \pm 0.6$  and  $4.9 \pm 0.1 \mu\text{M}$  in abiotic microcosms with 1% and 0.5% headspace O<sub>2</sub> after 120 hours. In contrast, O<sub>2</sub> accumulated to a maximum of  $30.6 \pm 1.7 \mu\text{M}$  in biotic microcosms with 3% O<sub>2</sub> after 120 hours and only to  $3.5 \pm 1.3$  and  $2.0 \pm 0.1 \mu\text{M}$  in 1% and 0.5% O<sub>2</sub> microcosms (Fig. 4, bottom).

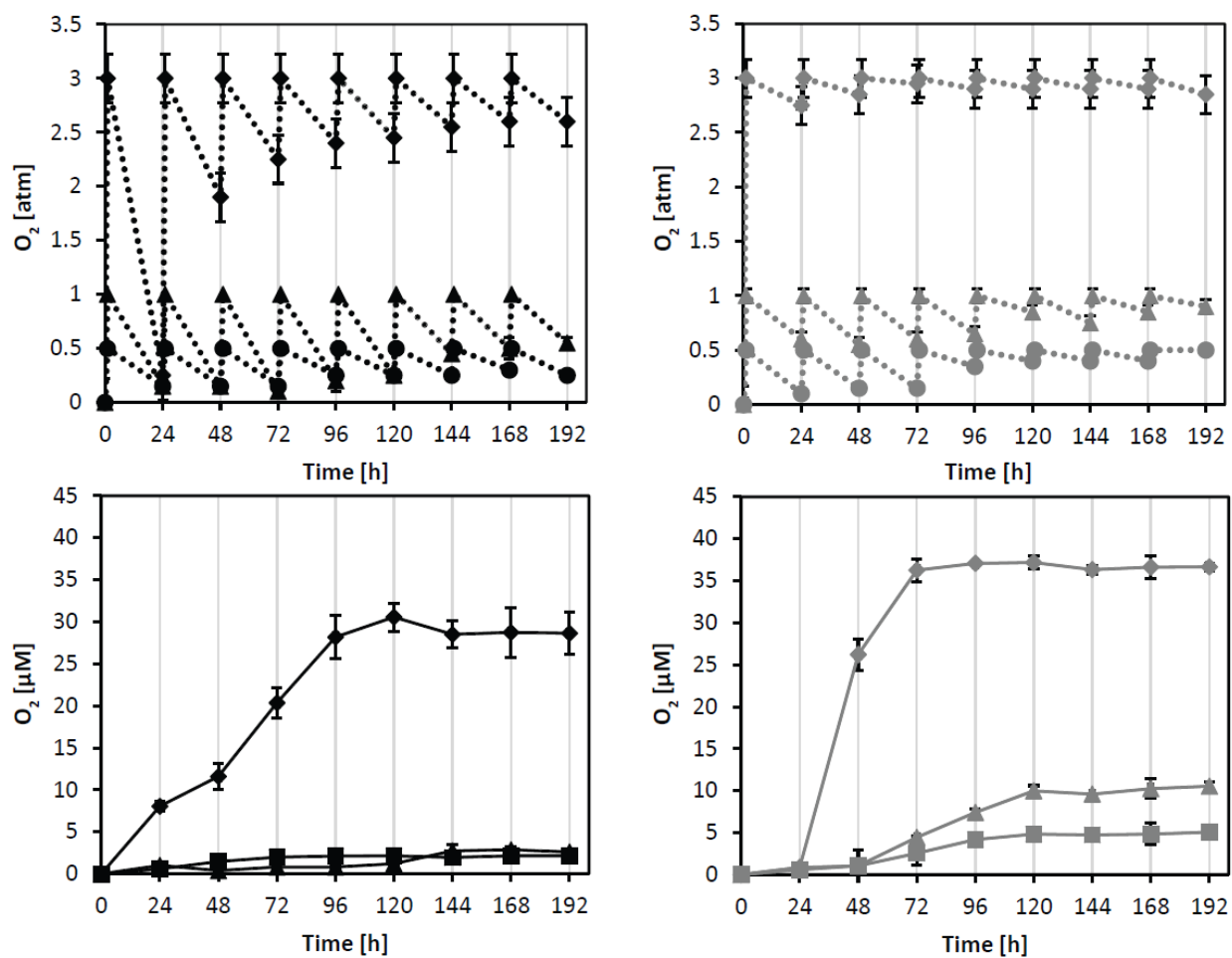


**Fig. 4:** Oxygen concentrations in the microcosm headspace (top) and slurry (bottom) over time. Diamonds show setups containing 3% headspace O<sub>2</sub>, triangles show 1% headspace O<sub>2</sub> and squares show 0.5% headspace O<sub>2</sub> microcosms.

**Fe(III) reduction under anoxic conditions.** Despite extensive homogenization of the sediment during the experimental setup, the initial Fe(II)/Fe(III) ratio in the slurry phase of the microcosms varied between 0.27 and 1.45 at the start of the experiment. Generally, Fe(II)/Fe(III) ratios changed in the first 2 to 4 days of incubation in all abiotic microcosms, but stabilized afterwards until the end of the experiment. No significant discrepancies were observed between light and dark incubated microcosms in the slurry phase (Fig. 5 & 6), while light-dependent trends could be observed in the dissolved phase (Fig. 7 & 8).

Major differences were observed between microcosm with active and inhibited sulfate reduction. Under active sulfate reduction conditions, complete Fe(III) reduction was observed only in microcosms that were amended with additional organic carbon in form of acetate and lactate (Fig. 5, top right) or with a combination of acetate, lactate and ferrihydrite (Fig. 5, bottom right). In unamended microcosms (Fig. 5, top left), a remaining Fe(III) pool of  $16.1 \pm 2.4$  and  $15.8 \pm 1.6\%$  was recorded at 17 days, while  $33.0 \pm 1.6$  and  $36.3 \pm 0.4\%$  Fe(III) were found in ferrihydrite-spiked microcosms that were incubated in the light and in the dark, respectively (Fig. 5, bottom left).

Under inhibited sulfate reduction conditions, Fe(III) reduction was complete in non-amended and organic carbon-spiked microcosms (Fig. 6 top left and top right). In microcosms spiked with ferrihydrite- and a combination of ferrihydrite and organic carbon, Fe(III) reduction was found to be incomplete with a remaining pool of  $29.0 \pm 1.9$  and  $31.1 \pm 6.5\%$  as well as  $17.5 \pm 2.5$  and  $18.8 \pm 3.3\%$  Fe(III) in light and dark incubated conditions, respectively (Fig. 6, bottom left).

Overall, the highest total increase in Fe(II) was observed in microcosms with active sulfate reduction that were amended with acetate, lactate and ferrihydrite, as the complete reduction of initially  $71.8 \pm 4.0$  and  $71.6 \pm 3.3\%$  Fe(III) over 17 days was observed in light and

dark incubated microcosms, respectively (Fig. 5, bottom right). Following on this were microcosms with active sulfate reduction that were spiked with additional organic carbon with a total of  $50.7 \pm 2.3$  and  $54.5 \pm 3.7\%$  Fe(III) having been reduced. Similarly contents of Fe(III) were reduced in microcosms with inactive sulfate reduction that were spiked with organic carbon ( $53.4 \pm 10.9$  and  $47.3 \pm 1.5\%$  Fe(III), Fig. 6, top right), and spiked with organic carbon and ferrihydrite ( $51.9 \pm 1.5$  and  $49.2 \pm 3.7\%$  Fe(III), Fig. 6, bottom right), incubated in the light and in the dark, respectively. The lowest relative amount of Fe(III) that was reduced was found in microcosms with active sulfate reduction that were not amended ( $39.9 \pm 4.6$  and  $39.9 \pm 2.7\%$  Fe(III)) or spiked with ferrihydrite ( $43.6 \pm 2.7$  and  $38.8 \pm 1.9\%$  Fe(III)) and in microcosms with inhibited sulfate reduction that were not amended ( $37.9 \pm 4.8$  and  $39.8 \pm 3.2\%$  Fe(III)) or spiked with ferrihydrite ( $37.7 \pm 2.0$  and  $33.6 \pm 6.8\%$  Fe(II), incubated in the light or in the dark, respectively).

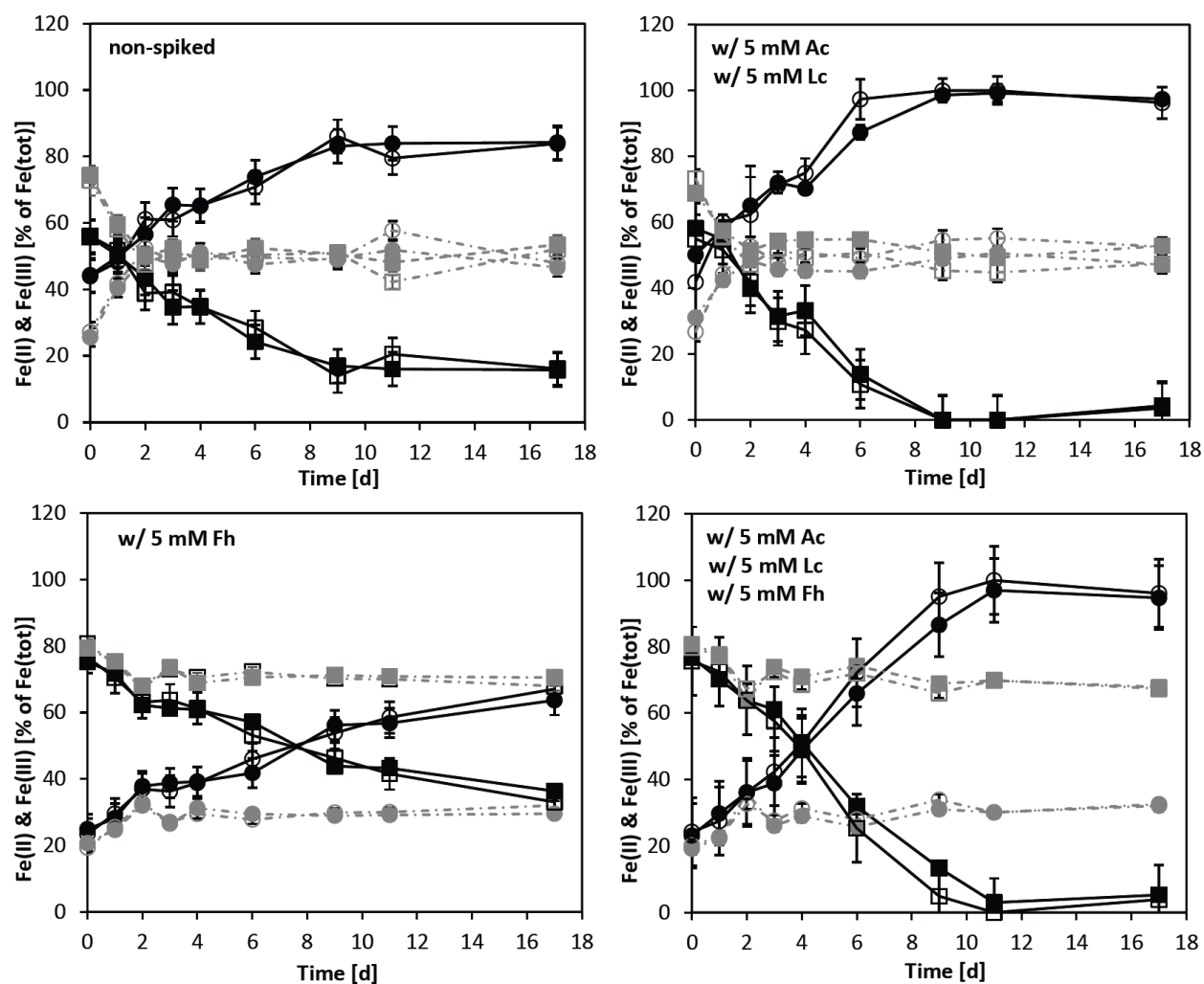


**Fig. 5:** Fe(II) oxidation and Fe(III) reduction in the slurry phase of microcosms with active sulfate reduction. Black graphs correspond to biotic microcosms, grey graphs to abiotic microcosms. Circles indicate Fe(II), squares Fe(III). Filled symbols correspond to incubation in the dark, empty symbols to light incubation. Shown are means of triplicates. Error bars indicate standard deviations of three parallel incubations.

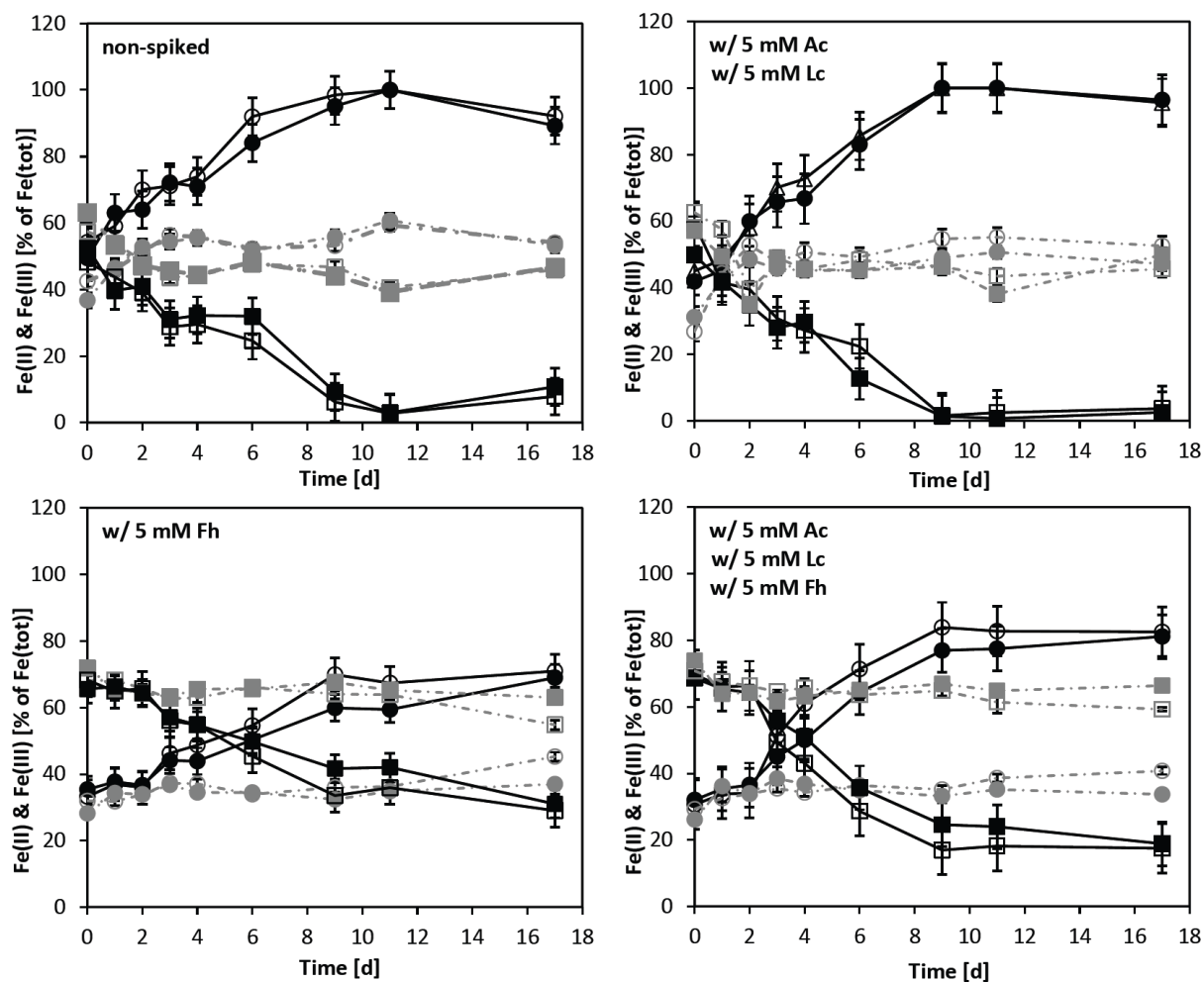


**Fig. 6:** Fe(II) oxidation and Fe(III) reduction in the slurry phase of microcosms with inactivated sulfate reduction. Black graphs correspond to biotic microcosms, grey graphs to abiotic microcosms. Circles indicate Fe(II), squares Fe(III). Filled symbols correspond to incubation in the dark, empty symbols to light incubation. Shown are means of triplicates. Error bars indicate standard deviations of three parallel incubations.



The highest dissolved phase Fe(II) concentrations were quantified in microcosms with active sulfate reduction that were amended with organic carbon and ferrihydrite and incubated in the dark at 6 days ( $1.0 \pm 0.0$  mM, Fig. 7, bottom right). Slightly lower Fe(II) concentrations were found in their light incubated counterparts ( $0.8 \pm 0.1$  mM Fe(II)) and in microcosms amended with organic carbon only ( $0.8 \pm 0.0$  and  $0.8 \pm 0.1$  mM Fe(II) in light and dark incubated microcosms, respectively). Fe(II) concentrations were found to be much lower in not amended ( $0.4 \pm 0.0$  and  $0.6 \pm 0.0$  mM Fe(II)) and ferrihydrite-spiked microcosms ( $0.5 \pm 0.0$  and  $0.7 \pm 0.0$  mM Fe(II) in light and dark incubated microcosms, respectively).

Similar observations were made for dissolved phase Fe(II) in microcosms with inhibited sulfate reduction (Fig. 8). The highest Fe(II) concentrations were quantified at  $0.9 \pm 0.1$  mM and  $0.9 \pm 0.0$  mM in microcosms amended with organic carbon (Fig. 8, top right) and with organic carbon and ferrihydrite (Fig. 8, bottom right), both incubated in the dark. Slightly lower Fe(II) concentrations were recorded for their light incubated counterparts with  $0.9 \pm 0.0$  mM and  $0.8 \pm 0.0$  mM Fe(II) respectively. Fe(II) concentrations were lower in microcosms that were not amended with additional organic carbon, with  $0.7 \pm 0.0$  and  $0.7 \pm 0.0$  mM in unamended microcosms (Fig. 8, top left) and  $0.6 \pm 0.0$  and  $0.6 \pm 0.0$  mM Fe(II) in ferrihydrite-spiked microcosms (Fig. 8, bottom left).

Fe(II) concentrations were observed to decrease after reaching their highest concentration in all of the microcosms. Thereby, the decrease was much faster and steep in organic-spiked microcosms than in those without organic carbon amendment.

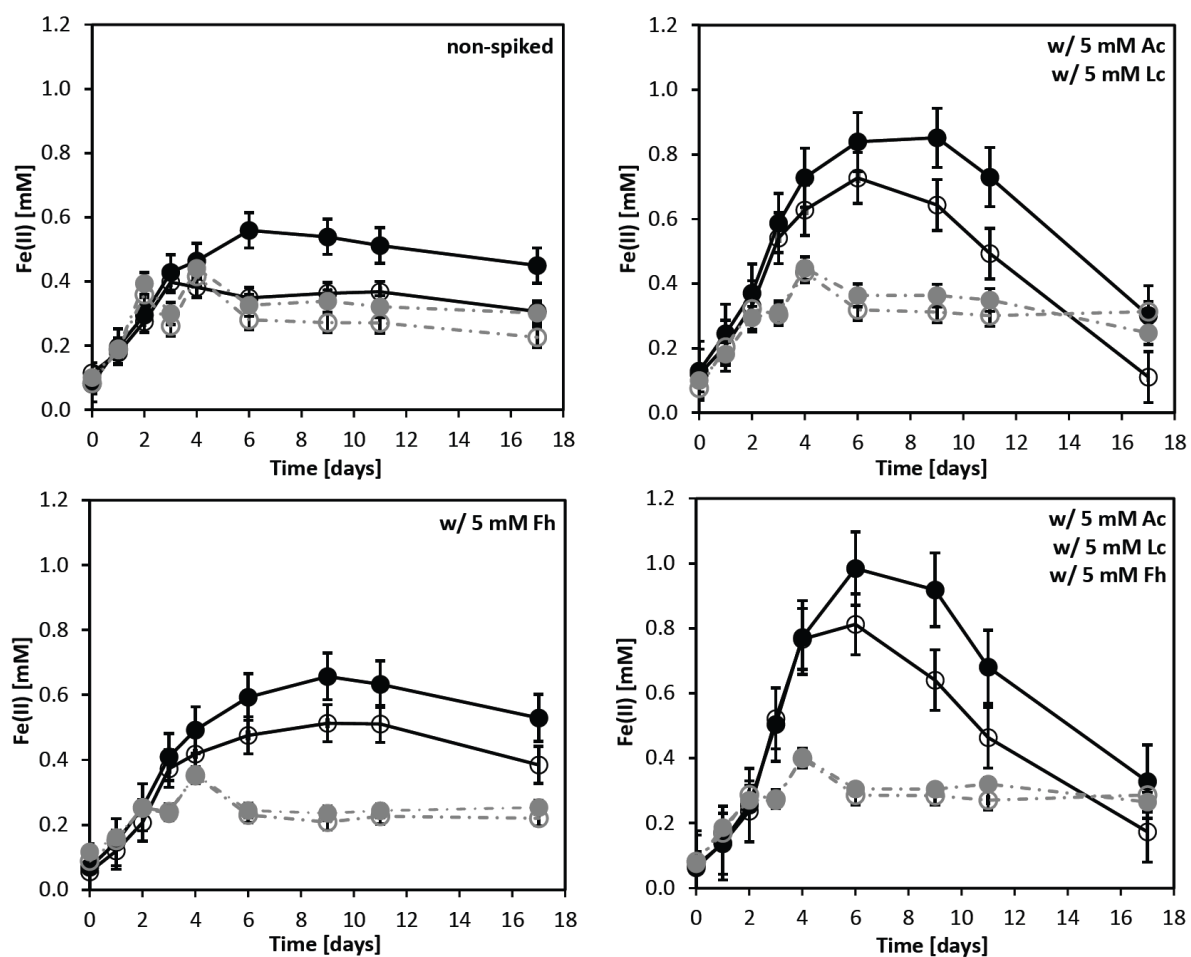


**Fig. 7:** Fe(II) in the dissolved phase of microcosms with active sulfate reduction.

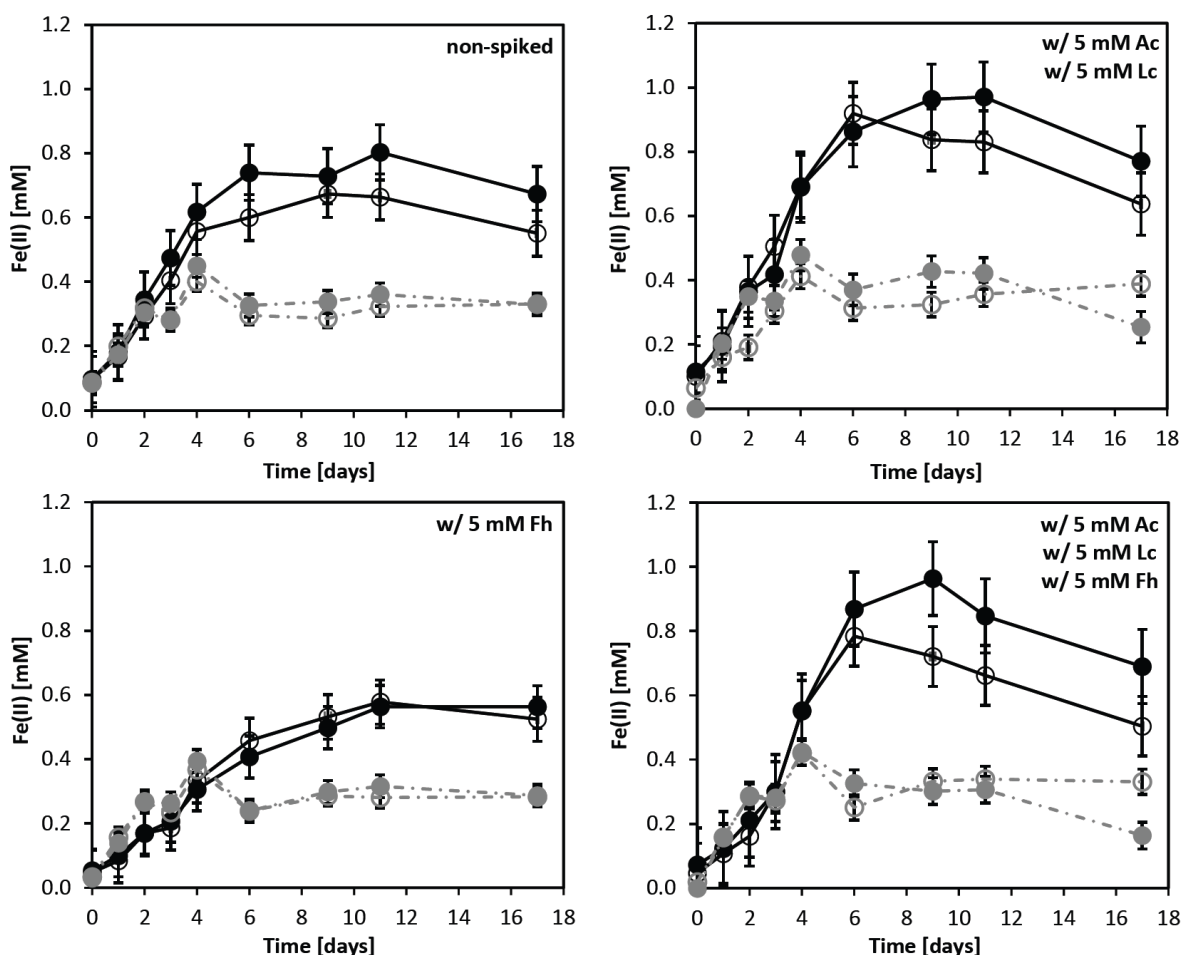


**Fig. 8:** Fe(II) in the dissolved phase of microcosms with inactivated sulfate reduction.

## Discussion

**Fe(II) oxidation under anoxic conditions.** The results for the Fe(II)/Fe(III) development were quite similar between phototrophic and nitrate-reducing Fe(II) oxidation microcosms. We showed that there was no net increase in the Fe(III) content in phototrophic Fe(II) oxidation microcosms, but instead the initially available Fe(III) to have been reduced completely within 12 to 16 days. The Fe(II) development was similar in nitrate-amended microcosms. Only a decrease in the Fe(II) content in dark incubated biotic microcosms after

12 days indicates Fe(II) oxidation to have started in respective microcosms towards the end of the experiment. We therefore suggest Fe(II) oxidation to possibly have proceeded in both, phototrophic and nitrate-reducing Fe(II) oxidation microcosms, over the course of the experiment and with certainty to have started in dark incubated biotic nitrate-reducing Fe(II) oxidation microcosms after 12 days. However, the net increase in Fe(II) implies Fe(III) reduction to have been the dominating process, masking potential Fe(II) oxidation. Unfortunately it was not possible in our approach to distinguish between the relative contributions of Fe(II) oxidation and Fe(III) reduction to net Fe(II)/Fe(III) development.

As phototrophic Fe(II)-oxidizers had been shown to exist in the Arvadi sediment before in long-term incubation experiments of about two months by Koeksoy et al. (in press), a reason for their missing or low activity could be the comparably short duration of our Fe(II) oxidation microcosm experiment. Fe(II)-oxidizers may have required a lag phase longer than 16 days before metabolic activity could have been recorded (except for dark incubated nitrate-reducing Fe(II) oxidation microcosms). To examine this possibility, additional experiments with longer incubation times would be required in future tests. Reasons for low metabolic activities could have been the lack of suitable ecological niches in the oxygen saturated Arvadi Spring pond. Anoxic niches for the anaerobic lifestyle of phototrophic and nitrate-reducing Fe(II)-oxidizers may be located too deep in the Arvadi sediment where the wavelength spectrum presumably does not allow for photoferrotrophy, hence forcing these microorganisms to either perform chemolithotrophic metabolisms (e.g. sulfide oxidation) or to switch into a dormant state [43]. In case of the latter, microorganisms may have required longer incubation periods in order to become fully metabolically active again.

We generally expected nitrate-reducing Fe(II)-oxidizers to be metabolically inactive due to the scarcity of nitrate and its intermediate products in the Arvadi Spring [44, 45]. However, the intense reduction of nitrate in nitrate-amended microcosms was against our expectations. Nitrite was shown not to accumulate, which on the one hand can be explained by its transition into ammonia (that in fact accumulated) or N<sub>2</sub> [46], while on the other hand, nitrite may have partially oxidized Fe(II). Generally, we cannot assign the observed reduction of nitrate to Fe(II) oxidation with certainty for several reasons: (1) To evaluate a

dependence of nitrate reduction and Fe(II) oxidation, additional test microcosms amended with nitrate but not with Fe(II) are required; however, for such microcosms, the Arvadi Spring sediment would be required to be devoid of Fe itself. Furthermore, control experiments without organic carbon are necessary to evaluate whether nitrate reduction is a heterotrophic process, but for this purpose, the Arvadi Spring sediment would be required to be devoid of organic carbon. (2) A calculated stoichiometry of reduced nitrate per oxidized Fe(II) would give further indications on nitrate-dependent Fe(II) oxidation. However, based on the large fluctuations in the total Fe concentrations over time, it was not possible to compile the Fe(II) development with the nitrate decrease. (3) Data on the consumption of organic carbon in respective microcosms could give additional hints on whether nitrate was reduced mainly by heterotrophic, mixotrophic or autotrophic nitrate-reducers that would be required to be tested in future experiments. (4) We cannot rule out analytical mistakes in the presented nitrogen data since the measured initial nitrate concentrations were approximately 2 mM lower than the intentionally added 10 mM  $\text{NaNO}_3^{2-}$ . We therefore are cautious with drawing conclusions on the relative importance of nitrate-reducing Fe(II) oxidation in the overall cycling of Fe in the Arvadi Spring.

The increasing Fe(II) levels in abiotic phototrophic and nitrate-reducing Fe(II) oxidation microcosms implies a role for abiotic Fe(III) reduction in the Arvadi Spring. Koeksoy et al. (submitted) showed sulfide to be present in the Arvadi Spring water and sediment in form of dissolved sulfide, polysulfides and amorphous and higher crystalline Fe(II) sulfides. We therefore assume abiotic Fe(III) reduction coupled to the oxidation of sulfide [47, 48] to have caused the increase in Fe(II) in abiotic microcosms, and to have also played a role in biotic microcosms in addition to dissimilatory Fe(III) reduction. We exclude the reduction of Fe(III) by dissolved sulfide from contemporaneously ongoing sulfate reduction in phototrophic and nitrate-reducing Fe(II) oxidation microcosms as on the one hand, these microcosms were amended with molybdate and hence sulfate reduction was inhibited during the microcosm incubation, while on the other hand, dissolved phase sulfide concentrations were shown to be below the detection limit of the Cline assay throughout the experiment. We rather suggest

sediment-bound sulfide to have been released during acidic Fe-extraction and to have reduced Fe(III) in the extract prior to Fe quantification by the ferrozine assay.

**Fe(II) oxidation under microoxic conditions.** Na-azide was shown by Otte et al. (unpublished data) to require 3 to 4 days to block all respiratory cytochromes in microorganisms of environmental soil and sediment samples [39]. Accordingly, we chose a 4 day pre-incubation to prevent microbial Fe-cycling in the microcosms after the addition of oxygen. Consequently, the Fe(II)/Fe(III) ratios were observed to be generally higher. The higher Fe(II) content in abiotic microcosms compared to biotic microcosms likely was the result of active dissimilatory Fe(III) reduction during these 4 days of the microcosm pre-incubation with Na-azide under anoxic conditions.

We could show a clear dependence between the time required to reach the smallest Fe(II)/Fe(III) ratio and the headspace O<sub>2</sub> content in microoxic microcosms, with the fastest, near complete Fe(II) oxidation recorded in 3% headspace O<sub>2</sub> microcosms already after 24 hours and the slowest Fe(II) oxidation in 0.5% O<sub>2</sub> microcosms that was not completed after 192 hours yet. The maximal increase in Fe(III) was generally higher in abiotic microcosms compared to biotic microcosms. This likely depended on the one hand on the higher Fe(II) content that was available for oxidation and on the other hand on the lack of dissimilatory Fe(III) reduction that could continuously supply Fe(II). Furthermore, O<sub>2</sub> was more available for Fe(II) oxidation in abiotic microcosms compared to biotic microcosms, in which much of the added O<sub>2</sub> was readily consumed within 24 hours (Fig. 4, top). Koeksoy et al. (in press) could show that heterotrophic microorganisms are abundant in the Arvadi Spring microbial community, hence we assume much of the added oxygen in biotic microcosms to have been consumed by aerobic respiration of heterotrophic microorganisms, whereby this assumption could not be evaluated quantitatively. Partially, the decrease in the headspace O<sub>2</sub> levels can be assumed to have been based on the oxidation of reduced compounds as well, including Fe(II) and sulfide. With a decreasing prevalence of reduced compounds upon their

oxidation and the accumulation of oxygen in the slurry phase, the discrepancies between measured and desired headspace O<sub>2</sub> levels became smaller after each O<sub>2</sub>-spiking event.

Overall, Fe(II) oxidation was not complete in any of the microcosms, indicating Fe(II) to be continuously supplied by Fe(III) reduction in biotic and abiotic microcosms. This observation indicates an abiotic source for Fe(II) and similar to anoxic Fe(II) oxidation microcosms, we suggest a role for sulfide-dependent Fe(III) reduction in both types of microcosms.

While the near complete consumption of oxygen in biotic microcosms certainly slowed down abiotic Fe(II) oxidation, the impact of fluctuating O<sub>2</sub> concentrations on the microbial activity remain uncertain. While continuous exchange of the headspace with a gas mixture containing defined amounts of O<sub>2</sub> may have prevented big fluctuations in the O<sub>2</sub> levels in biotic microcosms, gradient formation in the slurry phase would have been an accompanying side-effect.

We suggest abiotic Fe(II) oxidation by O<sub>2</sub> to be the dominant source for Fe(III) in microoxic microcosms and microaerophilic Fe(II) oxidation not to play a role at the O<sub>2</sub> concentrations tested in this study. However, considering microaerophiles to be the dominating type of Fe- and S-metabolizers in the Arvadi Spring (Koeksoy et al. (in press)), further tests with lower oxygen concentrations could reveal a larger impact of microaerophilic Fe(II) oxidation. Already at 0.5% headspace O<sub>2</sub>, abiotic Fe(II) oxidation slowed down significantly compared to 1% and 3% headspace O<sub>2</sub> microcosms (Fig.3).

**Fe(III) reduction under active and inactive sulfate reduction.** We could demonstrate Fe(III) reduction in the Arvadi Spring to be limited by the availability of organic carbon. Complete Fe(III) reduction was observed in microcosms with active sulfate reduction only if they were spiked with additional organic carbon in form of acetate and lactate (Fig. 5 top and bottom right). We could show that the Arvadi Spring is not limited in Fe(III) as no significant improvement in the total Fe(II) increase was achieved by the amendment with ferrihydrite

(Fig. 5, bottom left). Only by the combined amendment with ferrihydrite and organic carbon, an increase in the Fe(II) content and complete Fe(III) reduction was observed (Fig. 5, bottom right), that further supported our finding that the system is limited in organic carbon availability.

The complete reduction of Fe(III) in microcosms with inhibited sulfate reduction that were not amended with either organic carbon or ferrihydrite (Fig. 6, top left) implies much of the Arvadi Spring organic carbon to be consumed by sulfate-reducers and hence sulfate reduction to be indirectly limiting Fe(III) reduction in the Arvadi Spring. The incomplete reduction of Fe(III) and the significantly lower increase in Fe(II) in ferrihydrite-spiked microcosms with inhibited sulfate reduction indicates the organic carbon content of the Arvadi Spring to be sufficient only for the available amount of Fe(III). For a higher demand, as for instance in ferrihydrite-spiked microcosms or at contemporaneously ongoing dissimilatory sulfate reduction as in microcosms with active sulfate reduction, the available organic carbon in the Arvadi Spring was demonstrated to be insufficient.

While a slight improvement in the Fe(III) reduction capacity could be monitored in microcosms that were spiked with organic carbon and ferrihydrite with inhibited sulfate reduction, Fe(III) was not reduced completely in these microcosms (Fig. 6, bottom right). These results, compared to the complete reduction of Fe(III) in organic carbon- and ferrihydrite-spiked microcosms with active sulfate reduction (Fig. 5, bottom right), indicate the highest yield of Fe(II) to be achieved under the contemporaneous presence of active sulfate reduction and additional organic carbon that is sufficient for both, dissimilatory Fe(III) and sulfate reduction together. Thereby, Fe(II) is produced on the one hand by dissimilatory Fe(III) reduction and on the other hand abiotically by sulfide from sulfate reduction. Our observation of sulfide levels to be below detection limit in dissolved phase samples from all Fe(III) reduction microcosms supports its rapid reaction with either Fe(III), reducing it to Fe(II), or with Fe(II), precipitating as Fe(II) sulfide.

It was not possible to identify the Fe(II)/Fe(III) development in absolute concentrations in microcosms with the Arvadi Spring sediment due to its heterogeneous composition. To avoid



great deviations among the total Fe concentrations through varying amounts of Fe particles in samples from different sampling time points, we suggest future microcosms to be set up with enrichment cultures of the original Arvadi Spring sediment that were grown on specific substrates. Microcosms inoculated with respective enrichment cultures could aid in the collection of absolute concentrations of Fe(III), Fe(II), sulfate, sulfide and organic carbon, with which mass balances for the specific metabolic and abiotic processes could be set up to quantitatively evaluate the impact of the respective processes under Arvadi Spring and controlled conditions.

## **Implications for Precambrian Fe-cycling**

Our results indicate the cycling of Fe in ferro-euxinic transition zones of the ocean to have been spatially separated to a great extent into anoxic ocean zones, where Fe(III) got reduced and into oxic ocean parts, where Fe(II) was oxidized mainly abiotically by O<sub>2</sub>. We suggest a diminished role for anaerobic Fe(II)-oxidizers in ferro-euxinic transition zones of the Proterozoic Ocean under anoxic conditions with elevated Fe(II) levels. Phototrophic Fe(II)-oxidizers presumably played a major role in photic zones of ferro-euxinic waters, where their required wave length spectrum for photosynthetic Fe(II) oxidation was available. In contrast, photoferrotrophs probably were in a dormant state in oxygenated parts of ferro-euxinic intermixed waters, where most of the Fe(II) was rather oxidized abiotically by oxygen. In zones where less than 3.5 μM O<sub>2</sub> was present, microaerophiles may have played a bigger role in the oxidation of the present Fe(II) as well.

Our data generally indicates Fe(II) production and hence the formation of ferruginous conditions to have been triggered by sulfate reduction under the contemporaneous presence of sufficient organic carbon for both, dissimilatory Fe(III) and sulfate reduction. Only if the organic carbon content would have been insufficient for both processes, the prevalence of sulfate-reducers would have diminished Fe(II) levels, not only by its precipitation as Fe(II) sulfide through emerging euxinic water masses, but also by limiting Fe(III)-reducers by

organic carbon availability. In this assumption, the contribution of hydrothermal venting however is not considered, which additionally elevates total Fe(II) concentrations. Generally, we could not observe the development of euxinic conditions. To evaluate the conditions under which sulfide starts accumulating with Fe(II), additional tests with anoxic and microoxic microcosms with elevated sulfate levels would be required. Furthermore, column experiments for the simulation of geochemical gradient formation and additional factors such as wave action are necessary in future experiments, in which the accumulating concentrations of Fe(II) and sulfide in the dissolved phase could be taken as representative for ancient ferruginous and euxinic seawater. Our batch culture approach does not represent ocean conditions and hence, the observed Fe(II) concentrations in the dissolved phase of Fe(III) reduction microcosms cannot be taken as representative values for ferruginous conditions in the ancient global ocean. However, our experiments set the onset for further tests focusing on the interplay of Fe(III) reduction, sulfate reduction and organic carbon limitation, that once tested under different conditions with different approaches, could reveal how ferruginous and euxinic waters formed, were controlled and persisted over geologic timescales.

### **Acknowledgements**

We thank E. Roehm, F. Schaedler and V. Nিকেleit for support during the microcosms sampling and sample analyses process. We acknowledge U. Lueder, M. Maisch and N. Blackwell for inspirations and improvements during project design and development. This project was funded by the DFG grant (No. KA 1736/27-1).

## REFERENCES

1. Klein, C., *Some Precambrian banded iron-formations (BIFs) from around the world: Their age, geologic setting, mineralogy, metamorphism, geochemistry, and origins*. American Mineralogist, 2005. **90**(10): p. 1473-1499.
2. Huston, D.L. and G.A. Logan, *Barite, BIFs and bugs: evidence for the evolution of the Earth's early hydrosphere*. Earth and Planetary Science Letters, 2004. **220**(1): p. 41-55.
3. Planavsky, N.J., et al., *Widespread iron-rich conditions in the mid-Proterozoic ocean*. Nature, 2011. **477**(7365): p. 448-451.
4. Canfield, D.E., et al., *Ferruginous conditions dominated later neoproterozoic deep-water chemistry*. Science, 2008. **321**(5891): p. 949-952.
5. Canfield, D.E., *The early history of atmospheric oxygen: homage to Robert M. Garrels*. Annu. Rev. Earth Planet. Sci., 2005. **33**: p. 1-36.
6. Crosby, C.H., J.V. Bailey, and M. Sharma, *Fossil evidence of iron-oxidizing chemolithotrophy linked to phosphogenesis in the wake of the Great Oxidation Event*. Geology, 2014. **42**(11): p. 1015-1018.
7. Planavsky, N., et al., *Iron-oxidizing microbial ecosystems thrived in late Paleoproterozoic redox-stratified oceans*. Earth and Planetary Science Letters, 2009. **286**(1-2): p. 230-242.
8. Dodd, M.S., et al., *Evidence for early life in Earth's oldest hydrothermal vent precipitates*. Nature, 2017. **543**(7643): p. 60-64.
9. Yamaguchi, K.E., et al., *Biogeochemical cycling of iron in the Archean-Paleoproterozoic Earth: Constraints from iron isotope variations in sedimentary rocks from the Kaapvaal and Pilbara Cratons*. Chemical Geology, 2005. **218**(1): p. 135-169.
10. Heimann, A., et al., *Fe, C, and O isotope compositions of banded iron formation carbonates demonstrate a major role for dissimilatory iron reduction in ~2.5Ga marine environments*. Earth and Planetary Science Letters, 2010. **294**(1): p. 8-18.
11. Li, W., B.L. Beard, and C.M. Johnson, *Biologically recycled continental iron is a major component in banded iron formations*. Proceedings of the National Academy of Sciences, 2015. **112**(27): p. 8193-8198.
12. Czaja, A.D., et al., *Iron and carbon isotope evidence for ecosystem and environmental diversity in the ~2.7 to 2.5Ga Hamersley Province, Western Australia*. Earth and Planetary Science Letters, 2010. **292**(1): p. 170-180.
13. Johnson, C.M., et al., *Iron isotopes constrain biologic and abiologic processes in banded iron formation genesis*. Geochimica et Cosmochimica Acta, 2008. **72**(1): p. 151-169.

14. Jacobsen, S.B. and M.R. Pimentel-Klose, *A Nd isotopic study of the Hamersley and Michipicoten banded iron formations: the source of REE and Fe in Archean oceans*. Earth and Planetary Science Letters, 1988. **87**(1-2): p. 29-44.
15. Holland, H.D., *The oceans; a possible source of iron in iron-formations*. Economic Geology, 1973. **68**(7): p. 1169-1172.
16. Krepeski, S., et al., *Morphology of biogenic iron oxides records microbial physiology and environmental conditions: toward interpreting iron microfossils*. Geobiology, 2013. **11**(5): p. 457-471.
17. Chan, C., D. Emerson, and G. Luther, *The role of microaerophilic Fe-oxidizing micro-organisms in producing banded iron formations*. Geobiology, 2016. **14**(5): p. 509-528.
18. Chan, C.S., et al., *Lithotrophic iron-oxidizing bacteria produce organic stalks to control mineral growth: implications for biosignature formation*. The ISME journal, 2011. **5**(4): p. 717.
19. Kappler, A., et al., *Deposition of banded iron formations by anoxygenic phototrophic Fe (II)-oxidizing bacteria*. Geology, 2005. **33**(11): p. 865-868.
20. Michiels, C.C., et al., *Iron-dependent nitrogen cycling in a ferruginous lake and the nutrient status of Proterozoic oceans*. Nature Geoscience, 2017. **10**(3): p. 217-221.
21. Holland, H.D., *The chemical evolution of the atmosphere and oceans*. 1984: Princeton University Press.
22. Schirrmeister, B.E., et al., *Evolution of multicellularity coincided with increased diversification of cyanobacteria and the Great Oxidation Event*. Proceedings of the National Academy of Sciences, 2013. **110**(5): p. 1791-1796.
23. Planavsky, N.J., et al., *Sulfur record of rising and falling marine oxygen and sulfate levels during the Lomagundi event*. Proceedings of the National Academy of Sciences, 2012. **109**(45): p. 18300-18305.
24. Bachan, A. and L.R. Kump, *The rise of oxygen and siderite oxidation during the Lomagundi Event*. Proceedings of the National Academy of Sciences, 2015. **112**(21): p. 6562-6567.
25. Olson, S.L., L.R. Kump, and J.F. Kasting, *Quantifying the areal extent and dissolved oxygen concentrations of Archean oxygen oases*. Chemical Geology, 2013. **362**(Supplement C): p. 35-43.
26. Partin, C., et al., *Large-scale fluctuations in Precambrian atmospheric and oceanic oxygen levels from the record of U in shales*. Earth and Planetary Science Letters, 2013. **369**: p. 284-293.
27. Reinhard, C.T., et al., *Proterozoic ocean redox and biogeochemical stasis*. Proceedings of the National Academy of Sciences, 2013. **110**(14): p. 5357-5362.
28. Hardisty, D.S., et al., *An iodine record of Paleoproterozoic surface ocean oxygenation*. Geology, 2014. **42**(7): p. 619-622.

29. Canfield, D.E., *A new model for Proterozoic ocean chemistry*. *Nature*, 1998. **396**(6710): p. 450-453.
30. Li, C., et al., *A stratified redox model for the Ediacaran ocean*. *Science*, 2010. **328**(5974): p. 80-83.
31. Reinhard, C.T., et al., *A Late Archean Sulfidic Sea Stimulated by Early Oxidative Weathering of the Continents*. *Science*, 2009. **326**(5953): p. 713-716.
32. Koeksoy, E., et al., *Using modern ferruginous habitats to interpret Precambrian banded iron formation deposition*. *International Journal of Astrobiology*, 2016. **15**(3): p. 205-217.
33. Crowe, S.A., et al., *Photoferrotrophs thrive in an Archean Ocean analogue*. *Proceedings of the National Academy of Sciences*, 2008. **105**(41): p. 15938-15943.
34. Zegeye, A., et al., *Green rust formation controls nutrient availability in a ferruginous water column*. *Geology*, 2012. **40**(7): p. 599-602.
35. Busigny, V., et al., *Iron isotopes in an Archean ocean analogue*. *Geochimica et Cosmochimica Acta*, 2014. **133**: p. 443-462.
36. Canfield, D.E., J. Farquhar, and A.L. Zerkle, *High isotope fractionations during sulfate reduction in a low-sulfate euxinic ocean analog*. *Geology*, 2010. **38**(5): p. 415-418.
37. Widdel, F. and N. Pfennig, *Studies on dissimilatory sulfate-reducing bacteria that decompose fatty acids*. *Archives of microbiology*, 1981. **129**(5): p. 395-400.
38. Widdel, F., G.-W. Kohring, and F. Mayer, *Studies on dissimilatory sulfate-reducing bacteria that decompose fatty acids*. *Archives of Microbiology*, 1983. **134**(4): p. 286-294.
39. Wilson, D. and B. Chance, *Azide inhibition of mitochondrial electron transport I. The aerobic steady state of succinate oxidation*. *Biochimica et Biophysica Acta (BBA)-Bioenergetics*, 1967. **131**(3): p. 421-430.
40. Klueglein, N. and A. Kappler, *Abiotic oxidation of Fe (II) by reactive nitrogen species in cultures of the nitrate-reducing Fe (II) oxidizer Acidovorax sp. BoFeN1—questioning the existence of enzymatic Fe (II) oxidation*. *Geobiology*, 2013. **11**(2): p. 180-190.
41. Stookey, L.L., *Ferrozine---a new spectrophotometric reagent for iron*. *Analytical chemistry*, 1970. **42**(7): p. 779-781.
42. Cline, J.D., *Spectrophotometric determination of hydrogen sulfide in natural waters*. *Limnology and Oceanography*, 1969. **14**(3): p. 454-458.
43. Behrens, C.S.S. and A. Kappler, *Ecosystem functioning from a geomicrobiological perspective—a conceptual framework for biogeochemical iron cycling*. 2010.
44. Strauss, H., et al., *Multiple sulphur and oxygen isotopes reveal microbial sulphur cycling in spring waters in the Lower Engadin, Switzerland*. *Isotopes in environmental and health studies*, 2016. **52**(1-2): p. 75-93.
45. Koeksoy, E., Halama, M., Hagemann, N., Weigold, P.R., Laufer, K., Kleindienst, S., Byrne, J.M., Sundman,

- A., Hanselmann, K., Halevy, I., Schoenberg, R., Konhauser, K.O. and Kappler, A., *A case study for late Archean and Proterozoic biogeochemical iron- and sulphur-cycling in a modern habitat – the Arvadi Spring*. *Geobiology*, 2018.
46. Francis, C.A., J.M. Beman, and M.M. Kuypers, *New processes and players in the nitrogen cycle: the microbial ecology of anaerobic and archaeal ammonia oxidation*. *The ISME journal*, 2007. **1**(1): p. 19.
47. Yao, W.S. and F.J. Millero, *Oxidation of hydrogen sulfide by hydrous Fe(III) oxides in seawater*. *Marine Chemistry*, 1996. **52**(1): p. 1-16.
48. Lohmayer, R., et al., *Sulfur species as redox partners and electron shuttles for ferrihydrite reduction by *Sulfurospirillum deleyianum**. *Applied and environmental microbiology*, 2014. **80**(10): p. 3141-3149.

## GENERAL CONCLUSIONS AND OUTLOOK

The primary goals of this thesis were to evaluate the suitability of the Arvadi Spring as an analogue for ferro-euxinic transition zones of oxygenated ancient oceans and to transfer our observations on its geochemical, mineralogical and microbiological composition on existing models for biogeochemical Fe-S-cycling in respective parts of the ancient ocean.

To follow our objectives, we primarily conducted a detailed characterization of the Arvadi Spring water geochemistry and compared our results to the modeled composition of ancient seawater in the current literature (see Chapter 2). We could show that the Arvadi Spring combines the presence of dissolved Fe(II), sulfide and sulfate under fully oxygenated conditions, providing a geochemical framework that is suitable for studying biogeochemical Fe-S-cycling in ancient oceans under natural conditions. The conditions that the Arvadi Spring resembles presumably prevailed mostly during the late Archean in oxygen oases (Olson et al., 2013) and in shallow waters of the Proterozoic ocean (Partin et al., 2013, Kipp et al., 2017).

However, several aspects that appear as problematic in using modern model habitats to study ancient ocean biogeochemistry specifically also apply to the Arvadi Spring and therefore require consideration for a proper evaluation of its value as an ancient ocean analogue. For instance, the salinities of certain modern analogues, including Lake Matano (Crowe et al., 2008), Lake Pavin (Busigny et al., 2014) and Lake La Cruz (Walter et al., 2014), are far below those of marine systems (35‰ for the modern ocean and 1.5 to 2x the modern value in ancient oceans (Knauth, 2005)). The Arvadi Spring salinity is in the lower brackish range with 0.7‰, hence not resembling the ionic strength of a marine environment either. Similarly, the temperature ranges estimated for ancient oceans are much higher (55-85°C (Knauth, 2005)) than those present in the listed analogues and specifically of the Arvadi Spring temperature. Furthermore, the Arvadi Spring O<sub>2</sub> content presumably exceeds the O<sub>2</sub> concentrations of late Archean oxygen oases and shallow Proterozoic ocean waters that are estimated to have contained at least 0.4 to 5 μM O<sub>2</sub> (Olson et al., 2013, Kipp et al., 2017).

Despite the listed discrepancies to anticipated ancient seawater conditions, we conclude that the Arvadi Spring resembles ferro-euxinic conditions in redox-stratified shallow waters of ancient oceans to a certain extent (Fig. 1). Overall, it is important to emphasize that no potential ancient ocean analogue on modern Earth, including the Arvadi Spring, can fully resemble past conditions. Rather, the major insights we can gather from such an approach is the functioning of complex biogeochemical processes and ecosystems in their natural environment that presumably were present to a certain degree in specific spatio-temporal parts of the ancient ocean as well.

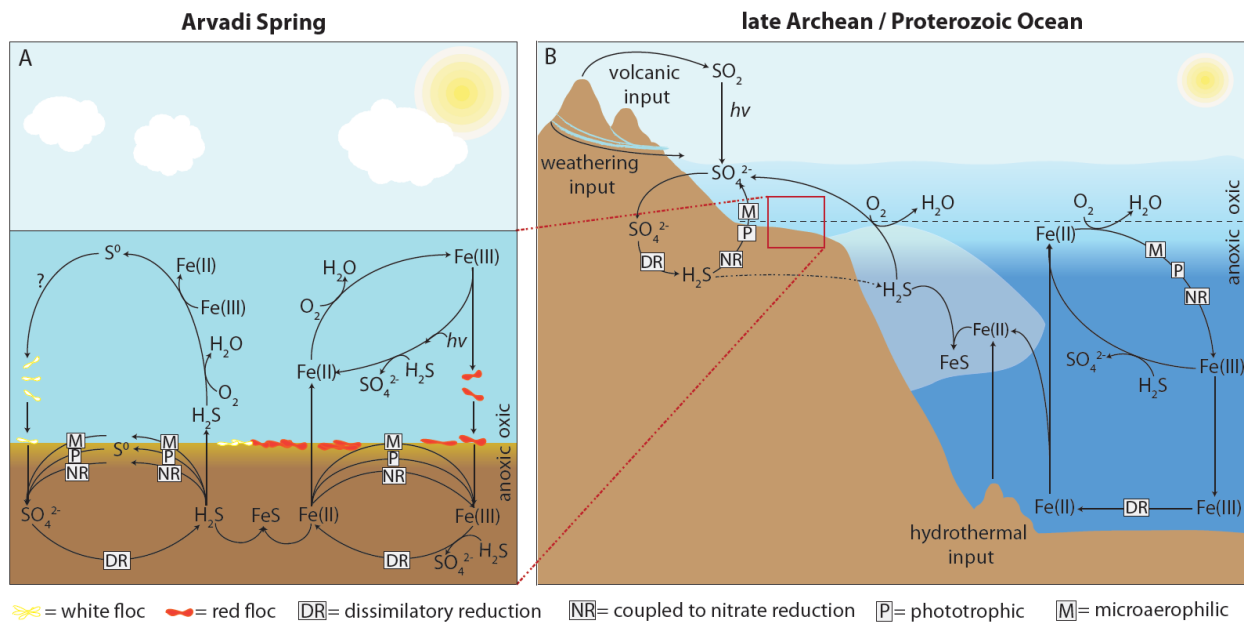


**Fig. 1:** Arvadi Spring Fe-S-cycling (A) and the corresponding zones of ancient oceans where the Arvadi Spring model fits in (B).

The emergence of euxinic seawater as a consequence of intense oxidative weathering of terrestrial pyrite during the Lomagundi Event (Planavsky et al., 2012; Canfield et al., 2013) is pictured in form of sulfide-‘wedges’, i.e. sulfidic waters that accumulated in intermediate depths of neritic ocean zones (Reinhard et al., 2009). Addressing the factors that controlled



the expansion of euxinia versus ferruginous conditions requires a full understanding of the composition of ferro-euxinic transition zones that we partly examined by generating a geochemical profile of the Arvadi Spring water (see Chapter 2). We showed that dissolved Fe(II) and sulfide can coexist in micromolar concentrations at contemporaneous full oxygen saturation and conclude similar concentrations to have prevailed in ferro-euxinic transition zones of late Archean and Proterozoic oceans. A calculated saturation index of -7.42 for amorphous Fe(II) sulfide in the Arvadi Spring water (see Chapter 3) implies that Fe(II) and sulfide could have indeed accumulated to higher concentrations in the Arvadi Spring water before reaching saturation. However, under the oxygen saturation of the Arvadi Spring water, Fe(II) and sulfide consumption by abiotic oxidation with oxygen prevented Fe(II) and sulfide to accumulate to higher amounts. Dissolved Fe(II) and sulfide presumably could have coexisted at somewhat higher micromolar concentrations in ferro-euxinic ocean transition zones as well, depending on the oxygen content and the relative intensity of Fe(II)- and sulfide-producing and consuming processes in respective waters. Overall, we suggest the determined Fe(II) and sulfide concentrations in the Arvadi Spring to be a good basis for future experiments with controlled conditions, in which a variety of environmental conditions including pH, salinity and oxygen concentrations could be tested for controls on the formation of ferruginous versus euxinic conditions.

Another objective in this thesis was to identify the Fe- and S-mineralogy in the Arvadi Spring to assess the primary origin of the observed rock record mineralogy in late Archean and Proterozoic deposits. For this purpose, we examined the Fe- and S-mineralogy in mineral precipitates in the Arvadi Spring pond by XRD, XAS, EXAFS and Mössbauer spectroscopy (see Chapter 3). We could demonstrate that the mineral precipitates in the Arvadi Spring were dominated by quartz, dolomite and calcite, but the major Fe-mineralogy to be characterized by green rust, lepidocrocite and ferrihydrite. Furthermore, we could show that the S-mineralogy was dominated by elemental sulfur. Despite the calculated saturation index of -7.42 for amorphous Fe(II) sulfide in the Arvadi Spring water, we identified minor amounts of Fe(II) sulfides including pyrite and mackinawite at hot spots of red flocs, while Fe(II) sulfides indeed were found not to dominate the bulk Fe-S-mineralogy (see Chapter 3). Based

on their spatially restricted and rather low appearance, we assume Fe(II) sulfides in the Arvadi Spring mineral assemblages to be the results of locally high rates of Fe(III) and sulfate reduction. Nevertheless, the scenario could have been different in zones with higher Fe(II) and sulfide concentrations that reached saturation, resulting in the abundant precipitation of Fe(II) sulfides and the ultimate formation of pyrite that deposited in Black Shales (Canfield, 1998; Werne et al., 2002; Reinhard et al., 2009). Our results imply a rather bigger role for green rust, lepidocrocite, ferrihydrite and  $S^0$  as precursors to geologic rock formations. Unfortunately, due to the high surface reactivities of green rust and  $S^0$  tracking their presence as original mineral phases in geologic deposits is challenging. However, together with recent studies that suggest green rust as a BIF precursor (Halevy et al., 2017; Zegeye, 2014), our findings provide a fundament for future experiments to identify the signals that are produced during the biotic and abiotic formation of green rust and  $S^0$  from solutes and during their transformation into more stable mineral phases.

We examined the Arvadi Spring microbial community composition and structure by a suite of cultivation-based and molecular biological techniques combined with SEM imaging (see Chapter 3) and microcosm experiments (see Chapter 4). Generally, we found the microbial community in the Arvadi Spring sediment to be very diverse, with the microaerophilic sulfide-oxidizer *Thiothrix* spec. being the dominating genus on the 16S rRNA gene level. Furthermore, we could demonstrate the Arvadi Spring mineral assemblages to be densely colonized by microbial networks (see Chapter 2) that already implied a close association between the observed Fe- and S-mineralogy and microbial Fe-S-turnover. In fact, the Arvadi mineral-microbe-assemblages contained a community of coexisting Fe- and S-metabolizers, including microaerophilic, phototrophic and nitrate-reducing Fe(II)-oxidizers, microaerophilic sulfide-oxidizers and dissimilatory Fe(III)- and sulfate-reducers. The relatively low abundance of anaerobic Fe- and S-metabolizers compared to microaerophilic Fe(II)- and sulfide-oxidizers implies anaerobes to be limited in the availability of suitable ecological niches, while microaerophiles are implied to flourish under the oxygen saturation of the Arvadi Spring. However, comparing the results of the relative abundances of the different types of Fe-metabolizers to our microcosm data, microaerophilic Fe(II) oxidation

seems rather not to play a major role in the overall cycling of Fe in the Arvadi Spring under the oxygen concentrations that we tested (Chapter 4). Instead, most of the available Fe(II) was consumed by abiotic Fe(II) oxidation with O<sub>2</sub>, indicating microaerophiles not to be able to outcompete the abiotic reaction at O<sub>2</sub> concentrations above 2 μM O<sub>2</sub>. In order to assess under which conditions microaerophiles can outcompete abiotic Fe(II) oxidation, while Fe(III) reduction still does not prevail under same incubation conditions, additional experiments with a detailed range of oxygen ranges requires to be tested between 0 and 2 μM O<sub>2</sub>.

We conclude a microbial network to have inhabited ferro-euxinic transition zones of the ancient oceans that was similar to the Arvadi Spring microbial community and that showed approximately the same abundances of the different types of Fe – and S-metabolizers. Our results generally support recent studies that suggest microaerophiles to have emerged and colonized the topmost ocean surface layers (Field et al., 2016). However, the actual metabolic activity of microaerophiles in the Arvadi Spring requires further investigation with lower oxygen levels in order to draw conclusions on the impact of microaerophilic Fe(II) oxidation on the overall cycling of Fe. Independently of their metabolic activity, we suggest that the emergence of microaerophiles and their colonization of the topmost oxygenated surface ocean/coastal sediment layers would have caused a rearrangement of the present microbial community. Assuming that the sequence of geochemical gradients would have been fairly similar in the ancient ocean water column and sediment to the present gradients in the modern ocean, the depth distribution of microorganisms presumably would have followed the sequence of microaerophiles - phototrophs - anaerobic chemolithotrophs with increasing depth (Laufer et al., 2016). Our understanding about the structure and depth distribution of ancient marine microbial communities is vague, and a possibility to evaluate this would be the use of graded columns to reconstruct the ancient ocean stratification with which the water geochemistry, mineralogy and microbial community could be examined at different depths.

Such experiments have been conducted in the past and a recent study with a graded column by Swanner et al. (2018) showed dissolved Fe(II) concentrations to have been maintained in

oxic layers of the column by the continuous supply of Fe(II) from Fe(III) reduction in higher depths. The authors showed the major sink for Fe(II) to have been abiotic oxidation by O<sub>2</sub>, suggesting a steady cycling of Fe in Precambrian continental margins between abiotic Fe(II) oxidation and dissimilatory Fe(III) reduction. The results of the batch microcosm experiments that we conducted with sediment from the Arvadi Spring revealed similar results (see Chapter 4), supporting a major fraction of ancient Fe(II) to have been consumed by O<sub>2</sub> from oxygenic photosynthesis. Also, the major source of Fe(II) was found to be Fe(III) reduction in anoxic microcosms. To extend our knowledge from the batch microcosms experiments conducted within the framework of this thesis, we suggest Arvadi sediment to be used for column experiments as described by Swanner et al. (2018), with a focus being set on organic carbon availability and the presence of sulfate reduction in higher depths of the column and a controlled variation in oxygen concentrations in surface parts of the column. By this, the conditions under which ferruginous and euxinic waters form could be fully evaluated and also the establishment of microbial communities with different metabolisms in different depths of the water column could be reconstructed.

In summary, the results presented in this thesis provide a good basis for future work that combine simulation-based laboratory experiments in form of column experiments with samples from modern model habitats such as the Arvadi Spring, following the aim to fully decipher under which conditions ferruginous and euxinic conditions form, when ferro-euxinic transition zones enlarge and narrow down and when nutrient and trace metal scavenging becomes limiting for the apparent microbial community.

## REFERENCES

- Busigny, V., Planavsky, N.J., Jezequel, D., Crowe, S., Louvat, P., Moureau, J., Viollier, E., and Lyons, T.W. (2014) Iron isotopes in an Archean ocean analogue. *Geochimica et Cosmochimica Acta*, **133**, 443-462.
- Canfield, D.E. (1998) A new model for Proterozoic ocean chemistry. *Nature*, **396**, 450-453.
- Canfield, D.E. (2005) The early history of atmospheric oxygen: homage to Robert M. Garrels. *Annual Review of Earth and Planetary Sciences*, **33**, 1-36.
- Canfield, D.E., Ngombi-Pemba, L., Hammarlund, E.U., Bengtson, S., Chaussidon, M., Gauthier-Lafaye, F., Meunier, A., Riboulleau, A., Rollion-Bard, C., Rouxel, O., Asael, D., Pierson-Wickmann, A.C., El Albani, A. (2013) Oxygen dynamics after the Great Oxidation of Earth's atmosphere. *Proceedings of the National Academy of Sciences*, **42**, 16736-16741.
- Crowe, S.A., Jones, C., Katsev, S., Magen, C., O'Neill, A.H., Sturm, A., Canfield, D.E., Haffner, G.D., Mucci, A., Sundby, B. and Fowle, D.A. (2008) Photoferrotrophs thrive in an Archean Ocean analogue. *Proceedings of the National Academy of Sciences of the United States of America*, **105**, 15938-15943.
- Dodd M.S., Papineau D., Grenne T., Slack J.F., Rittner M., Pirajno F., O'neil J. and Little C.T.S. (2017) Evidence for early life in Earth's oldest hydrothermal vent precipitates. *Nature*, **543**, 60-64.
- Field, E. K., Kato, S., Findlay, A. J., MacDonald, D.J., Chiu, B.K., Luther, G. W. and Chan, C.S. (2016) Planktonic marine iron oxidizers drive iron mineralization under low-oxygen conditions. *Geobiology*, **14**, 499-508.
- Halevy, I., Alesker, M., Schuster, E.M., Popovitz-Biro, R., Feldman, Y. (2017) A key role for green rust in the Precambrian oceans and the genesis of iron formations. *Nature Geoscience*, **10**, 135-139
- Kipp, M., Stuecken, E., Bekker., A., Buick., R. (2017) Selenium isotopes record extensive marine suboxia during the Great Oxidation Event. *Proceedings of the National Academy of Sciences*, **114**, 875-880.
- Knauth, L.P. (2005) Temperature and salinity history of the Precambrian ocean: implications for the course of microbial evolution. *Paleogeography, Paleoclimatology, Paleoecology*, **219**, 53-69.
- Laufer, K., Nordhoff, M., Roy, H., Schmidt, C., Behrens, S., Jorgensen, B.B. And Kappler, A. (2016) Coexistence of Microaerophilic, Nitrate-Reducing, and Phototrophic Fe(II) Oxidizers and Fe(III) Reducers in Coastal Marine Sediment. *Applied and Environmental Microbiology*, **82**, 1433-1447.
- Olson S.L., Kump L.R., Kasting J.F. (2013) Quantifying the areal extent and dissolved oxygen concentrations of

- Archean oxygen oases. *Chemical Geology*, **362**, 35-43.
- Partin C.A., Lalonde S.V., Planavsky N.J., Bekker A, Rouxel O.J., Lyons T.W., and Konhauser K.O. (2013) Uranium in iron formations and the rise of atmospheric oxygen. *Chemical Geology*. **362**, 82-90.
- Planavsky, N.J., Bekker, A., Hofmann, A., Owens J.D. and Lyons, T.W. (2012) Sulfur record of rising and falling marine oxygen and sulfate levels during the Lomagundi event. *Proceedings of the National Academy of Sciences*, **109**, 18300-18305.
- Reinhard C.T., Raiswell R., Scott C., Anbar A.D., Lyons T.W. (2009) A late Archean sulfidic sea stimulated by early oxidative weathering of the continents. *Science*, **326**, 713-716.
- Schmidt C., Behrens S., Kappler A. (2010) Ecosystem functioning from a geomicrobiological perspective – a conceptual framework for biogeochemical iron cycling. *Environmental Chemistry*, **7**, 399-405.
- Swanner, E.D., Maisch, M.P., Wu, W. and Kappler, A. (2018) Oxidic Fe(III) reduction could have generated Fe(II) in the photic zone of Precambrian seawater. *Nature Scientific Reports*, **8**, 1-9.
- Walter X.A., Picazo A., Miracle M.R., Vicente E., Camacho A., Aragno M. and Zopfi J. (2014) Phototrophic Fe(II)-oxidation in the chemocline of a ferruginous meromictic lake. *Frontiers in Microbiology*, **5**, 713.
- Werne, J.P., Sageman, B.B., Lyons, T.W., and Hollander, D.J. (2002) An integrated assessment of a “type euxinic” deposit: evidence for multiple controls on black shale deposition in the Middle Devonian Oatka Creek Formation: *American Journal of Science*, **302**, 110-143
- Zegeye, A., Bonneville, S., Benning, L.G., Sturm, A., Fowle, D.A., Jones, C., Canfield, D.E., Ruby, C., MacLean, L.C., Nomosatryo, S. (2012) Green rust formation controls nutrient availability in a ferruginous water column. *Geology*, **40**: 59

# STATEMENT OF PERSONAL CONTRIBUTION

The work described in this thesis was funded by the Deutsche Forschungsgemeinschaft. The conceptual background to this project was designed by Prof. Andreas Kappler, Prof. Ronny Schönberg and Prof. Harald Strauss. Prof. Kappler was the main supervisor throughout the project and Dr. Halevy was the second supervisor. Unless stated otherwise, experiments were either conceptualized by myself or together with Prof. Kappler and/or Dr. Halevy and were carried out by me. The discussion and analysis of the obtained results, as well as writing all manuscripts were completed in cooperation with Prof. Kappler and for chapter 2, 3 and 4 also in cooperation with Dr. Halevy.

In detail the contributions of people other than Prof. Kappler and Dr. Halevy or myself were:

Several people were involved in the fieldwork during the sampling campaigns at the Arvadi Spring. During the sampling in October 2014 Prof. A. Kappler, Prof. Schoenberg, Dr. K. Hanselmann, Dr. S. Eroğlu, G. Albut, U. Lüder, M. Maisch and T. Bayer helped with the field work. During the sampling in April 2015 I had help from A. Sundman, C. Scholze and T. Bayer. During the sampling in July 2015, T. Warchola, A. Mishra and C. Scholze supported me in collecting the samples. During the sampling in November 2015 I had help from A. Sundman, A. Mlloszewska and A. Mishra during sampling and field measurements. During the sampling in March 2016 I had help from M. Patzner and G. Albut. During the sampling in September 2016 I had help from M. Patzner, S. Rughöfft and V. Nickeleit. During the sampling in March 2017 M. Maisch and J. Otte supported during water flow rate analyses and field measurements. During the sampling in September 2017 I had help from M. Schad and T. Bayer.

**Chapter 1:** M. Halama and K. O. Konhauser wrote parts of the manuscript.

**Chapter 2:** N. Hagemann did the SEM sample preparation and sample imaging. M. Halama and Dr. J. M. Byrne performed Mössbauer spectroscopy and XRD analyses on the prepared samples. P. Weigold and Dr. Sara Kleindienst were involved in the 16S rRNA gene sequencing

and sequence analyses. K. Laufer trained me in MPN counts. A. Sundmann, K. Hanselmann and K. O. Konhauser revised the manuscript.

**Chapter 3:** A. Sundmann helped me in field sampling and was responsible for the data fitting and for most of the sample preparation for the synchrotron radiation facilities. She wrote a significant part of the manuscript. Dr. J.M. Byrne performed Mössbauer spectroscopy and evaluated the data. He partly wrote the material and methods as well the results part with respect to Mössbauer spectroscopy and XRD. He revised the manuscript. R. Lohmayer and B. Planer-Friedrich were involved in the polysulfide analyses.

**Chapter 4:** E. Roehm, F. Schaedler and V. Nিকেleit helped during the microcosm preparation, sampling and analyses. C. Schmidt was involved in the project development.

I state hereby that I have not plagiarized or copied any of the text. Chapters 1-4 have been or will be submitted to different scientific journals, so that they may be published in a slightly modified version elsewhere in the future.



# ACKNOWLEDGEMENTS

In the first place, I would like to thank Prof. Andreas Kappler for enabling me to enter the world of fancy science by offering me a project for my doctoral thesis for which I could burn, and that made me enjoy every single day of my time as a grad student. I especially am thankful for his 'open ear' and motivational character that helped me tremendously in overcoming challenging situations. I am happy he was my mentor and am grateful for his trust into my scientific development, considering the high risk he took by offering an early Earth topic to a pure (partly medical) microbiologist with no knowledge in the field of Geoscience.

Furthermore, I would like to acknowledge Dr. Itay Halevy, who accepted co-supervising my project without doubt. I am very thankful for his invitation to the Weizmann Institute in Israel, where I could meet his heartwarming and hospitable research group members. It was quite an interesting journey for me and I will always remember my days there.

It would not have been possible to realize my doctoral thesis without the financial support. I therefore would like to thank the Deutsche Forschungsgemeinschaft (DFG) for funding my project.

My biggest thanks go to a group of scientists, that I don't count as colleagues but as my friends, and that I know I will stay connected with my entire life. I could always be myself without concerns and could trust them in every sense. Their friendship made me waking up earlier than my biological clock allowed, just to have coffee together and start the day cheerful. Specifically, I would like to thank Ellen Röhm, without who my thesis would not have been realizable. Her efficient way of working has always impressed and inspired me, and most of my laboratory experience is based on what I have learned from her. Ulf Lüder and Markus Maisch have helped me tremendously in developing my projects and critically reviewing the outcome, but most importantly, they motivated me and thought me to have more trust into myself. I am thankful for their support in the trickiest situations and for all the laughter we had together in the daily lab life. I am happy I could meet Lars Grimm, even if it was at a later stage of my PhD, and will always keep thinking of our discussions through

the lab benches about life's endlessness, about Ratingen and Herrenberg, about flea markets and Turkish culture, but mostly about what makes good music. I will always remember Lars whenever Fleetwood Mac will be on in the radio. I thank Monique Patzner for having been my friend since my very first days in the Kappler group, and that she never stopped believing in me. Many thanks go to countless others, including Caroline Schmidt, Franziska Schädler, Manuel Schad, Viola Warter, Verena Nিকেleit, Akanksha Mishra, Katja Laufer, Tina Gauger, Anneli Sundman, James Byrne, Nia Blackwell, Casey Bryce, Gregor Schmid, Eirini Adaktylou and many more that accompanied me during my best years in Tübingen that I will never forget.

I would never have approached the path of geomicrobiology without having stepped into biology, for which I thank Dr. Susanne Zimmermann, my former Abitur teacher in biotechnology and my lifelong friend, who inspired and supported me further ever since school. I thank also the cat-ladies Samantha Basile and Petra Horvatek for accompanying me from the beginning of way in biology and for having been friends in good and bad days.

Further thanks go to my new colleagues at Bigelow, especially Jake, Jelena, Nicolas, Jackie and Rose for having eased my start with their friendliness and for having supported me in the very last stages of my PhD thesis. I thank Dave Emerson for his patience during my transition between still being a grad student and finally becoming a postdoc.

I thank my entire family from far and close, for their support and their trust into the path I chose that what anything but what they would have expected. I am lucky to be part of a family that held together in impossible times, that taught me to be resistant and to take the challenge which made me going through my doctoral thesis without fears and tears. Anne, Sinem, Sinan, baba, Haja, babaanne, Edo, Aysun, Musti, Tülin, Yaso, teyzeler, dayı, Çiçek, Ziya, sizler olmadan buralara gelemezdim, ve ancak sizin inanciniz ve gayretiniz sayesinde kendimi daha da ileride görebildim.

I especially thank my beloved husband Dilovan, who helped me to find trust into myself in times that would not have allowed for that and who stayed patient with me at all times, supporting and motivating me throughout very intense years.

## Acknowledgements

---

Last but not least, I would like to thank Tübingen, the little town in Southwest Germany that became my home for eight incredible years, where I could grow up, find peace and security and where my heart will be beating my entire life.

# CURRICULUM VITAE

## Personal data

---

Name Elif Köksoy  
Current address 60 Bigelow Drive  
East Boothbay  
04544 Maine, USA  
Email ekoeksoy@bigelow.org  
Mobile phone +49 176 62747001  
Work phone +1 207 315 2329 412  
Date and place of birth May 20<sup>th</sup> 1990  
Böblingen, Germany  
Citizenship German

## Academic Education

---

**Ph.D. in Geoscience, U. of Tuebingen, Germany** Expected 04/2018

Thesis title: *Biogeochemical Fe-S-cycling in a late Archean and Proterozoic Ocean Model Habitat – the high alpine Arvadi Spring.*

Geomicrobiology Dep., Center for Applied Geoscience, U. of Tuebingen

Supervisors: Prof. Andreas Kappler & Dr. Itay Halevy

---

**M.Sc. Microbiology, U. of Tuebingen, Germany** 2012 – 2014

Thesis title: *Arvadi Spring – a Modern Analogue for the Redox Transition from Ferruginous to Euxinic to Oxic Conditions in Proterozoic Oceans.*

Geomicrobiology Dep., Center for Applied Geoscience, U. of Tuebingen

Supervisors: Prof. Andreas Kappler & Dr. Katja Laufer

---

**B.Sc. Biology, U. of Tuebingen, Germany** 2009 – 2012

Thesis title: *Analyses of protein-protein-interactions involved in the bacterial peptidoglycan synthesis of Staphylococcus carnosus TM300.*

Dep. of Microbial Genetics, Interfaculty Inst. for Microbiology and Infectious Diseases, U. of Tuebingen

Supervisors: Dr. Ute Bertsche & Dr. Julia Deibert

---

## Conference contributions

---

**Goldschmidt Conference**, Paris, France (08/2017)

*Session convener:* New insights into the evolution of Archean-Paleoproterozoic environments and the biosphere

*Oral presentation:* Identity and Abundance of Iron- and Sulfur-Metabolizers in a Paleoproterozoic Ocean Analogue

**Scottish Planetary Science Research Network Meeting**, Edinburgh, UK (02/2017)

*Poster presentation:* Biogeochemical Fe-S-cycling in a Paleoproterozoic ocean model habitat - the Arvadi Spring

**Workshop: 'Building Habitable Worlds'**, Edinburgh, UK (02/2017)

**Geobiology Gordon Research Conference**, Galveston, USA (02/2016)

*Poster presentation:* Reconstructing Proterozoic ocean Fe-S biogeochemistry using the Arvadi spring (Switzerland) as a modern model analogue

**American Chemical Society Conference**, Denver, USA (03/2015)

*Oral presentation:* Iron mineral formation in an iron- and sulfide-rich early ocean model habitat

**Biom mineralization Short Course, CNRS, Paris, France** (12/2014)

*Poster presentation:* Iron mineral formation in an iron- and sulfide-rich early ocean model habitat

**'The role of Earth Sciences in the Origin of Life Problem' microsposium**, Goettingen, Germany (05/2014)

*Oral presentation:* Evaluation of the Arvadi Spring as a modern model for Paleoproterozoic Oceans

## Training Experience

---

### Visiting scientist experience

**Weizmann Inst. of Science, Dep. Of Earth and Planetary Science**, Rehovot, Israel (12/2017)

Data integration and mineral sample discussion in collaboration with Dr. Itay Halevy

**Center for Geomicrobiology**, Aarhus U., Denmark (01/2015 & 06/2015)

Training in voltammetric analysis of geochemical gradients in marine sediment cores during assistance in two sampling campaigns in collaboration with Prof. Bo Barker Jorgensen and Dr. Hans Roy

**ANKA Synchrotron Facility**, KIT, Germany (05/2015)  
Training in synchrotron-spectroscopic analyses of Fe- and S-rich mineral precipitates on the Fe- and K-edge by the SUL-X line comprising XAS and EXAFS

**Novartis AG**, Basel, Switzerland (10/2012)  
Meeting with research staff for the isolation of novel antibiotics from soil microbial communities, Dep. of Microbiology & Biotechnology, Interfaculty Inst. for Microbiology and Infectious Diseases, U. of Tuebingen

---

### **Participation in field excursions and lab courses**

**Field excursion 'Geomicrobiology and Biogeochemistry of High Alpine Fe-rich Cold water springs'** (09/2013)  
Geomicrobiology Dep., U. of Tuebingen

**Lab course 'Geomicrobiology and Environmental Microbiology'** (10/2013)  
Geomicrobiology Dep., U. of Tuebingen

**Electron microscopy short course** (03/2014)  
Geomicrobiology Dep., U. of Tuebingen  
Training in preparation and analyses of environmental biofilm samples with CLSM, SEM, CLSM of FISH samples and image processing with ImageJ

**Electron microscopy short course** (02/2012)  
Cent. for Molecular Biology of Plants, U. of Tuebingen  
Preparation of thin sections of rock samples, staining and microscopic analyses of human tissue, blood and microbial culture samples

### **Supervising Activity**

---

**Student supervision and co-organization of field excursion 'Geomicrobiology & Biogeochemistry of High Alpine Fe-rich Cold-Water Springs'**  
(09/2015 – 09/2017)  
Geomicrobiology Dep., U. of Tuebingen

**Assistance in lab course 'Geomicrobiology and Environmental Microbiology'**  
(10/2014 – 10/2016)  
Geomicrobiology Dep., U. of Tuebingen

**Training of students and interns in basic skills of anoxic work**  
(10/2014 – 02/2015, 10/2014 – 12/2014, 09/2014 – 11/2014)  
Geomicrobiology Dep., U. of Tuebingen

**Teaching assistance in lecture 'structure and function of plants'**

(11/2011 – 12/2011)

Cent. for Molecular Biology of Plants, U. of Tuebingen

**Publication Record**

---

**Koeksoy E.**, Halama M., Konhauser K. O., Kappler A. (2016) Using modern ferruginous habitats to interpret Precambrian banded iron formation deposition. *International Journal of Astrobiology*, **15**, 205-2017.

Deibert J., Kuehner D., Stahl M., **Koeksoy E.**, Bertsche U. (2016) The Peptidoglycan Pattern of *Staphylococcus Carnosus* TM300—Detailed Analysis and Variations Due to Genetic and Metabolic Influences, *Antibiotics*, **5**, 33.

**Koeksoy E.**, Halama M., Hagemann N., Laufer K., Kleindienst S., Byrne J. M., Sundman A., Hanselmann K., Halevy I., Schoenberg R., Konhauser K. O., Kappler A. (accepted with minor reviews) Biogeochemical Iron- and Sulphur-Cycling in the Arvadi Spring – a Paleoproterozoic Ocean Analogue. Accepted for publication in *Geobiology*.

**Koeksoy E.**, Sundman A., Byrne J. M., Lohmayer R., Planer-Friedrich B., Halevy I., Konhauser K. O., Kappler A. Formation of green rust and elemental sulfur in a late Archean and Proterozoic Ocean Analogue. Submitted to: *Geology*.

**Koeksoy E.**, Schaedler F., Nিকেleit V., Schmidt, C., Halevy, I. Schoenberg, R. and Kappler A. (in prep.) Microbial Fe-cycling in a late Archean and Proterozoic Ocean analogue. Target Journal: *Applied and Environmental Microbiology*. Anticipated submission: September 2018.

---